
Arnold Schwarzenegger
*Governor*

# EFFECTS OF ANTHROPOGENIC AEROSOL PARTICLES AND THEIR PRECURSOR GASES ON CALIFORNIA AND SOUTH COAST CLIMATE

**CONSULTANT REPORT**

*Prepared For:*
**California Energy Commission**
Public Interest Energy Research Program

*Prepared By:*
**Mark Z. Jacobson**
**Stanford University**

November 2004
CEC-500-2005-003


**California Climate Change Center**
**Report Series Number 2005-002**

***Prepared By:***
Stanford University
Mark Z. Jacobson
Stanford, California
Contract No. 700-99-019
Work Authorization No. 18

***Prepared For:***
**California Energy Commission**
Public Interest Energy Research (PIER) Program

Guido Franco,
***Contract Manager***

Kelly Birkinshaw,
***Program Area Team Lead***
***Energy-Related Environmental Research***

Ron Kukulka,
***Acting Deputy Director***
**ENERGY RESEARCH AND DEVELOPMENT DIVISION**

Robert L. Therkelsen
***Executive Director***

# Acknowledgements

This work was funded by California Energy Commission's Public Interest Energy Research (PIER) program. I would like to thank Guido Franco and Daniel Rosenfeld for helpful comments.


Please cite this report as follows:

Jacobson, Mark Z. 2004. *Effects of Anthropogenic Aerosol Particles and their Precursor Gases on California and South Coast Climate.* California Energy Commission, PIER Energy-Related Environmental Research. CEC-500-2005-003.

# Preface

The Public Interest Energy Research (PIER) Program supports public interest energy research and development that will help improve the quality of life in California by bringing environmentally safe, affordable, and reliable energy services and products to the marketplace.

The PIER Program, managed by the California Energy Commission (Energy Commission), annually awards up to $62 million to conduct the most promising public interest energy research by partnering with Research, Development, and Demonstration (RD&D) organizations, including individuals, businesses, utilities, and public or private research institutions.

PIER funding efforts are focused on the following RD&D program areas:

- Buildings End-Use Energy Efficiency
- Energy Innovations Small Grant Program
- Energy-Related Environmental Research
- Energy Systems Integration Environmentally Preferred Advanced Generation
- Industrial / Agricultural / Water End-Use Energy Efficiency
- Renewable Energy Technologies

**The California Climate Change Center (CCCC)** is sponsored by the PIER program and coordinated by its Energy-Related Environmental Research area. The Center is managed by the California Energy Commission, Scripps Institution of Oceanography at the University of California at San Diego, and the University of California at Berkeley. The Scripps Institution of Oceanography conducts and administers research on climate change detection, analysis, and modeling; and the University of California at Berkeley conducts and administers research on economic analyses and policy issues. The Center also supports the Global Climate Change Grant Program, which offers competitive solicitations for climate research.

**The California Climate Change Center Report Series** details ongoing Center-sponsored research. As interim project results, these reports receive minimal editing, and the information contained in these reports may change; authors should be contacted for the most recent project results. By providing ready access to this timely research, the Center seeks to inform the public and expand dissemination of climate change information; thereby leveraging collaborative efforts and increasing the benefits of this research to California's citizens, environment, and economy.

The work described in this report was conducted under the Effects of Aerosols on California Climate and Weather: An Exploratory Study contract, Contract Number 700-99-019, Work Authorization 18, by Mark Z. Jacobson, Stanford University.

For more information on the PIER Program, please visit the Energy Commission's Web site www.energy.ca.gov/pier/reports.html or contract the Energy Commission at (916) 654-4628.

## 1. Abstract

*Effects of Anthropogenic Aerosol Particles and their Precursor Gases on California and South Coast Climate* reviews the literature and presents new numerical model results on the potential effects of anthropogenic aerosol particles and their precursor gases on California and California's South Coast Air Basin (SCAB) climate. It first discusses the current understanding of the direct radiative effects of aerosol particles and the climate responses of aerosol particles. The paper then summarizes the literature relating to the effects of aerosol particles on regional climate and global climate. Some studies of temperature trends in California are subsequently described. Finally, it presents results from numerical simulations of the short-term effects of aerosol particles on California climate and air pollution. Comparisons with measurements were performed for some parameters. Nested global-through-urban scale model simulations were run for February and August 1999. Three nested grids were treated in each case: a global grid ($4^o$-SN x $5^o$-WE resolution), a California grid ($0.2^o$ x $0.15^o$ ~ 21.5 km x 14.0 km) and a South Coast Air Basin grid ($0.045^o$ x $0.05^o$ ~ 4.7 km x 5 km). Three simulations were run for each period: one baseline simulation with 1999 emission of gas and aerosol components as determined by the U.S. National Emission inventory (for the United States), one simulation in which all anthropogenic aerosol and precursor gas emissions were removed from the California grid only, and one simulation in which emissions were removed from the South Coast grid only. The purpose of perturbing emissions on only one grid at a time was to eliminate potential exaggerated perturbations at the boundaries from coarser grids in each case. Aerosol emissions removed included those for particulate black carbon, organic carbon, sulfate, nitrate, and fugitive dust. Aerosol precursor gas emissions removed included those for anthropogenic sulfur oxides ($SO_x$), nitrogen oxides ($NO_x$), ammonia ($NH_3$), and speciated reactive organics gases (ROGs), but not carbon dioxide ($CO_2$), methane ($CH_4$), nitrous oxide ($N_2O$), or chlorofluorocarbons (CFCs). The main findings of the study are:

(a) Anthropogenic aerosol particles and their precursor gases (AAPPG) were modeled to reduce precipitation in the Sierra-Nevada Mountains and the Central Valley in February and August. Slight increases in precipitation in some locations beyond the mountains were also seen in both months, but the net effect was a precipitation reduction over land. Similarly, AAPPG were modeled to reduce precipitation in February and August over most of the SCAB grid, including in mountainous regions. Increases in precipitation occurred beyond the mountains in both months. Again, the net effect of particles was to reduce precipitation.

(b) AAPPG were modeled to decrease both California-grid-averaged and South-Coast-grid-averaged ground temperatures in both February and August.

(c) AAPPG decreased near-surface air temperatures in February in both grids, but slightly increased near-surface air temperatures in the South-Coast grid and caused no net change in near-surface air temperatures in the California grid in August.

(d) AAPPG increased California temperatures in the boundary layer and lower troposphere above the boundary layer in August and kept them relatively constant in February. A similar result was found over the SCAB grid. The effects of individual aerosol components were not isolated. The effect of historic changes in greenhouse gas changes, which would enhance warming, were also not isolated.

Present emission of greenhouse gases was treated in all cases to isolate the effect of aerosols and their precursor gases.

(e) In all cases, AAPPG stabilized the boundary layer. More stable boundary layers enhance pollutant concentrations.

(f) AAPPG were modeled to reduce net downward minus upward surface solar radiation and increase net downward thermal-IR radiation in the Central Valley and South Coast Air Basin in February and August. Increases in thermal-infrared (thermal-IR) offset decreases in solar to a greater extent in February than in August. The reduction in solar radiation has implications for photosynthesis rates and crop yields, although such effects were not quantified.

(g) AAPPG were modeled to increase cloud optical depths by up to a factor of two in some areas (reducing visibility through clouds) in the California and SCAB grids in February and August, demonstrating the first indirect effect of aerosols in all cases.

(h) AAPPG were modeled to increase cloud liquid water and decrease cloud ice in California in February and August. Increases in cloud liquid may have been due to the longer lifetimes of clouds and the reduction in precipitation caused by aerosol particles. In the SCAB, liquid water contents increased in February and slightly decreased in August.

(i) AAPPG were modeled to decrease downward surface ultraviolet (UV) radiation in the Central Valley and SCAB in February and August. The reduction in UV come at the expense of high particle and gas pollutant loadings. Increases in particle loadings, in particularly, exacerbate human health to a greater extent than reductions in UV radiation improve it.

(j) AAPPG were modeled to increase the rainwater concentration of aerosol particles. Thus, rainwater contamination is a consequence of air pollution buildup.

These and additional results are discussed more thoroughly in the paper.

## 2. Effects of aerosol particles on climate

Aerosol particles affect temperatures and other weather parameters directly by scattering and absorbing solar and thermal-IR radiation and indirectly through a variety of feedbacks (climate responses). This section discusses direct effects and climate responses of aerosol particles, in turn.

### 2.A. Direct effects of particles

All aerosol particle components scatter thermal-IR and solar radiation and absorb thermal-IR and near-IR radiation. However, only a few components absorb visible and UV radiation.

The strongest aerosol particle absorber in the visible spectrum is black carbon (BC)—the main component of soot (which is emitted mainly as BC and high-molecular-weight organic matter, OM). Black carbon consists of agglomerates of spherules, where the spherule diameters are generally 15–30 nanometers (nm) in diameter. Other visible absorbers include iron and aluminum, which are found in soil dust and industrial particles. Aerosol particle absorbers in the UV spectrum include BC, iron (Fe), aluminum (Al), and certain organic compounds. The organics absorb UV radiation but little visible radiation. The strongest near-UV absorbing organics include certain nitrated aromatics,

polycyclic aromatic hydrocarbons (PAHs), benzaldehydes, benzoic acids, aromatic polycarboxylic acids, and phenols (*Jacobson,* 1999b).

Most particle components, though, are weak absorbers of visible and UV radiation. For example, silicon dioxide [$SiO_2$(s), silica]—which is the white, colorless, crystalline compound found in quartz, sand, and other minerals—is a weak absorber. Sodium chloride [NaCl(s)], ammonium sulfate [$(NH_4)_2SO_4$(s)], and sulfuric acid [$H_2SO_4$(aq)] are also weak absorbers of visible and UV radiation. Soil-dust particles—which contain $SiO_2$(s), aluminum oxide ($Al_2O_3$(s)), iron oxide ($Fe_2O_3$(s)), calcium carbonate ($CaCO_3$ (s)), magnesium carbonate ($MgCO_3$(s)), and other substances—are moderate absorbers of such radiation. Their absorptivity increases from the visible to the UV spectra (e.g., *Gillette et al*. 1993; *Sokolik et al*. 1993).

When an absorbing particle component, such as a BC agglomerate, becomes coated by a relatively nonabsorbing material, such as sulfuric acid or organic carbon, the absorption efficiency of the BC increases, as shown through numerical models that have treated coated particles (e.g., *Toon and Ackerman* 1981; *Bohren*, 1986; *Chylek et al*., 1988; 1995; *Jacobson*, 1997a,b; 2000, 2001; *Fuller et al*., 1999; *Lesins et al*., 2002) and experiments of the optical properties of coated particles (e.g., *Chylek et al.*, 1988; *Schnaiter et al.*, 2004).

The reasons for the enhanced absorption of BC when it is coated versus when it is not are as follows: (1) in the case of particles larger than the wavelength of light, geometric optics implies that $n_\lambda^2$ more light is incident on a small sphere when it is at the center of a much larger transparent sphere with real refractive index $n_\lambda$ than when it is in air (e.g., *Bohren* 1986; *Twohy et al*. 1989). This is called the *optical focusing effect*, because more light is focused into the core of a sphere due to refraction when a shell surrounds the core compared with when it does not. (2) In the case of particles near or smaller than the wavelength of light, enhanced diffraction at the edge of a particle increases the exposure of the core to waves in comparison with exposure of the core to waves in the absence of a shell.

The enhancement of absorption due to the coating of soot in the atmosphere may be sufficiently great to make soot from fossil fuels and biomass burning the second most important component of global warming, after $CO_2$ and ahead of $CH_4$, in terms of its direct radiative effect (*Jacobson* 2000, 2001b; *Chung and Seinfeld*, 2002). However, the climate effects of soot and other particle components depend not only on their direct radiative effects but also on their feedbacks to climate (the climate responses that they initiate). Section 2 briefly discusses climate responses of aerosol particles.

**2.B. Climate responses to particles**

Aerosol particles feed back to climate in many ways. This subsection discusses several feedback mechanisms.

2.B.i. The *particle effect through large-scale meteorology*

Aerosol particles affect local temperatures through their direct effects, which affect local air pressures, winds, relative humidities, and clouds. Changes in local meteorology and heating feed back to the large scale through energy transport and by shifting the locations and magnitudes of semipermanent and thermal pressure systems and jet streams. The effect of local particles on large-scale temperatures is referred to as the *particle effect through large-scale meteorology*. The effect is illustrated in more detail below with respect to black carbon.

Black carbon, the main component of soot, directly warms the air by absorbing sunlight, converting the solar radiation into internal energy (raising the temperature of the soot). The soot then emits thermal-IR radiation at the higher temperature, and greenhouse gases (GHGs) absorb the thermal-IR at selective wavelengths. The warmer air molecules, which generally have long lifetimes, are transported to the large-scale environment, where they may mix vertically. The soot particles, which are removed within days to weeks by rainout, washout, and dry deposition, do not travel so far. As such, the energy trapped and reemitted by soot travels to a larger scale than does the soot itself. This becomes important, because soot particles absorb sunlight, preventing that radiation from reaching the ground, cooling the ground immediately below them during the day. *If soot's energy is transported by air but the soot itself is not, the air can warm on a large scale without causing a simultaneous surface cooling.* During the day and night, BC absorbs the Earth's thermal-IR radiation, a portion of which is redirected back to the ground, warming the ground. This becomes important at high latitudes, where little sunlight is present during much of the year. In such cases, aerosol particles trap heat energy exclusively, like GHGs, and have little solar effect.

In sum, soot particles create three major types of vertical temperature gradients: (1) a daytime gradient in the immediate presence of soot, where the atmosphere warms and the ground cools, (2) a nighttime gradient in the immediate presence of soot, where the atmosphere warms and the ground warms, and (3) a large-scale day- and nighttime gradient in the absence of soot but in the presence of advected air heated by soot, where the atmosphere warms and the ground temperature is unchanged. In only one of these cases, which covers only a portion of the globe and only during the day, does soot cool the ground. In the other two cases, soot warms the ground. These three types of temperature gradients set in motion feedbacks to meteorology. In case (3), the feedback is to the large scale.

2.B.ii. The *self-feedback effect*

When aerosol particles are emitted into to the air, they change the surface area available for gases to condense upon, the air temperature, and the relative humidity, all of which affect the composition, liquid water content, size, and optical properties of new and existing particles. This process is the *self-feedback effect* (*Jacobson*, 2002a). For example, when BC is emitted in one location, it increases the surface area available for sulfuric acid to condense upon, increasing the formation of sulfate locally. Second, when BC absorbs sunlight and warms the air, it decreases the relative humidity, decreasing the liquid water content and reflectivity of aerosol particles containing sulfate and nitrate, warming the air further. In other words, *the reflectivity of sulfate and other reflective particle components decrease in the presence of soot.* Reduced aerosol-particle liquid-water also decreases the liquid-phase chemical conversion of sulfur dioxide to sulfate and the dissolution of ammonia, nitric acid, and hydrochloric acid into particles; further reducing particle size and reflectivity. Treatment of the *self-feedback effect* in a numerical model requires the treatment of nucleation, electrolyte hydration, dissolutional growth, condensational growth, aqueous chemistry, and the effect of aerosol-particles on temperatures and the relative humidity through the thermodynamic energy equation (*Jacobson*, 1994; 1997a,b, 1998a).

2.B.iii. The *photochemistry effect*

Aerosol particles alter photolysis coefficients of gases, affecting their concentrations and those of other gases (through chemical reactions) (e.g., *Jacobson*, 1994; 1997b, 1998b, *Dickerson et al*., 1997). Because many gases absorb solar and/or thermal-IR radiation, changing the concentration of such gases affects temperatures. The process by which aerosol particles change photolysis coefficients (thereby affecting temperatures) is the *photochemistry effect* (*Jacobson*, 2002a).

2.B.iv. The *smudge-pot effect*

During the day and night, all aerosol-particles trap the Earth's thermal-IR radiation, warming the air (*Bergstrom and Viskanta*, 1973a; *Zdundowski et al.*, 1976). This warming is well known to citrus growers who, at night, used to burn crude oil in smudge pots to fill the air with smoke and trap thermal-IR radiation, preventing crops from freezing. The warming of air relative to a surface below increases the stability of air, reducing vertical fluxes of horizontal momentum, slowing surface winds (and increasing them aloft), reducing the wind-speed-dependent emission rates of sea-spray, soil-dust, road-dust, pollens, spores, and some gas-phase particle precursors. The reduction in concentration of these particle types affects daytime solar reflectivity and day- and nighttime thermal-IR heating. Changes in stability and winds due to thermal-IR absorption by aerosols also affect vertical and horizontal energy and pollutant transport. The effect of thermal-IR absorption by particles on emissions of other particles and gases and on local energy and pollutant transport is referred to as the *smudge-pot effect* (*Jacobson*, 2002a).

2.B.v. The *daytime stability effect*

If airborne particles absorb solar radiation, the air warms. Whether the particles absorb or only scatter, they prevent solar radiation from reaching the surface, cooling the surface and increasing the air's stability (*Bergstrom and Viskanta*, 1973a,b; *Venkatram and Viskanta*, 1977a,b; *Ackerman*, 1977). Like with the *smudge-pot effect*, enhanced daytime stability slows surface winds, reducing emission of wind-driven particles and gases and affecting local pollutant and energy transport. At the same time, heating at the top of the boundary layer due to aerosol absorption destabilizes the air above the boundary layer. This destabilization slightly increases venting of particles at the top of the boundary layer to the free troposphere. The effect of solar absorption and scattering by particles on the emission of other particles and gases and on local energy and pollutant transport is referred to as the *daytime stability effect* (*Jacobson*, 2002a).

2.B.vi. *Indirect effects*

An increase in the number of particles increases the number and decreases the size of cloud drops ("first indirect effect," *Twomey*, 1977), reducing rates of drizzle, thereby increasing liquid water content and fractional cloudiness of low-level clouds ("second indirect effect," *Albrecht*, 1989). *Rosenfeld* (2000), for example, found that the presence of aerosol particles from air pollution shut off precipitation from clouds that had top temperatures of $-10^{o}$C. *Borys et al.* (2003) found that the presence of aerosol particles inhibited the riming growth of snow crystals, reducing the snow water content of precipitation. *Givati and Rosenfeld* (2004) found that air pollution particles suppressed precipitation over the upslope side of mountains and enhanced it over the downslope side. They also found that, during the twentieth century, the ratio of precipitation over hills/mountains relative to the coast has decreased.

The increased number of small cloud drops and ice crystals and the longer lifetime of all drops and crystals increases the reflectivity of clouds, reducing the transmission of solar radiation to the Earth's surface and increasing the downward thermal-infrared transfer of energy since enhanced cloudiness acts like a blanket to trap emission of the Earth's thermal-infrared radiation.

Most aerosol particles can serve as cloud condensation nuclei (CCN) and, therefore, have strong indirect effects. However, some, such as diesel soot particles, which consist mostly of black carbon plus unburned lubricating oil and some sulfate, are relatively hydrophobic when emitted, so water does not readily condense upon them. On the other hand, some types of soot may exhibit CCN activation characteristics of the least-

hydrophobic wood smoke particles (*Lammel and Novakov*, 1995). Due to the relatively hydrophobic nature of emitted soot, *Ishizaka and Adhikari* (2003) found from a field experiment in an urban area that "soot particles contributed hardly to the CCN." *Jacobson* (2002a) found that, on a global scale, "sulfate increased cloud optical depths more than did BC + OM" (which is also expected since sulfate is a secondary pollutant, formed from atmospheric oxidation of sulfur dioxide; whereas, soot is a primary pollutant and should not spread so far). *Kristjansson* (2002) concluded, "…black carbon only contributes marginally to the overall indirect effect."

Although soot is relatively hydrophobic initially, other hygroscopic chemicals coat it during aging by condensation and coagulation, increasing soot's ability to act as a CCN. In some cases, this internal mixing may occur within an urban area itself. For example, tunnel studies indicate that 85% of fossil-fuel-derived BC mass is emitted in particles smaller than 0.12 μm in diameter (*Venkataraman et al.*, 1994; *Berner et al.*, 1996), but ambient measurements, such as those in Los Angeles and other cities, show that BC in the accumulation mode often exceeds that in the emissions mode away from sources (e.g., *Hitzenberger and Puxbaum*, 1993; *Venkataramn and Friedlander*, 1994; *Berner et al.*, 1996). The only way the ambient size distribution of BC can differ so significantly from that of the emission distribution is if BC particles coagulate and/or grow. Whereas self-coagulation of BC occurs, self-coagulation alone cannot account for the volume-growth of BC from the emission mode to the upper accumulation mode or coarse-particle mode, as seen in Figures 2b and 4b of *Jacobson* (1997a). Heterocoagulation of BC with other particles already in these modes and condensation can account for such growth (same figures).

2.B.vii. The *effect on BC absorption of the first indirect effect*

Clouds enhance the direct forcing of soot lying within and above them (e.g., *Haywood et al.*, 1997). In addition, when the *first indirect effect* occurs, cloud scattering is enhanced, increasing: (1) the absorption of all solar radiation by BC, and (2) solar-IR radiation by water vapor and $CO_2$ within and above the cloud, warming the air there (*Jacobson*, 2002a).

2.B.vii. The *semidirect effect*

Solar absorption by a low cloud increases stability below the cloud, reducing vertical mixing of moisture to the cloud base, thinning the cloud (*Nicholls*, 1984). Decreases in relative humidity correlate with decreases in low-cloud cover (*Bretherton et al.*, 1995; *Klein*, 1997). Similarly, absorbing particles warm the air, decreasing its relative humidity and increasing its stability, reducing the low-cloud cover (*Hansen et al.*, 1997; *Ackerman et al.*, 2000; *Koren et al.*, 2004). Reduced cloud cover increases sunlight reaching the surface, warming the surface in a process called the "semidirect effect" (*Hansen et al.*, 1997).

2.B.ix. The *BC-low-cloud positive feedback loop*

When BC reduces low-cloud cover by increasing stability and decreasing relative humidity, enhanced sunlight through the air is absorbed by BC (and by water vapor and $CO_2$ in the solar-IR), further heating the air and reducing cloud cover in a positive feedback loop, identified as the *BC-low-cloud positive feedback loop* (*Jacobson*, 2002a). Whereas $CO_2$ also warms the air by absorbing thermal- and solar-IR radiation, reducing low cloud cover and enhancing surface solar radiation in some cases, it absorbs solar radiation much less effectively than does BC, so it partakes less in this positive feedback loop than does BC.

2.B.x. The *Rainout effect*

When BC increases stability of and vertical moisture transport in the boundary layer, it may decrease cumulus convection, much of which starts in the boundary layer, reducing cumulus precipitation. The addition of BC also triggers the second "indirect effect," which reduces precipitation. Reducing precipitation reduces rainout of soluble gases and all aerosol-particles, increasing their concentrations in the air; increasing warming in some cases and cooling in others. This suppression of aerosol removal due to suppression of rainout caused by increased aerosol loadings was described by *Jacobson* (2002a) and has been observed to occur in biomass-burning plumes (*Andreae et al*., 2004).

2.B.xi. The *BC-water-vapor positive feedback*

When BC is present, it warms the air relative to the surface. The warmer air decreases the relative humidity, evaporating cloud water to vapor (a GHG), warming the air further. The resulting vertical temperature gradient, in the presence of mechanical or thermal turbulence, increases the downward sensible heat flux, warming the surface (although less than the air is warmed). The increase in surface temperature relative to its initial temperature increases the evaporation rate of ocean and soil water. Since the air is now warmer, the saturation vapor pressure of water is now higher, allowing much of the additional water vapor to accumulate. The additional water vapor absorbs solar-IR and thermal-IR, warming the air further. (This feedback also applies to $CO_2$ for the most part).

2.B.xii. The *airborne particle snow-albedo effect*

During the day, airborne BC reduces sunlight to the ground, cooling it, increasing the lifetime of existing snow. Conversely, because BC warms the air, snow falling through the warmer air is more likely to melt. At night, airborne BC also enhances downward thermal-IR, increasing nighttime melting and sublimation of snow on the ground. Because the albedo of new snow exceeds that of sea ice—which exceeds those of soil or water—the melting of snow or sea ice increases sunlight to the surface. The effect of airborne aerosol-particles on temperatures through their change in snow and sea-ice cover is referred as the *airborne particle snow-albedo effect*, analogous to its well-known GHG counterpart, the *greenhouse-gas snow-albedo effect.*

2.B.xiii. The *effect of particle inclusions on snow and sea ice albedo*

When an absorbing aerosol particle, such as BC or soil dust, deposits directly onto a snow or sea grain surface or when the same particle becomes embedded within a snow flake that falls to the surface, the BC or soil dust absorbs sunlight, heating the snow or sea ice surface and reducing the albedo of the surface. Both factors feed back to climate. Several studies have modeled the albedo of snow containing BC inclusions (e.g., *Warren and Wiscombe*, 1980, 1985; *Chylek et al*., 1983; *Warren*, 1984; *Aoki et al*., 2000), the albedo of sea ice containing BC inclusions (*Light et al.,* 1998), and the optical properties of ice or snow containing other inclusions (e.g., *Higuchi and Nagoshi*, 1977; *Gribbon*, 1979; *Clark and Lucey*, 1984; *Woo and Dubreuil*, 1985; *Podgorny and Grenfell*, 1996). *Warren and Wiscombe* (1980), for example, found that a concentration of 15 nanograms per gram (ng/g) of soot in snow may be needed to reduce the albedo of snow by about 1%. *Light et al.* (1998) calculated that 150 ng/g of soot embedded in sea ice could decrease the spectral albedo of sea ice by up to 30%. *Twohy et al*. (1989) estimated that about 1000 times higher concentration of soot is needed for a cloud than for snow to cause the same albedo reduction, because: (1) snow optical thickness is much larger than is cloud optical thickness, and (2) cloud drops are much smaller than ice crystals. For both reasons, light has more encounters with absorbing material in snow than in a cloud. A third set of studies has examined the effect on climate of pre-estimated albedo changes due to assumed changes of soot in snow (*Vogelmann et al*., 1988; *Hansen and Nazarenko,* 2003). A fourth type of study has examined the effect on climate of soot

when snow and sea ice albedos were predicted with a radiative transfer code, rather than prescribed, and the concentration of soot in snow was calculated by treating the cycle of BC between emission and removal, by first principles (*Jacobson*, 2004).

## 3. Effects of aerosol particles on regional climate

This section discusses studies of the regional climate response of aerosol particles. Early studies of aerosol particles on regional climate focused on the instantaneous radiative impacts of aerosols. Early one-dimensional modeling studies examined absorption and extinction properties of urban aerosol particles (*Bergstrom*, 1972), the effects of urban particles on the vertical thermal structure of the atmosphere (*Atwater*, 1971a,b, 1972; *Rasool and Schneider*, 1971; *Zdunkowski and McQuage*, 1972; *Bergstrom and Viskanta*, 1973a; *Wang and Domoto*, 1974; *Zdunkowski et al*., 1976; *Welch and Zdunkowski*, 1976; *Venkatram and Viskanta*, 1977a; *Ackerman*, 1976, 1977; *Charlock and Sellers*, 1980), and the feedback of the change in thermal structure of the boundary layer due to aerosols on aerosol vertical dispersion (*Bergstrom and Viskanta*, 1973b; *Venkatram and Viskanta*, 1977b).

Some early measurement studies examined the difference in downward radiative fluxes between urban and rural areas of downward solar irradiance (*Peterson et al.*, 1978), downward solar and thermal-IR irradiance (*Estournel et al*., 1983), downward thermal-IR irradiance in the atmospheric window (*Lubin and Simpson*, 1994), and heating rates below an aerosol layer (e.g., *Kilsby*, 1990).

The first three-dimensional model to consider the effects of bulk (e.g., non-size- or composition-resolved) aerosols on urban or regional temperatures was that of *Atwater* (1975). Many additional studies have examined regional climate change in the absence of aerosols (e.g., *Dickinson et al*., 1989; *Giorgi and Bates*, 1989).

The first study on either the regional or global scale to examine the three-dimensional climate response of discrete *size-resolved* aerosol particles was the regional-scale study of *Jacobson* (1997b). In that study, particle evolution and short-term climate response was simulated for the Los Angeles basin over a two-day period, and model results were compared with data from the Southern California Air Quality Study of 1987. Aerosol particles in the model were distributed over a single internally mixed size distribution consisting of 16 size categories, or "bins," and 73 chemical constituents per bin over a grid with > 24,000 grid cells. Size-resolved particles were emitted and homogeneously nucleated and evolved by condensation, dissolution, coagulation, dry deposition, sedimentation, advection, convection, and diffusion. Black carbon was treated as a concentric core surrounded by a shell of all other constituents in each size bin, when it was present in the bin. As such, this was also the first three-dimensional modeling study to treat the evolution of the mixing state of BC and the enhancement of BC absorption due to size-resolved internal mixing.

The study found that aerosol particles in Los Angeles, which contained absorbing BC, decreased peak daytime surface and air temperatures slightly but increased nighttime temperatures to a greater extent, causing a net two-day warming. These three-dimensional results were generally consistent with one-dimensional results of *Bergstrom and Viskanta* (1973a), who calculated that aerosol particles in Los Angeles reduced daytime surface temperatures, increased daytime atmospheric temperatures, and increased nighttime surface temperatures to a greater extent than they decreased daytime surface temperature. The overall net warming found was also consistent with the one-dimensional result of *Ackerman* (1977), who found that "urban pollutants tend to warm the surface slightly." Finally, this study also found the near-surface warming of air in August in the South Coast Air Basin.

*Jacobson* (1997b) also found that aerosol particles in Los Angeles may have reduced peak surface solar radiation by about 58 watts per square meters ($W/m^2$) (6.5%), consistent with measured peak reductions in Los Angeles of 6%–8% (*Peterson et al.*, 1978). Aerosols were also found to have increased daytime downward thermal-IR radiation by about 19 $W/m^2$ and increased nighttime downward thermal-IR radiation by about 13 $W/m^2$, close to values of 22–25 $W/m^2$ and 15 $W/m^2$, respectively, from *Estournel et al.* (1982). Finally, aerosols were calculated to have increased the heating rate of the bottom atmospheric layer by about 0.52 K/hr at Claremont, which compares with a Moscow measurement of +0.55 K/hr reported by *Binenko and Harshvardhan* (1993, p. 213) and calculations of about +0.5 K/hr for a polluted boundary layer by *Welch and Zdunkowski* (1976).

**Figure 1.** Aerosol particles in Los Angeles smog December 19, 2000.

**Photo by M.Z. Jacobson.**

Figure 1 shows a photograph of an aerosol layer in Los Angeles. The layer is often relatively thin but dense in Los Angeles due to the Pacific high pressure system, which forces air to sink above the layer, compressing it.

The radiative properties of aerosols discussed in the studies above, performed mostly for Los Angeles, have many similarities to (but some differences from) aerosols found in other polluted regions during studies such as TARFOX (e.g., *Russell et al*., 1999a,b; *Hignett et al*., 1999; *Hegg et al.* 1997) and INDOEX (e.g., *Jayaraman et al.*, 1998; *Satheesh and Ramanathan*, 2000; *Ramanathan et al*., 2001a,b).

For example, like the aerosols in Los Angeles, aerosols studied during the INDOEX field campaign in the North Indian Ocean and South and Southeast Asia had high optical depths, strong absorption by black carbon, heavy anthropogenic sources, a large reduction in downward surface solar radiation due to the aerosols, and large atmospheric heating rates (e.g., *Ramanathan et al*., 2001a). Pollution layers during INDOEX,

however, generally rose to higher altitudes than do those in Los Angeles, and more clouds were present during the INDOEX study than are generally present in Los Angeles. As such, INDOEX allowed for studies of the impact of aerosol particles on cloud suppression (e.g., *Ackerman et al*., 2000) and other hydrologic-cycle features (e.g., *Chung et al*., 2002).

To date, several studies have examined the effect of aerosol particles on regional temperature in Asia (e.g., *Yu et al*., 2001a; *Jacobson*, 2002a, 2004b; *Menon et al*., 2002; *Krishnan and Ramanathan*, 2002), but the net effects vary with aerosol loading, absorption properties, and feedbacks, so the issue is not settled. Some additional recent studies have modeled the regional radiative heating due to aerosol particles (e.g., *Jacobson*, 1998a, 1999; *Park et al*., 2001, *Raga et al*., 2001; *Riemer et al.*, 2003) and measured radiative forcing below an aerosol layer (e.g., *Yu et al*., 2001b).

## 4. The net effects of aerosol particles on global climate

The net effect of aerosol particles on climate cannot be determined experimentally or through data analysis, simply because it is not possible to run a controlled experiment of the Earth system with and without aerosol particles. Although they have uncertainties associated with them, numerical models are the primary tools available to isolate the effect of aerosol particles on regional or climate.

Whereas, many papers have examined the direct effects of aerosol particles and many have quantified the indirect effects in terms of radiative forcing, relatively few papers have modeled the global-scale climate response of aerosol particles (e.g., the effect of aerosol particles on global temperatures and other meteorological parameters). The earliest three-dimensional studies of the effects of aerosol particles on global climate examined the effect of abnormally large injections of soot or dust (e.g., *Kahle and Deirmendjian*, 1973; *Joseph*, 1976). The next set of three-dimensional model climate response studies examined the effect of large injections of smoke due to a hypothetical nuclear war (e.g., *Covey et al*., 1984; *Coakley and Cess*, 1985; *Cess et al*, 1985; *Malone et al*., 1986; *Ghan et al.*, 1988). Some later studies examined the historic or future climate response of anthropogenic aerosols (e.g., *Hansen et al*., 1997; *Tett et al*., 2002; *Wang*, 2004).

All studies mentioned above assumed that aerosol particles were a bulk parameter rather than size resolved in the numerical model. In some cases, the parameter was in the form of a continuous lognormal distribution; whereas in others, it was in the form of a single-scattering albedo. In some cases, particle emission was not treated; instead aerosols were assumed to have a fixed ambient loading. Such treatment prevented the simulation of aerosol evolution—namely, treating distinct size-resolved emission, homogeneous nucleation, coagulation, condensation, dissolution, internal particle chemistry, cloud formation, nucleation scavenging, impaction scavenging, and dry deposition. These factors are important because aerosol radiative and climate impacts are inherently a complex function of their size, composition, and feedbacks.

In a set of recent studies, the time-dependent evolution and climate response of size-resolved aerosol-particles on a global scale was simulated from first principles (*Jacobson*, 2001a; 2002a; 2004a,b). The studies treated the cycling of size-resolved aerosol particles between emission and removal. In one case (*Jacobson*, 2001a), the time-dependent calculation was performed among 18 aerosol size distributions, 17 size bins per distribution, and an average of 6.8 components per bin per distribution. In the remaining cases, size-resolved cloud liquid, ice, graupel, and precipitation formed on a single distribution of size-resolved aerosol particles, accounting for the first indirect effect and part of the second indirect effect in *Jacobson* (2002a; 2004a) and the complete first and

second indirect effects in *Jacobson* (2004b). To date, these are the only studies to treat size-resolved cloud formation from size-resolved aerosols and to treat either the first or second indirect effects in a global model from first principles.

One finding from *Jacobson* (2002a) was that the magnitude of the climate response per unit direct forcing of aerosols differed from that for gases. The reason was that particles have several effects that major GHG do not (e.g., the *indirect effects*, the *self-feedback effect*, the *semidirect effect*, the *photochemistry effect*, and the *rainout effect*, among others). This finding of the difference between gas and aerosol climate sensitivity is also consistent with results of *Hansen et al.* (1997) and *Cook and Highwood* (2004), who similarly found a difference between gas and aerosol climate response, although those studies did not treat the size resolution of aerosol particles. The implication of this result is that direct forcing, while possibly a reasonable surrogate for the climate response of gases, is not a surrogate for the climate response of aerosols. Whereas, several studies try to account for the additional feedback of the indirect effect through the term "indirect forcing," this term does not account for the multitude of other feedbacks of aerosol particles described in Section 2.B.

## 5. Previous studies of California temperature trends and their causes

A review of the effects of aerosol-particles on California climate would not be complete without some discussion of past temperature and precipitation trends and their possible causes in California. Briefly, some studies of temperature trends in California and in the United States, where California data were extractable, include those of *Karl et al.* (1988, 1996); *Balling and Idso* (1989); and *Goodridge* (1992). *Goodridge* (1992), for example, examined 80 years of temperatures at 112 California sites and found an overall warming trend, with greater warming in populated regions. *Balling and Iso* (1989) found a net warming of temperatures in Southern California between 1920 and 1984 during both summer and winter and a simultaneous net cooling in the Southeastern United States. Nemani et al. (2001) found that air temperatures over the California coast warmed by $1.13^{o}$C between 1951 to 1997, with most warming occurring at night and during spring. Warming of coastal sea surface temperatures occurred simultaneously.

*Groisman et al*. (2001) examined trends in precipitation and streamflow in the United States in the twentieth century and found an overall increase in U.S. precipitation—especially heavy and very heavy precipitation—and a large reduction in spring snow cover extent over the western United States.

## 6. Simulations of aerosol effects on California weather and climate

This section discusses results from three-dimensional nested numerical simulations of the short-term effects of aerosol particles on California climate and air pollution. The numerical model used is first described, followed by a discussion of the setup of the simulations, followed by an analysis of model results.

### 6.A. Description of the Model

The model used was GATOR-GCMOM, a parallelized and one-way-nested global-through-micro-γ-scale Gas, Aerosol, Transport, Radiation, General Circulation, Mesoscale, and Ocean Model. The model treated time-dependent gas, aerosol, cloud, radiative, dynamical, ocean, and transport processes. Aerosol and cloud processes were treated among multiple aerosol size distributions and hydrometeor distributions, respectively. All processes described were solved in all grid cells in the stratosphere and troposphere. The model was parallelized with Message Passing Interface (MPI). All physical, chemical, and cloud, and radiative algorithms were parallelized by column. The model as a whole has been tested against meteorological, chemical, and radiative field data without nesting on urban scales (*Jacobson*, 1997a,b; 1998a, 1999), with nesting from

the global-through-urban scale (*Jacobson*, 2001b,c), with nesting from the global-through-regional scale (*Jacobson et al*., 2004), without nesting on the freeway scale (*Jacobson and Seinfeld*, 2004), and on the global scale (*Jacobson*, 2001a, 2002a; 2004a,b).

*6.A.i.Atmospheric Dynamical and Transport Processes*
On the global scale, the model solved the equations for momentum (under the hydrostatic assumption), thermodynamic energy, and total water with the potential-enstrophy, mass, and energy-conserving scheme of *Arakawa and Lamb* (1981). In all nested regional grids, it solved with an enstrophy-, mass-, and kinetic-energy-conserving scheme (*Lu and Turco*, 1995). Both modules used spherical and sigma-pressure coordinates in the horizontal and vertical, respectively.

*6.A.ii. Gas processes*
Gas processes included emission, photochemistry, advection, turbulence, cloud convection of gases, nucleation, condensation onto and dissolution into aerosols, clouds, and precipitation, washout, and dry deposition. Gases affected solar and thermal-IR radiation, aerosol formation, and cloud evolution, all of which fed back to meteorology. Gas photochemistry was solved with SMVGEAR II, a sparse-matrix vectorized Gear-type chemical ordinary differential equation solver (*Jacobson*, 1998b). The chemical mechanism included over 300 reactions relevant to urban, free tropospheric, and stratospheric chemistry.

*6.A.iii.Aerosol Processes*
Aerosol processes were treated among 17 size bins and multiple aerosol components per bin. *Jacobson* (2002b) describe the numerical techniques for solving aerosol processes in the model. *Jacobson* (2003) describe the techniques for solving interactions of aerosol particles with size-resolved hydrometeor distributions. Size- and distribution-dependent aerosol processes included emission, homogeneous nucleation, condensation, dissolution, aerosol-aerosol coagulation, aerosol-cloud/ice/graupel coagulation, equilibrium hydration of liquid water, internal-particle chemical equilibrium, irreversible aqueous chemistry, evaporation of cloud drops back to aerosol-particles, transport, sedimentation, dry deposition, rainout, and washout. Aerosols in the model affected solar and thermal-IR radiation, cloud evolution, gas concentrations, and surface albedo, all of which feed back to meteorology. The number concentration of particles and the mole concentrations of each component in each size distribution were prognostic variables. $H_2SO_4$-$H_2O$ homogenous nucleation rates were calculated with the parameterization of *Vehkamaki et al.* (2002). Homogeneous nucleation was solved simultaneously with condensation of $H_2SO_4$-$H_2O$ between the gas and all size bins of all distributions with a mass-conserving, noniterative, and unconditionally stable scheme (*Jacobson*, 2002b). The scheme was also used for condensation of organic gases onto size-resolved aerosols. The model treated dissolutional growth of $NH_3$, $HNO_3$, HCl, and soluble organics over all size bins with a mass-conserving, noniterative, and unconditionally stable dissolution scheme. Aerosol liquid water content, pH, and ion distributions in all bins are solved with EQUISOLV II, a chemical equilibrium solver (*Jacobson*, 1999c). Aerosol-aerosol coagulation is solved among all distributions and components and among total particles in each bin with a volume-conserving, noniterative algorithm (*Jacobson*, 2002b).

*6.A.iv. Gas-Aerosol-Cloud-Turbulence Interactions*
The numerical techniques for cloud thermodynamics and microphysics are described predominantly in *Jacobson* (2003). Cumulus and stratus clouds formed in the model by water growth onto the 17 aerosol size bins to form liquid water drops or ice crystals or both. Following the growth calculation, the liquid drops and crystals were repartitioned from the 17-bin aerosol distribution into separate 30-bin liquid and ice hydrometeor

distributions, where each bin contained all the chemical components of the underlying CCN aerosol particles. A third 30-bin hydrometeor distribution, graupel, was also tracked. This distribution formed upon the heterocoagulation of the liquid water and ice hydrometeor distributions, the contact freezing of aerosol particles with the liquid distribution, the heterogeneous-homogeneous freezing of the liquid distribution, and the evaporative freezing of the liquid distribution.

The water available for the original condensational/depositional growth calculation was determined as a function of height with stratus and cumulus parameterizations. The stratus cloud scheme was from *Mellor and Yamada* (1982) and was coupled with the calculation of turbulence (order 2.5). The stratus scheme predicted vertical cloud fraction and cloud water content in each layer given turbulence terms and vertical gradients in potential temperature and moisture. Turbulence parameters affected clouds, momentum, energy, and tracers, particularly in the boundary layer, which was resolved. Cumulus clouds were predicted with a modified Arakawa-Schubert algorithm (*Ding and Randall*, 1998). In each column, nearly 500 subgrid cumulus clouds could form (and 1–10 typically formed), each defined by a unique cloud base and top (when 23 layers exist below the tropopause, 22 bases and 22 tops are possible). For each subgrid cloud, water and energy transport were solved with a mass-flux convection scheme; gas and size-resolved aerosol component transport are solved with a positive-definite, stable convective plume transport scheme. For each subgrid cloud, the model also generated adjustments to large-scale potential temperature, momentum, and water vapor.

Following convection, the bulk water predicted in each layer from the cumulus and stratus parameterizations was evaporated/sublimated, then regrown (simultaneously for liquid and ice) onto the size-resolved aerosol distributions transported to that layer. The critical radius for liquid growth accounted for Raoult's law and the Kelvin effect and that for ice growth accounted for the Kelvin effect. Because aerosols were transported vertically with cloud water in all cases, aerosol activation was consistent with that in a rising plume.

Following growth, size-resolved processes treated were hydrometeor-hydrometeor coagulation (liquid-liquid, liquid-ice, liquid-graupel, ice-ice, ice-graupel, and graupel-graupel), aerosol-hydrometeor coagulation, large liquid drop breakup, settling, evaporative cooling during drop settling, evaporative freezing (freezing during drop cooling), heterogeneous-homogeneous freezing, contact freezing, melting, evaporation, sublimation release of aerosol cores upon evaporation/sublimation, coagulation of hydrometeors with interstitial aerosols, irreversible aqueous chemistry, gas washout, and lightning generation from size-resolved coagulation among ice hydrometeors. The coagulation kernel for all cloud interactions and aerosol-cloud interactions included a coalescence efficiency and collision kernels for Brownian motion, Brownian diffusion enhancement, turbulent inertial motion, turbulent shear, settling, thermophoresis, diffusiophoresis, and charge.

Aerosol particles of different size were removed by size-resolved clouds and precipitation through two mechanisms: nucleation scavenging and aerosol-hydrometeor coagulation. Both processes were size-resolved with respect to both aerosol particles and hydrometeor particles.

*6.A.v.Radiative and Surface Processes*

Radiation processes included UV, visible, solar-IR, and thermal-IR radiative interactions with gases, size/composition-resolved aerosols, and size/composition-resolved hydrometeor particles. Radiative transfer was solved with the scheme of *Toon et al.* (1989). Calculations were performed over more than 600 wavelengths/probability

intervals and affected photolysis and heating. Column calculations treat shading by structures (e.g., buildings) and topography. The model treated ground temperatures over subgrid surfaces (up to 12 soil classes and roads over soil, roofs over air, and water in each cell). It also treated vegetation over soil, snow over bare soil, snow over vegetation over soil, sea-ice over water, and snow over sea-ice over water (*Jacobson*, 2001b). For all surfaces except sea ice and water, surface and subsurface temperatures and liquid water were found with a time-dependent 10-layer module. Ocean mixed-layer velocities, energy transport, and mass transport were calculated with a gridded 2-D potential-enstrophy, energy, and mass-conserving shallow-water equation module, forced by wind stress (*Ketefian and Jacobson*, 2004), based on the shallow-water scheme of *Arakawa and Lamb* (1981). Water (ocean and lake) temperatures were also affected by sensible, latent, and radiative fluxes. Nine additional layers were added below each ocean mixed-layer grid cell to treat energy diffusion from the mixed layer to the deep ocean and ocean chemistry.

**6.B. Description of Simulations**

For the present study, the model was run for August and February, 1999. Three one-way nested grids were used: a global grid ($4^o$-SN x $5^o$-WE resolution), California grid ($0.2^o$ x $0.15^o$ ~ 21.5 km x 14.0 km with the southwest corner grid cell centered at $30.0^o$ N and $-126.0^o$ W and 60 SN cells x 75 WE cells) and a South Coast Air Basin grid ($0.045^o$ x $0.05^o$ ~ 4.7 km x 5 km with the southwest corner grid cell centered at $30.88^o$ N and $-119.35^o$ W and 46 SN cells x 70 WE cells). The global grid treated 39 sigma-pressure layers between the surface and 0.425 hectaPascal (hPa). The nested regional grids included 27 layers between the surface and 103.5 hPa. Regional-grid sigma-pressure layer vertical boundaries matched each other and the bottom 27 global-model layers exactly. Each grid included four layers in the bottom 1 km.

The baseline emission inventory used was the U.S. National Emission Inventory for 1999, version 2 (*USEPA*, 2002). The inventory accounts for over 370,000 stack and fugitive sources, 250,000 area sources, and 1700 source classification code (SCC) categories of on-road and nonroad mobile sources. Emitted gases included $NO_x$, $SO_2$, $NH_3$, CO, $CH_4$, and speciated reactive organic gases (ROGs), including paraffins, ethane, other olefins, formaldehyde, higher aldehydes, toluene, and xylene. Emitted particle components included BC, organic carbon (OC), sulfate, nitrate, and "other." From the raw U.S. database inventory, special inventories were prepared for each model grid domain. Tables 1 and 2 show the emission rates by source for several chemical species and summed groups for the domains. Although the inventories appear to capture most of the important sources and species, some shortcomings can be seen from the inventory. For example, most onroad particulate matter is categorized as "other"; whereas much of this should be identified as BC or OM.

**Table 1.** Yearly emission rates of gas and particle components in the California grid (which includes some areas beyond California as well) based on 1999 National Emission Inventory Data. All units are metric tonnes per year.

| Species | Stack | Fugitive | Area | Nonroad | Onroad | Total |
|---|---|---|---|---|---|---|
| CO | 54,840 | 41,510 | 1,856,000 | 3,464,000 | 5,586,000 | 11,000,000 |
| $NO_x$ as $NO_2$ | 77,660 | 46,920 | 173,600 | 509,500 | 687,000 | 1,495,000 |
| ROG | 10,240 | 85,570 | 1,070,000 | 431,700 | 611,700 | 2,210,000 |
| $CH_4$ | 4822 | 35,640 | 501,400 | 62,930 | 77,240 | 682,000 |
| $SO_x$ as $SO_2$ | 29,730 | 17,590 | 14,500 | 52,180 | 12,140 | 126,100 |
| $NH_3$ | 3080 | 9915 | 175,100 | 3252 | 26,320 | 217,700 |
| | | | | | | |
| $OM_{2.5}$ | 8086 | 8957 | 253,000 | 13,370 | 360.3 | 283,800 |
| $BC_{2.5}$ | 842.2 | 982.3 | 29,170 | 19,650 | 633.4 | 51,290 |
| $SULF_{2.5}$ | 4964 | 4508 | 6869 | 940 | 13.66 | 17,300 |
| $NIT_{2.5}$ | 112.9 | 114.7 | 1394 | 107.5 | 1.738 | 1731 |
| $OTH_{2.5}$ | 15,750 | 18,570 | 403,100 | 4062 | 13,050 | 454,500 |
| | | | | | | |
| $OM_{10}$ | 11,130 | 14,270 | 456,200 | 14,930 | 516.4 | 497,000 |
| $BC_{10}$ | 1508 | 1611 | 49,130 | 21,310 | 751.4 | 74,310 |
| $SULF_{10}$ | 8766 | 7193 | 12,470 | 1016 | 21.68 | 29,470 |
| $NIT_{10}$ | 187.4 | 180.5 | 3402 | 119.8 | 2.232 | 3891 |
| $OTH_{10}$ | 32,770 | 39,350 | 1,657,000 | 4434 | 18,750 | 1,752,000 |

**Table 2.** Yearly emission rates of gas and particle components in the South Coast Air Basin grid (which includes some areas beyond the basin boundaries as well) based on 1999 National Emission Inventory Data. All units are metric tonnes per year.

| Species | Stack | Fugitive | Area | Nonroad | Onroad | Total |
|---|---|---|---|---|---|---|
| CO | 6802 | 17,290 | 288,900 | 1,739,000 | 2,721,000 | 4,773,000 |
| $NO_x$ as $NO_2$ | 21,570 | 23,710 | 47,830 | 222,800 | 342,400 | 658,300 |
| ROG | 1907 | 46,260 | 372,900 | 184,200 | 295,500 | 900,900 |
| $CH_4$ | 1089 | 17,160 | 180,100 | 26,760 | 37,450 | 262,600 |
| $SO_x$ as $SO_2$ | 947.9 | 8936 | 2625 | 23,720 | 5429 | 41,660 |
| $NH_3$ | 746.7 | 7014 | 20,510 | 1826 | 14,720 | 44,820 |
| | | | | | | |
| $OC_{2.5}$ | 1752 | 3265 | 64,140 | 5482 | 0 | 74,640 |
| $BC_{2.5}$ | 161.7 | 368.4 | 5486 | 7778 | 0 | 13,790 |
| $SULF_{2.5}$ | 714.4 | 2480 | 1987 | 368.7 | 0 | 5550 |
| $NIT_{2.5}$ | 17.96 | 43.54 | 422.8 | 44.24 | 0 | 528.5 |
| $OTH_{2.5}$ | 903.2 | 6597 | 104,800 | 2092 | 6985 | 121,400 |
| | | | | | | |
| $OC_{10}$ | 2063 | 4593 | 114,600 | 6153 | 0 | 127,400 |
| $BC_{10}$ | 256.2 | 598.9 | 9552 | 8460 | 0 | 18,870 |
| $SULF_{10}$ | 1048 | 3581 | 3693 | 400.3 | 0 | 8722 |
| $NIT_{10}$ | 24.01 | 63.24 | 993.9 | 49.49 | 0 | 1131 |
| $OTH_{10}$ | 1513 | 11,570 | 408,800 | 2284 | 10,220 | 434,400 |

Additional emissions treated in the model were biogenic emissions (isoprene, monoterpenes), wind-driven soil dust, sea spray, pollen, and spores, and $NO_x$ from lightning.

Three simulations were run for each February and August 1999: one with 1999 emission of gas and aerosol components, one in which all anthropogenic aerosol and precursor gas emissions were removed from the California grid only, and one in which all

anthropogenic aerosol and precursor gas emissions were removed from the South Coast grid only. Because perturbing the global grid (e.g., removing emissions) for the California simulation or perturbing the California grid for the South Coast simulation resulted in artificially high boundary fluxes of meteorological variables during preliminary simulations, it was decided to keep the emissions in all "parent" grid domains constant when examining the effect of aerosols on a "progeny" domain. Whereas this method smoothed results considerably, it resulted in slightly higher aerosol loadings during the sensitivity tests than should occur in reality, because 1999 aerosols entered the "progeny" (finer) domains from the "parent" (coarser) domains, even when emissions were removed from the "progeny" domains. As such, the actual effect of all anthropogenic aerosols and the gas-phase precursors should be slightly stronger than those predicted here.

In the sensitivity simulations, aerosol emissions removed included those for particulate black carbon, organic carbon, sulfate, nitrate, and fugitive dust. Aerosol precursor gases removed at the same time included anthropogenic $SO_x$, $NO_x$, $NH_3$, and speciated reactive organics gases (ROGs), but not $CO_2$, $CH_4$, $N_2O$, or CFCs.

The model dynamics time steps were 300 s (global grid), 10 s (California grid), and 5 s (South Coast grid). The time interval for nesting between the global to California grid and from the California to South Coast grid was 1 hour. Variables passed at the boundaries included temperature, specific humidity, wind velocity, gas concentrations, and size- and composition-resolved aerosol concentrations.

Initial meteorological fields were obtained from National Center for Environmental Prediction (NCEP) reanalysis fields for February 1 and August 1, 1999, at 12 GMT (*NCEP*, 2003). No data assimilation, nudging, or model spinup was performed during any simulation.

**6.C. Results**

6.C.1. Baseline Results, California Grid

Figure 2 shows baseline model results for the California grid, averaged over February and August (both day and night), for several parameters.

Figure 2a shows that the baseline monthly-averaged column abundance of black carbon (BC) was greater in August than in February. The major emission sources of BC were in the South Coast Air Basin, Central Valley, and San Francisco Bay Area.

The column abundance of BC was lower in winter than in summer because, as BC particles aged, they became coated with hygroscopic material (e.g., hygroscopic organic matter, sulfate, nitrate, ammonium), and such particles were readily removed by precipitation The two mechanisms of wet removal in the model were rainout (size-resolved nucleation scavenging) and washout (size-resolved aerosol-hydrometeor coagulation) (Section 6.A.iv). Figure 2b shows the baseline concentration of BC in precipitation. The removal of BC by precipitation was greatest in the Central Valley, particularly in the Northern Central Valley, in February, since BC concentrations were modestly high there but precipitation rates were higher there than in more southern locations. The precipitation distribution is shown shortly.

Figure 2c shows the baseline column abundance of primary organic matter (POM). The POM includes lubricating oil components in diesel and gasoline vehicle exhaust as well as primary organics from non-vehicle sources. The spatial distribution of POM roughly followed that of BC. The magnitude of POM concentration was about an order of

magnitude greater than that of BC because the number of POM sources exceeded those of BC.

Figure 2d shows the baseline column abundance of particulate secondary organic matter (SOM). Secondary organic matter formed in the model by condensation of low-vapor pressure organic gases onto size resolved aerosol particles. Condensing gases included by-products of toluene, xylene, and isoprene oxidation. Figure 2e shows the baseline column abundance of isoprene. The abundance was an order of magnitude greater in August than in February and peaked in mountainous forested regions. The high SOM column abundances in the southeast corner of the grids in Figure 2d appears to be due to advection of SOM from the global grid, and the source of most SOM in the global cell was isoprene and monoterpene oxidation. Because SOM was formed in the atmosphere, it was spatially distributed over a broader region than was POM.

Figure 2f shows that the baseline column abundance of sulfate was not so different in February than in August. Part of the reason was that, although more sulfate was removed by precipitation in February than in August, more sulfate was also produced by aqueous oxidation within aerosol particles, fog drops, and cloud drops in February than in August. When fog and cloud drops evaporated, for example, they released their aerosol cores, which now contained more sulfate due to aqueous oxidation.

Other aerosol particle components treated included nitrate, ammonium, sodium, chloride, and liquid water. Plots of some of these species when aerosols were present versus absent are shown shortly. Figure 2g shows the baseline column abundance of total aerosol liquid water content (ALWC). Aerosol liquid water content resulted from hydration of electrolytes such as sulfate, nitrate, ammonium, sodium, chloride, etc., and other solutes (e.g., oxalic acid, malonic acid) in aerosol particle solutions. Hydration occurred in the model for relative humidities (RHs) between 0% and 100%, although RHs between 99.5% and 100% were treated as RHs of 99.5%. Even though electrolyte concentrations were lower in February than August, ALWCs were higher in February than in August because of the superlinear effect of RH on hydration. Aerosol liquid water contents were generally high over the ocean, where the combination of sufficient sea spray ions and a high relative humidity led to significant absorption of liquid water onto particles.

Figure 2h shows the baseline total aerosol column abundance. It was greater in February than in August due to the dominance of liquid water in February. An effect of the greater total column abundance in February was to increase the aerosol optical depth (Figure 2i) in February relative to August.

The higher relative humidity in February invariably let to a greater baseline cloud optical depth (Figure 2j), and precipitation rate (Figure 2k) in February than in August. A comparison of the modeled precipitation maps shown in Figure 2k with a map of measured February, 1999 precipitation in California (Figure 2l) suggests that many regions of modeled high and low precipitation followed the measurements relatively well. For example, the peak observed precipitation rate in California was at the northwest corner of the state, which is where the model predicted it to be (Figure 2k). Measured high precipitation levels along the northern coast and Sierra-Nevada range were similarly modeled. The relatively low measured precipitation rate in the southern part of the state was also picked up by the model. The climatological average precipitation rate for February (Figure 2m) indicates greater precipitation in the southern part of the state than for February 1999. Magnitudes of measured precipitation were predicted less accurately than were locations.

**Figure 2.** Model baseline predictions on the California grid for February (left) column and August (right column), averaged over the respective months, of several variables.

2a. Baseline column BC

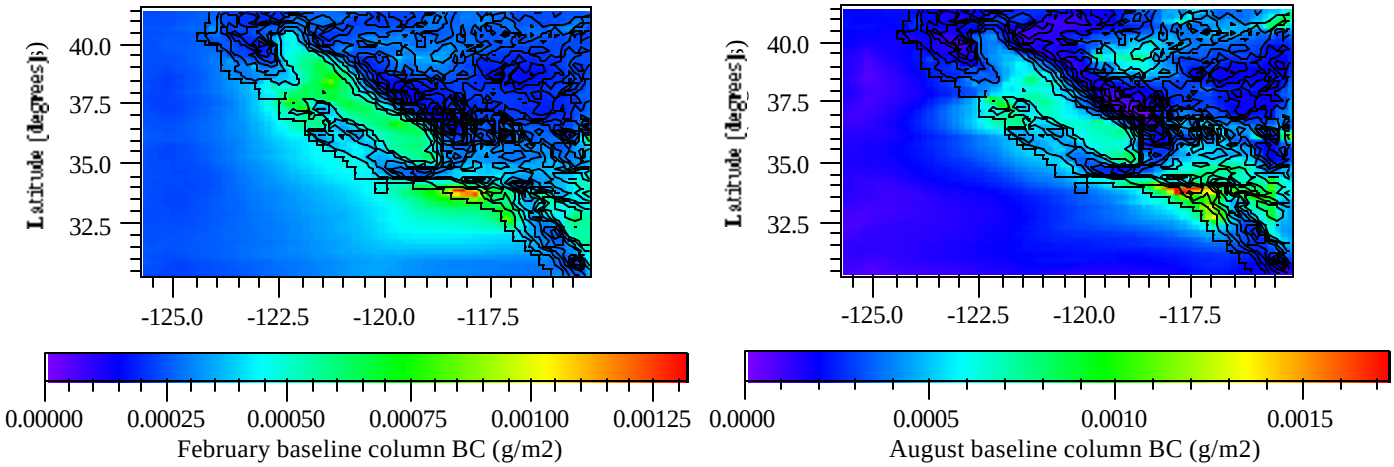


2b. Baseline BC in precipitation

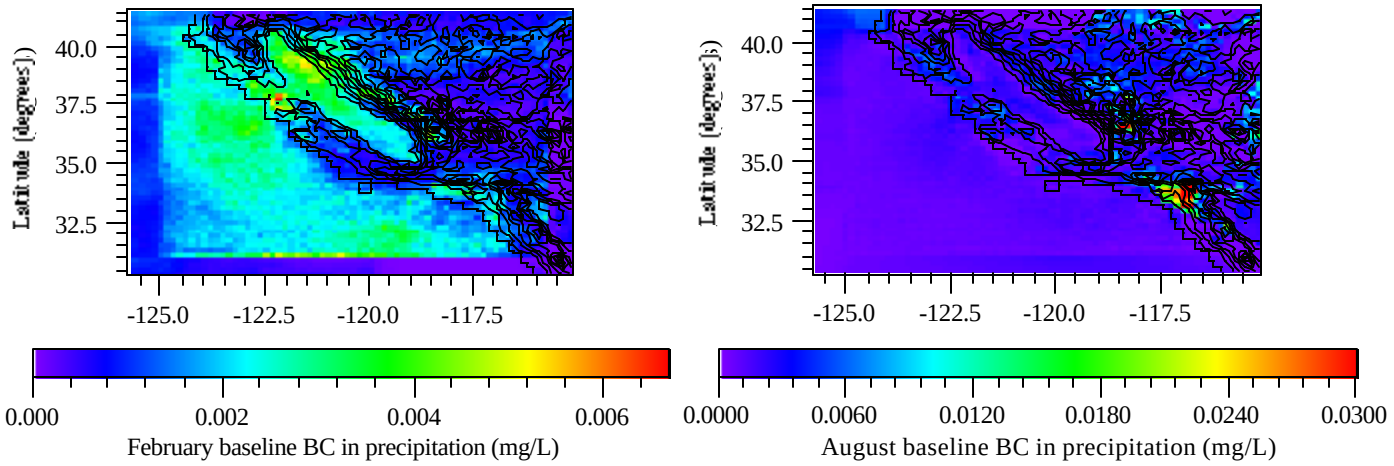


2c. Baseline column POM

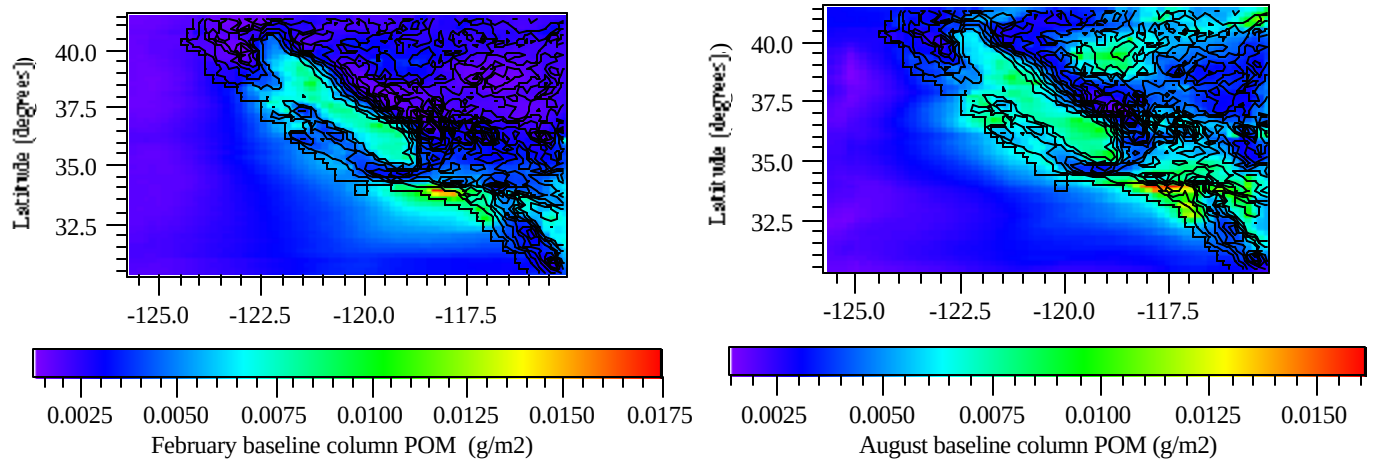

2d. Baseline column SOM

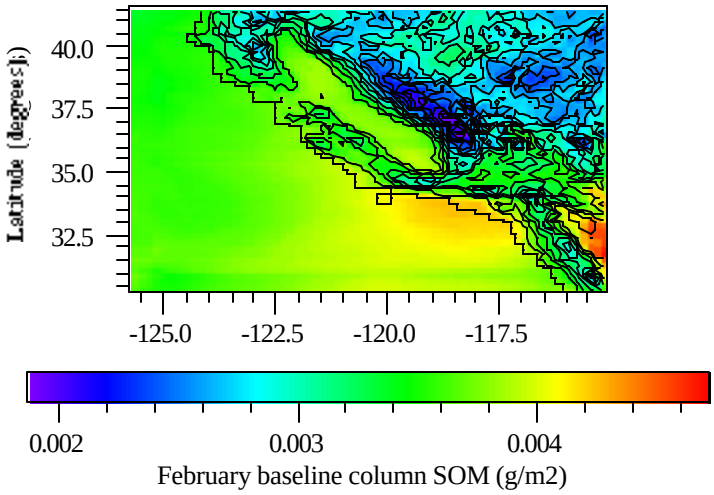


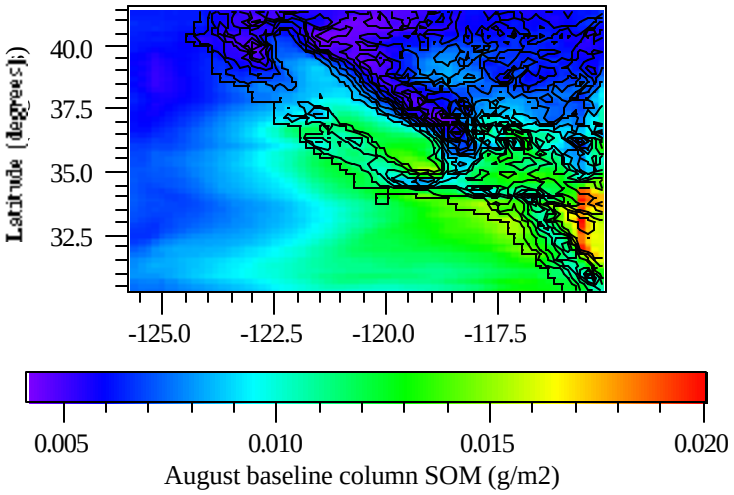


2e. Baseline column isoprene

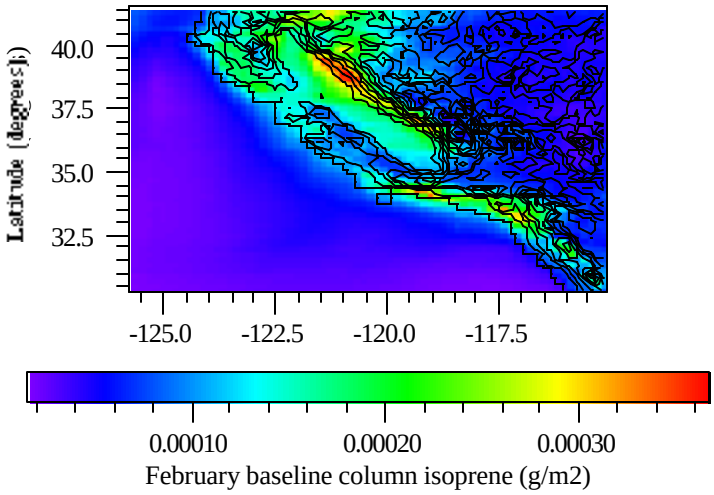


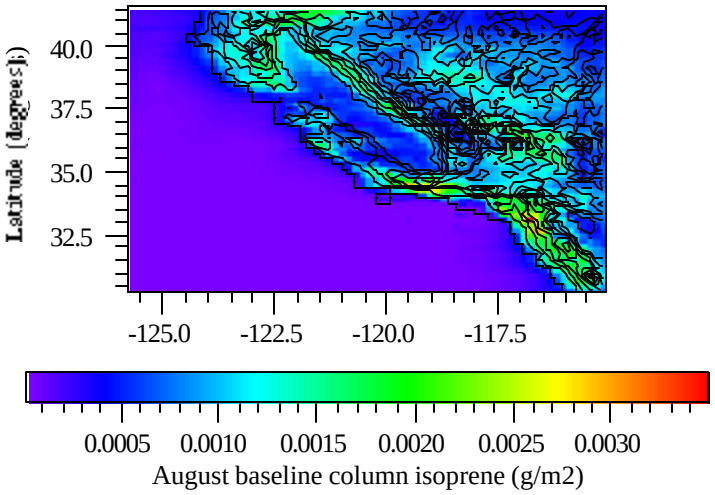


2 f. Baseline column particulate sulfate

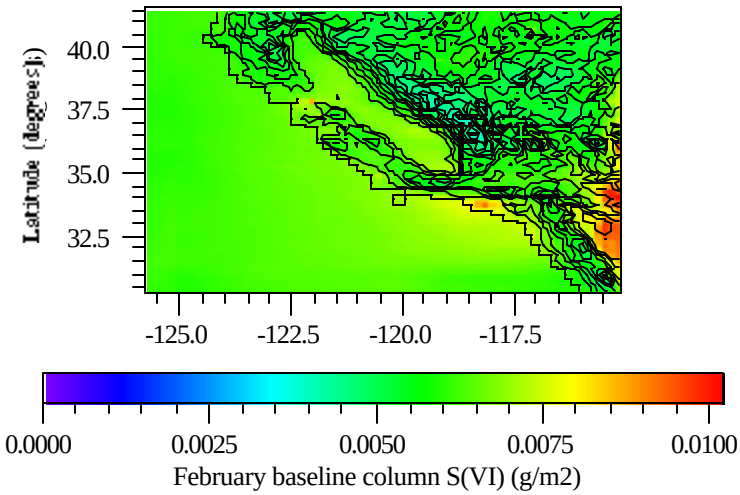


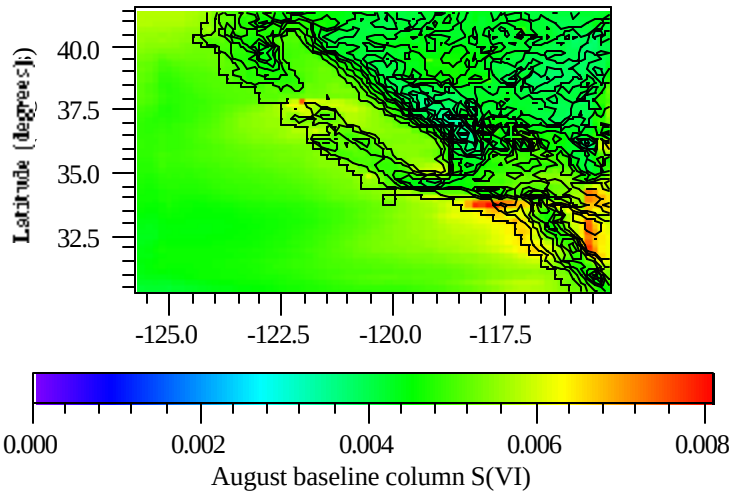

2g. Baseline column aerosol LWC

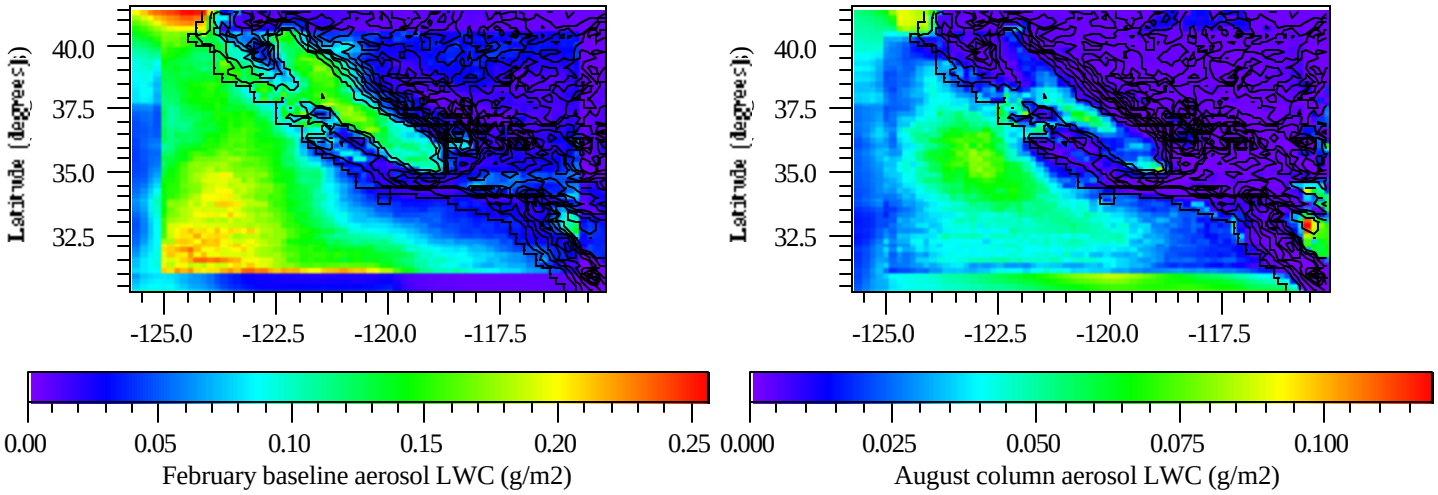


2h. Baseline column total aerosol

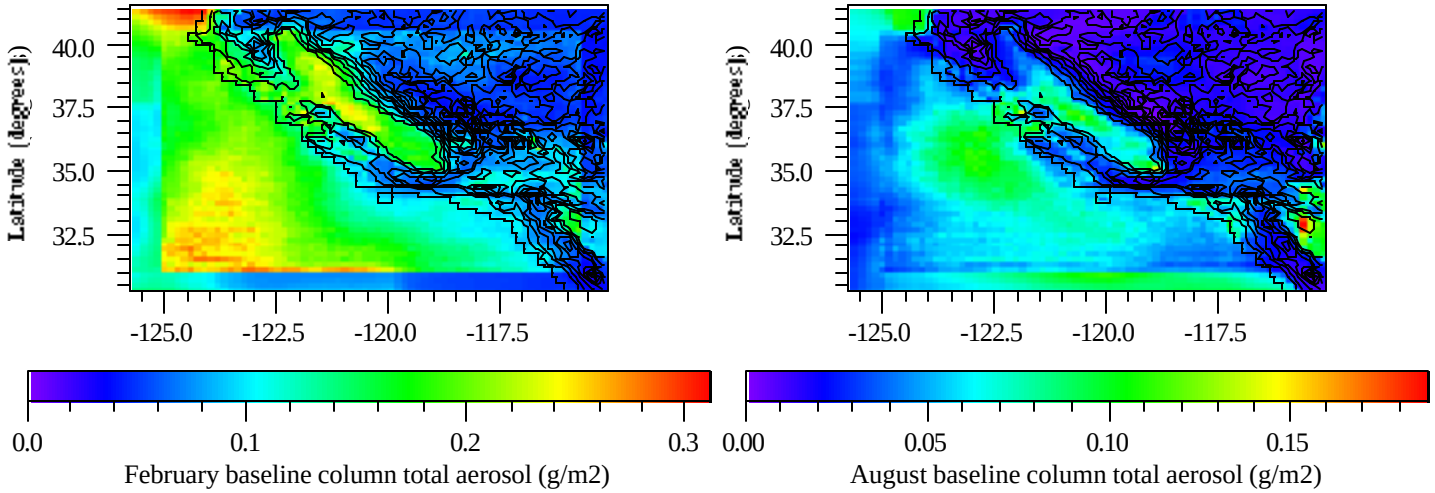


2i. Baseline aerosol optical depth

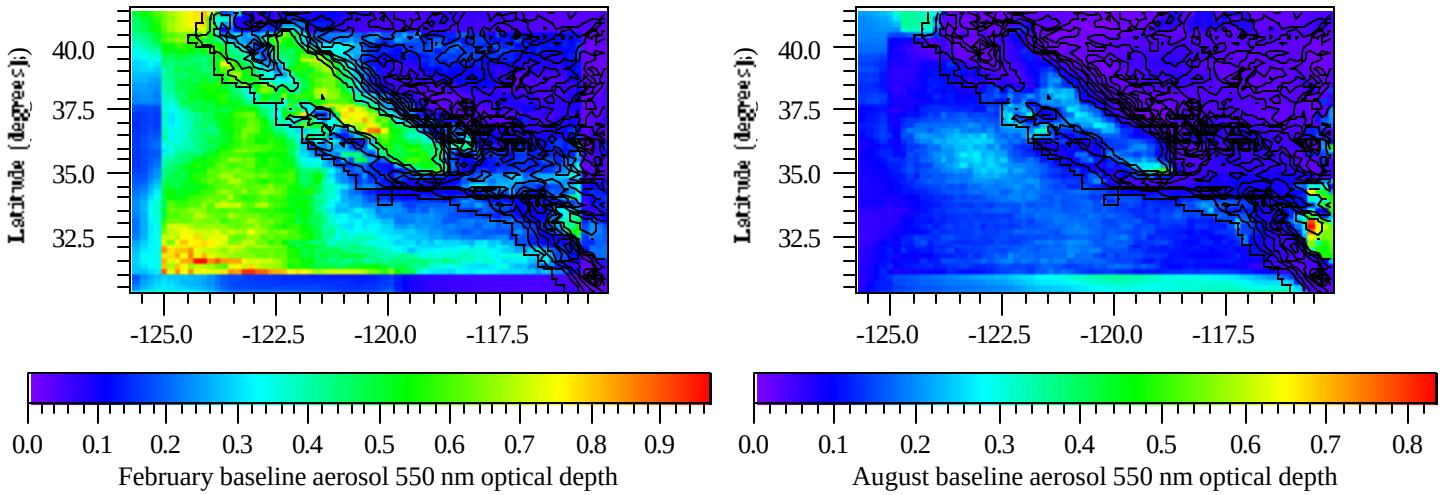

2j. Baseline cloud optical depth

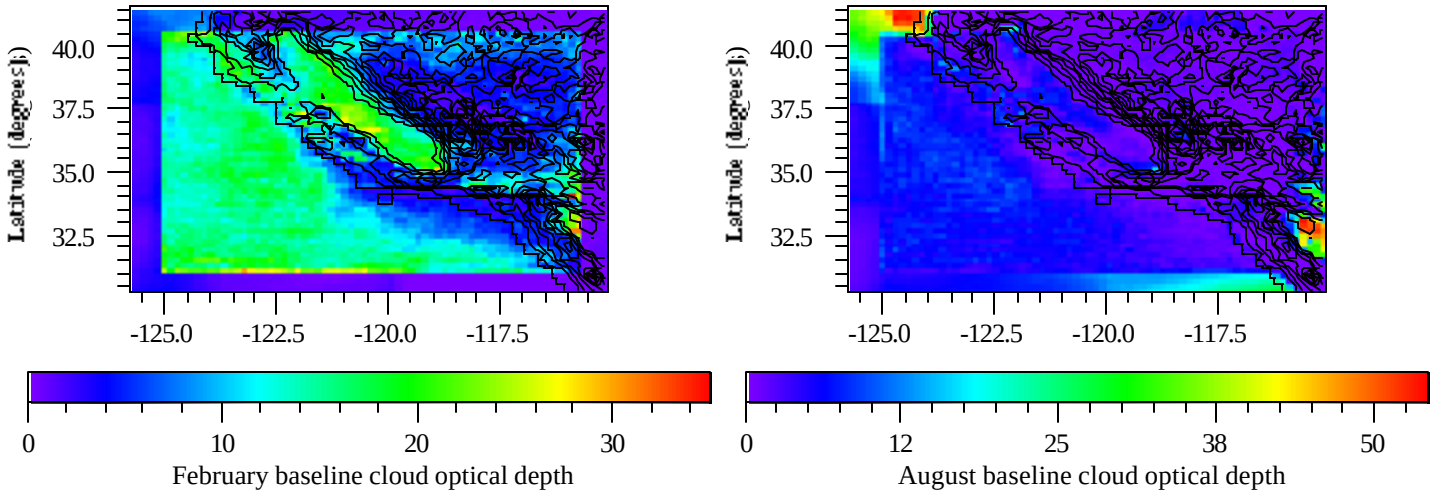


2k. Baseline precipitation

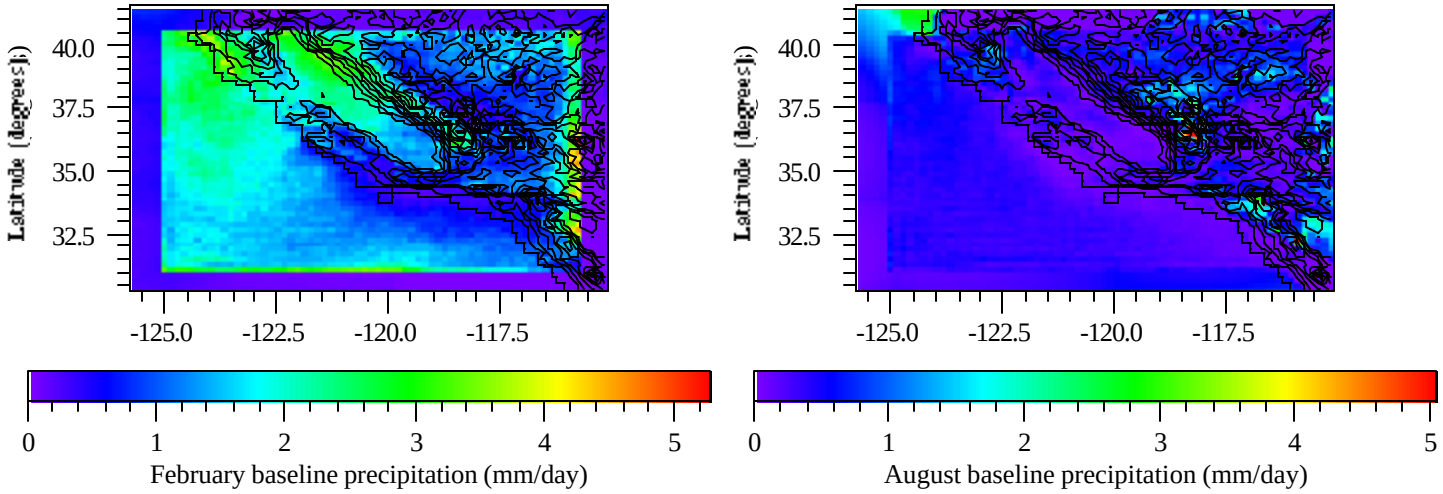

2l. Measured February 1999 precipitation (inches per month)

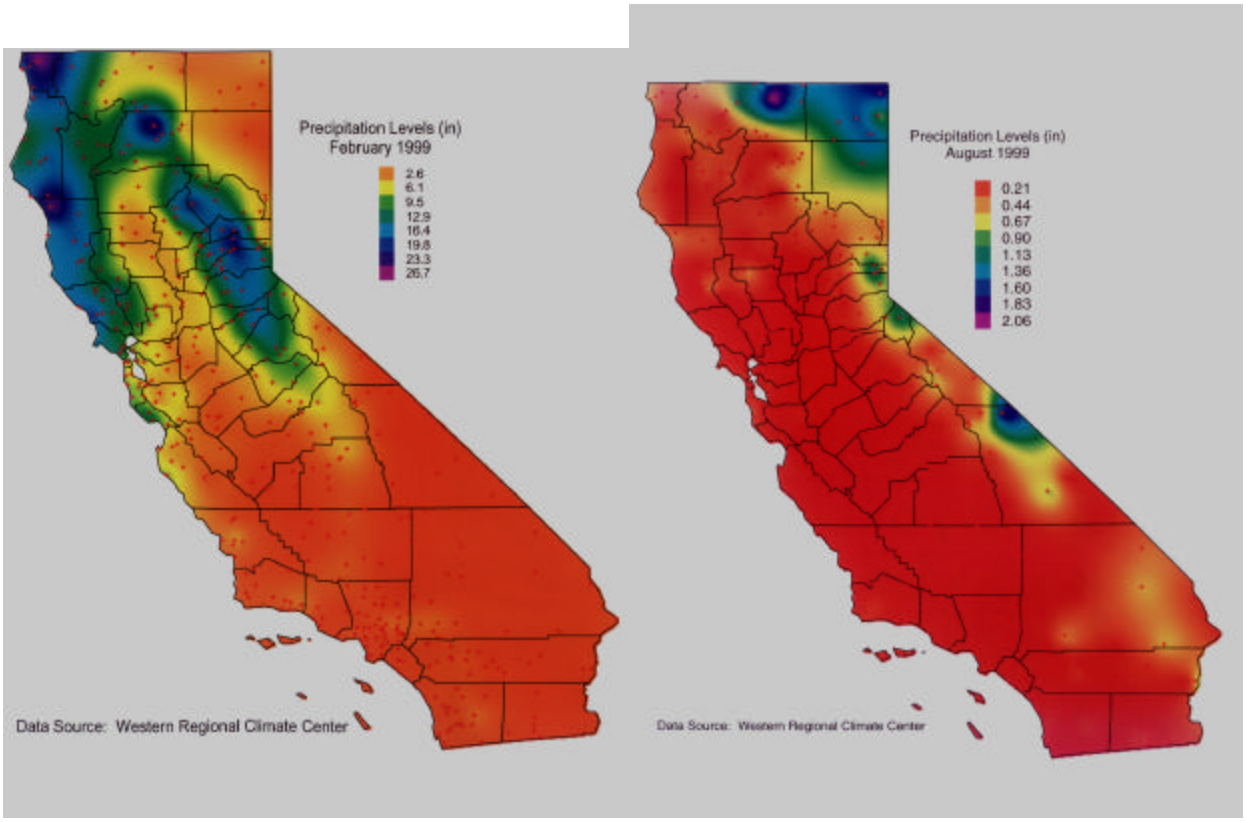


2m. Measured February climatological precipitation (1971-2000) (inches per month)

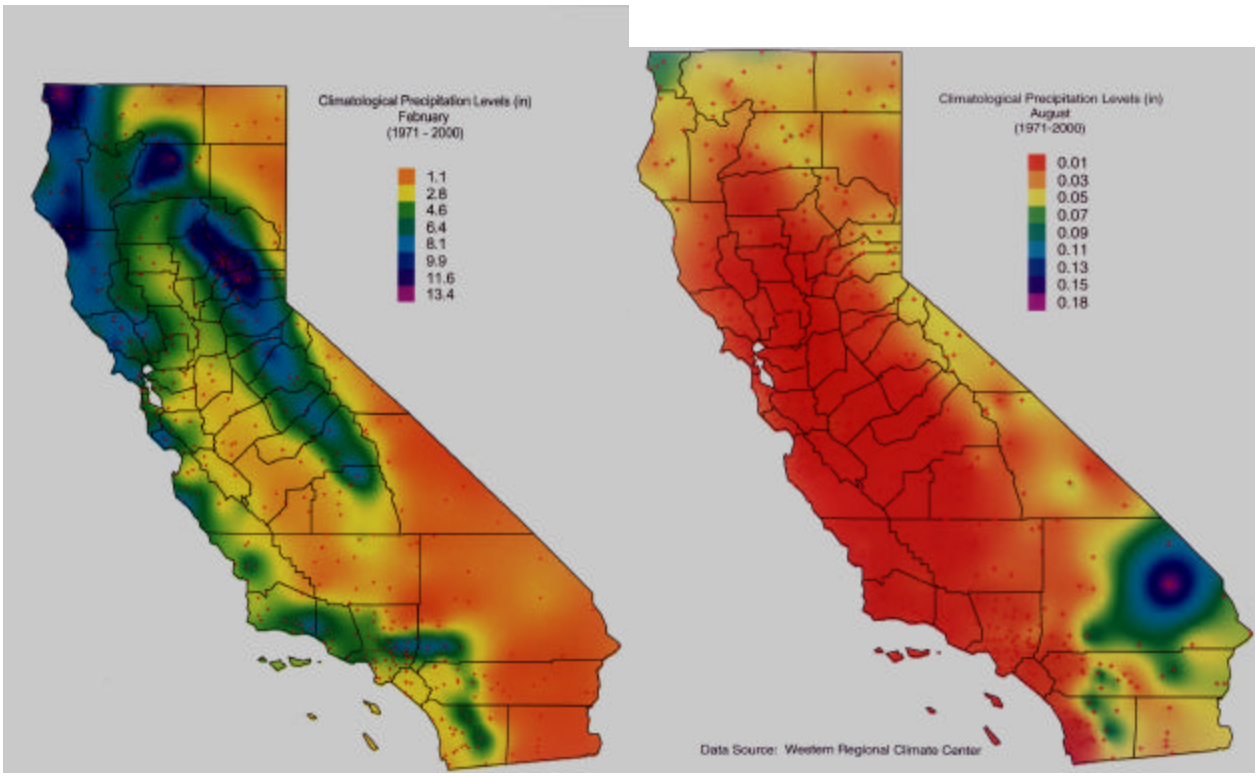

6.C.2. Sensitivity Results, California Grid

Figure 3 shows the monthly averaged and California-grid-averaged differences between the baseline case (with anthropogenic aerosols and their precursor gases) and the sensitivity case (without such aerosols and gases) in the vertical profile of several parameters. Figure 3a shows that anthropogenic aerosols enhanced cloud scattering optical depths at all altitudes in February and August, with the greatest increases in the boundary layer and small increases above it. The optical depths in the figure are layer optical depths (not cumulative between the layer and the top of the atmosphere).

The California-grid-averaged boundary-layer increase in scattering optical depths in both February and August was correlated with California-grid-averaged increases in cloud liquid water content (CLWC) (Figure 3b). Cloud liquid water content increased because of the longer lifetimes of clouds due to an enhanced aerosol loading, which is also one of the reasons for the reduction in precipitation. The increase in CLWC is an expected result of the second indirect effect of aerosol particles (Section 2.B.vi).

Aerosol particles caused a general decrease in lower-tropospheric cloud ice in February and August (Figure 3c), possibly due to slightly warmer lower-tropospheric temperatures in regions of cloud formation and/or due to decreased convection. Figure 3d shows that aerosol particles decreased water vapor in the boundary layer, most likely due to the suppression of surface evaporation due to net surface cooling resulting from aerosols (Figure 3f).

The California-grid-averaged increase in cloud and aerosol optical depths due to aerosols in August decreased the net downward solar irradiance above the boundary layer in August by about 2.5 $W/m^2$ in the day and night average (Figure 3e). Aerosols decreased the August net downward solar irradiance by another 2.5 $W/m^2$ (Figure 3e). Decreases in net downward solar irradiance above the boundary layer were due to increases in reflectivity caused by enhanced aerosol and cloud scattering optical depths. Decreases within the boundary layer were due to such scattering plus aerosol absorption.

Enhanced cloud optical depth together with the presence of anthropogenic aerosol particles increased the net downward thermal-IR irradiance in February and August (Figure 3e). Solar radiation reductions were greater in August than in February, because the absolute quantity of solar radiation was greater in August than in February and aerosols were present during both months. The relatively high thermal-IR increase in February was due to greater enhanced cloud cover in February. Clouds trap the Earth's emitted thermal-IR irradiance, sending some of it back to the surface. The net loss in surface radiation (surface solar irradiance loss minus the thermal-IR gain) was greater in August than in February.

The California-grid-averaged effect of anthropogenic aerosol particles on temperature was to decrease ground temperatures in August and February, decrease near-surface air temperatures in February, cause no net change in near-surface air temperatures in August, cause no net change in middle/upper boundary layer temperatures in February, and increase middle/upper boundary layer temperatures in August (Figure 3f). In all cases, aerosol particles stabilized the boundary layer, which has the effect of increasing pollutant concentrations. Decreases in ground temperatures were due primarily to a net reduction in downward solar plus thermal-IR irradiance in both months. Increases in boundary layer temperatures were due to absorption of solar radiation by absorbing components of aerosol particles (namely black carbon and organics in the UV spectrum). Absorption was greater in August than in February due to the greater solar irradiance, higher BC concentrations, and lower cloud cover in August.

**Figure 3.** Model monthly grid-averaged and California-grid-averaged differences in the vertical profiles of several parameters for February and August. The bottom value for temperatures is ground temperature.

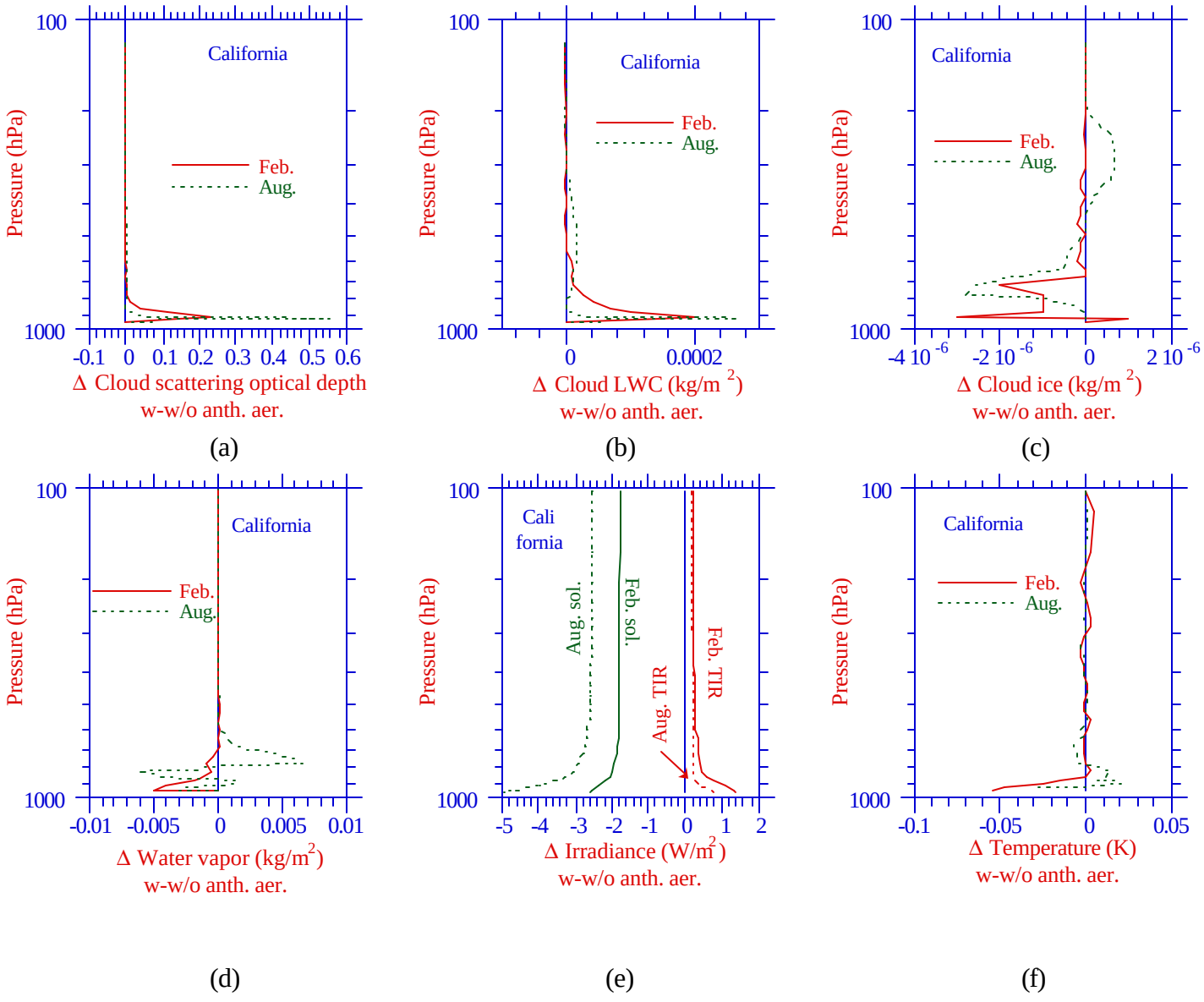

Figure 4, which shows spatial difference plots, provides further insight into some potential effects of anthropogenic aerosol particles and their precursor gases on short-term climate. Figures 4a–h show differences in the column abundances of several aerosol constituents and of total aerosol.

Figure 4i shows that AAPPGs had a greater effect on aerosol optical depth in February than in August. This was explained previously as being due to the higher relative humidity in February, which increased the aerosol liquid water content to a greater extent in February than in August (Figure 4g). AAPPGs increased cloud optical depth to a greater extent in February than August (Figure 4j), because clouds were more prevalent in February, so perturbations to the number concentration of aerosol particles had a greater chance of affecting the number and size of cloud drops. Figures 4i and 4j show an increase in aerosol and cloud optical depth, respectively, over the ocean in August. The aerosol optical depth increase appears to be due to the flow of some aerosols and their gas-phase precursors from polluted coastal regions to offshore.

Figure 4k shows that net down minus up surface solar irradiance decreased in locations of enhanced aerosol and cloud optical depth, including in the Central Valley, South Coast Air Basin, and some areas offshore. Slight increases in net solar irradiance occurred in some locations where cloud optical depth may have decreased during the day (but increased during the night, resulting in a net increase in optical depth).

Figure 4l shows that AAPPGs increased net down minus up surface thermal-IR irradiance. Irradiances increased primarily in locations where cloud and aerosol optical depths increased. Clouds and aerosols enhance net downward thermal-IR irradiance by trapping the Earth's emitted thermal-IR irradiance and sending some of it back toward the ground.

Figure 4m shows that AAPPGs decreased near-surface air temperatures in the Central Valley in February and August but tended to increase them slightly or cause little change in mountainous and ocean regions outside of the valley. Part of these increased temperatures was due to the advection of air warmed by aerosol particle absorption from the Central Valley and other locations of absorption, to areas around the Valley. Although absorbing aerosol particles are removed by precipitation, the thermal-IR radiation that such particles emit is absorbed by GHGs that have moderate or long lifetimes and are advected to areas where the particles are not substantially present. Figure 4n illustrates this point to some degree. It shows a latitude-altitude plot of the zonally averaged temperature differences with minus without AAPPGs. Although AAPPGs decreased or caused little change in near-surface air temperatures in February and August, averaged over the California domain, they increased temperatures above the surface. These increases were due primarily to aerosol particle absorption. The enhanced energy aloft, produced primarily over the Central Valley, was advected horizontally to regions beyond the Central Valley, where it was mixed vertically, enhancing near surface temperatures in such regions, as indicated by Figure 4m.

Another factor affecting temperatures was the feedback of aerosols to large-scale meteorology. Lower temperatures over the Central Valley caused a slight increase in air pressure there (Figure 4o). The increase caused a slight shift in winds (Figure 4o), which caused a shift in pressures in regions away from the valley. Increases in pressure generally increase compressional warming of descending air; decreases in pressure generally decrease compressional warming. Figure 4p shows that zonally averaged pressures generally increased slightly due to aerosol particles, suggesting that some of the enhanced near-surface warming, particularly in February, may have been due to compressional warming. Shifts in winds affect temperatures, because winds advect

energy into or away from a region. Figure 4q shows that aerosol particles may have slowed westerly winds slightly, in the zonal average, reducing the transport of cool, moist marine air to land.

Figure 4r shows that AAPPGs increased the near-surface relative humidity in the Central Valley but decreased it in many other locations. Figure 4s shows that, in the zonal average, a net decrease occurred near the surface, but an increase occurred aloft. The relative humidity is affected by the water vapor content of the air and temperature. Figure 4t shows that AAPPGs decreased the water vapor content of the air slightly, most likely by stabilizing the air, reducing the vertical turbulent flux of moisture from ground water and the oceans. The reduction in water vapor, combined with slight increases in near-surface temperature, was probably the major reason for the net decrease in the relative humidity near the surface outside of the Central Valley. Over the Central Valley, the decrease in near-surface temperature (Figure 4m) was probably the most important cause of the net increase in the near-surface relative humidity there.

Figure 4u shows that AAPPGs decreased precipitation in the Sierra Nevada mountains in February and August and slightly increased it beyond the mountains. Both results are generally consistent with those of *Givati and Rosenfeld* (2004), who found that air pollution particles may suppress precipitation over the upslope side of mountains and enhance it over the downslope side. Modeled decreases in precipitation also occurred in the Central Valley, on average, although some locations experienced increases. AAPPGs reduced precipitation, averaged over all land locations, during both February and August. The reduction in precipitation contributed to a general increase in cloud liquid water (Figure 4v) but a more ambiguous change in cloud fraction (Figure 4w).

6.C.3. Baseline and Sensitivity Results, South Coast Air Basin (SCAB) Grid

Figure 5 shows baseline model results for several parameters during February and August 1999 for the SCAB. Figure 6 and 7 show the difference between the baseline simulations and simulations in which all anthropogenic aerosol components and their gas-phase precursors were removed in the SCAB grid. Boundary conditions for the baseline and sensitivity simulations were fed in from the California grid, whose emissions and meteorology were from the baseline California simulation for both the SCAB baseline and SCAB sensitivity cases to ensure that perturbations in the South Coast grid were not due to meteorological perturbations from the California grid, which was more coarsely resolved than the SCAB grid. Results for the SCAB grid were obtained with convective cloud processes treated in that grid.

Figures 5a and 5b show baseline monthly averaged, near-surface concentrations of BC and nitrate, respectively. Black carbon has emission sources only; whereas, nitrate has emission and gas-to-particle conversion sources. As such, nitrate was spread over a greater area than was BC in the monthly average. Figure 5c shows that the areas of high baseline aerosol optical depth roughly followed the areas of high BC and nitrate loadings.

Figure 5d shows that the baseline cloud fraction was much greater in February than in August. Cloud liquid water content was similarly greater in February than in August (Figure 5e). Cloud optical depth (Figure 5f) was generally highest over the ocean and mountains in February and over the ocean in August. Cloud optical depths were greater in February than in August. Precipitation occurred primarily in mountainous regions. Precipitation was much greater in areal extent and magnitude in February than in August. Precipitation was most likely higher in the SCAB grid than it should have been in August for several reasons. First, the calculation of cloud thermodynamics was with a cumulus parameterization that is not strictly valid for scales in which clouds are on the order of the

**Figure 4.** Modeled differences between the baseline case (1999) and the sensitivity case (no anthropogenic aerosol or aerosol-precursor-gas emissions), for the California grid, averaged over February (left column) and August (right column).

4a. BC column difference

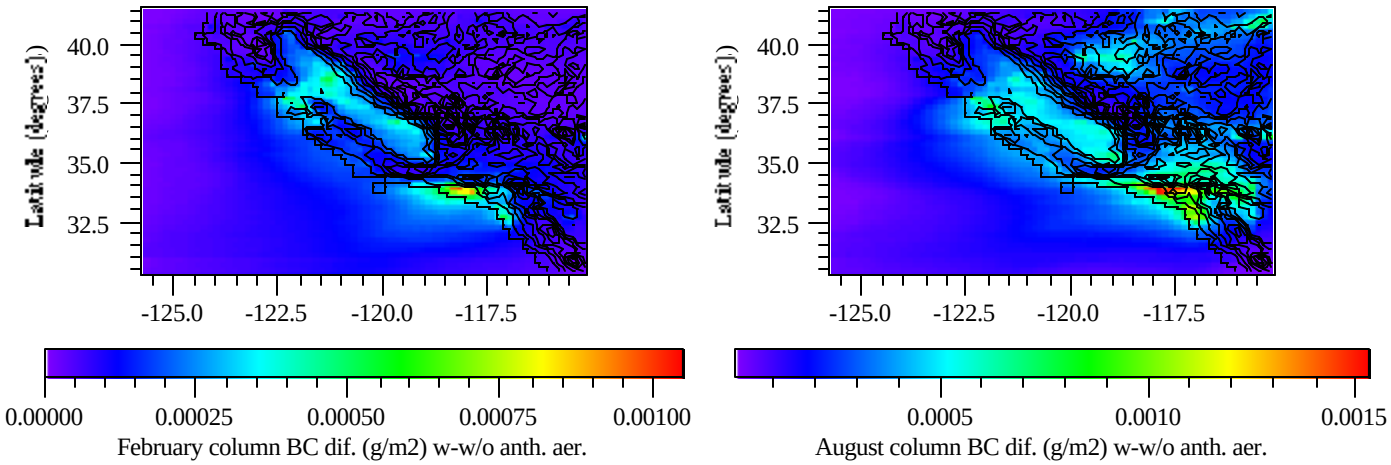


4b. POM difference

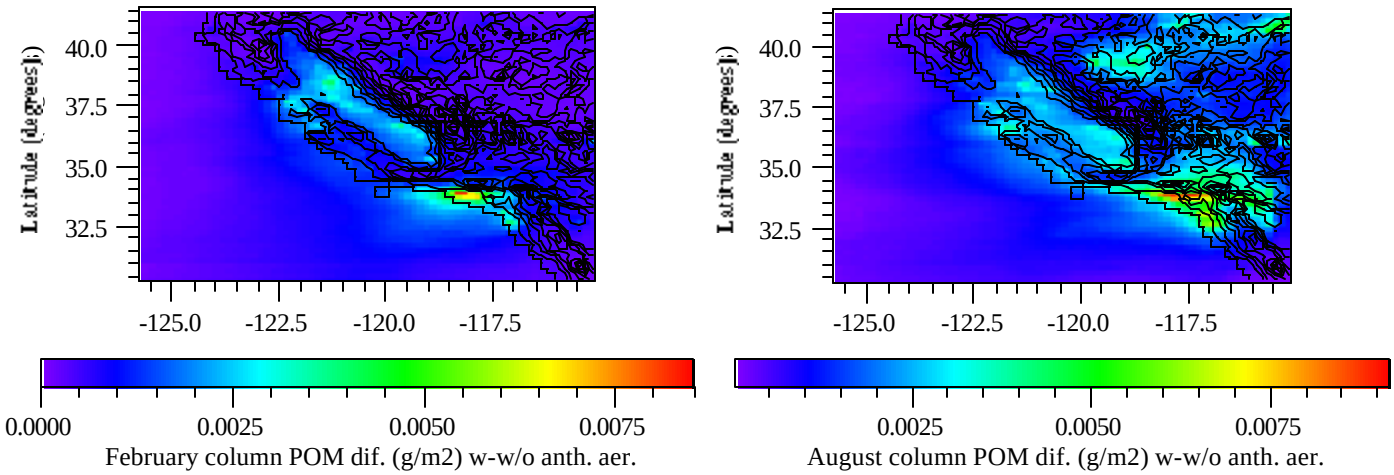


4c. Column SOM difference

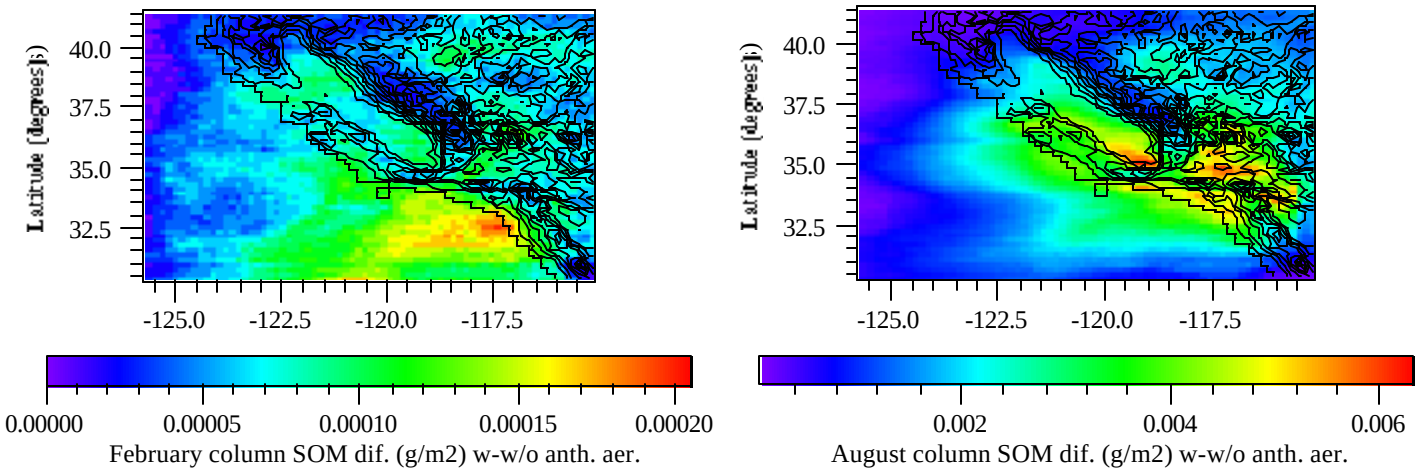

4d. Column S(VI) difference

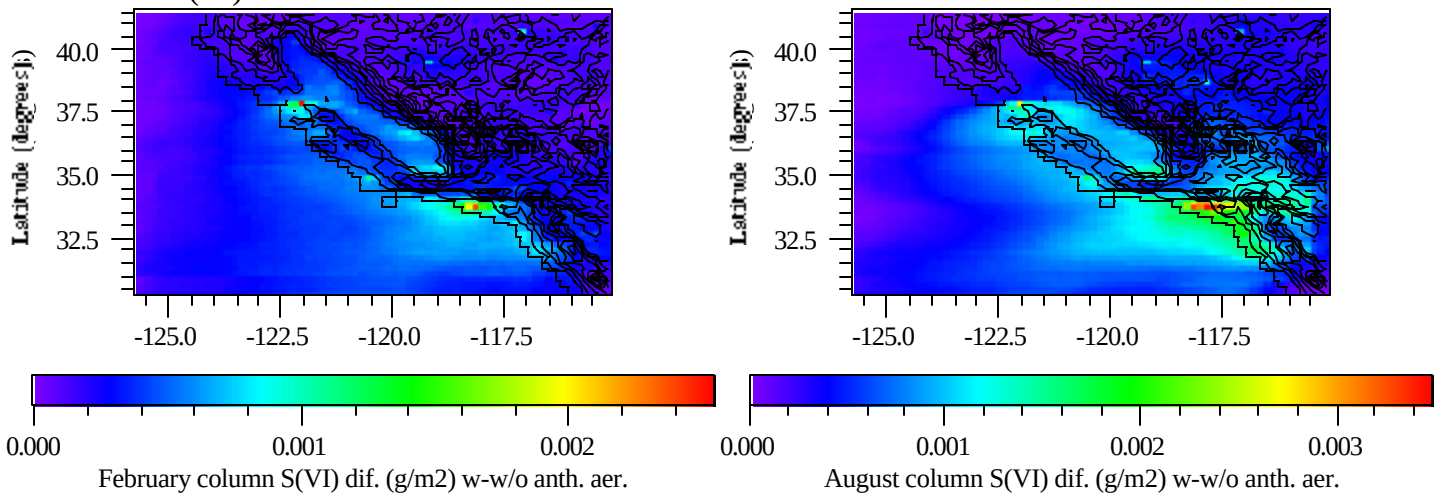


February column S(VI) dif. (g/m2) w-w/o anth. aer.

August column S(VI) dif. (g/m2) w-w/o anth. aer.

4e. Column $NO_3^-$ difference

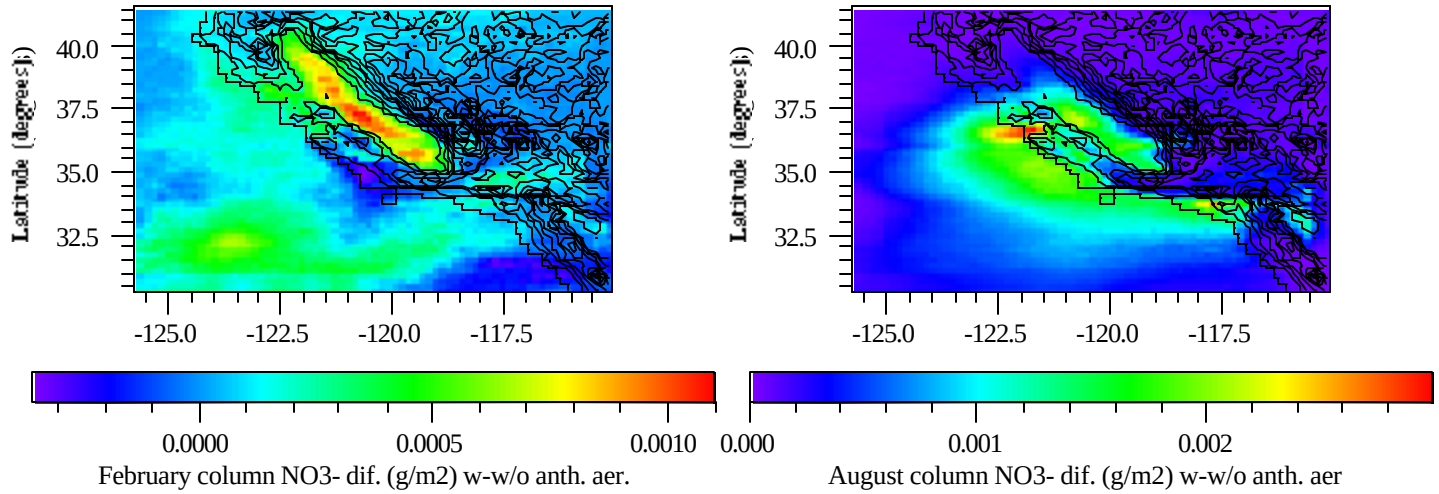


February column NO3- dif. (g/m2) w-w/o anth. aer.

August column NO3- dif. (g/m2) w-w/o anth. aer

4f. Column $NH_4^+$ difference

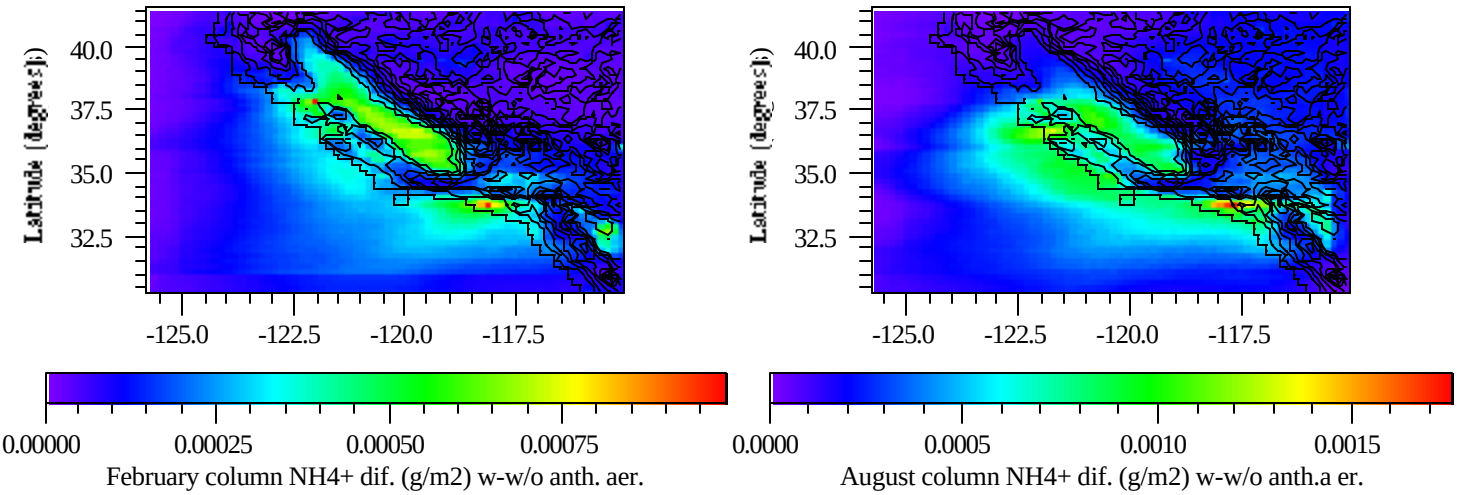


February column NH4+ dif. (g/m2) w-w/o anth. aer.

August column NH4+ dif. (g/m2) w-w/o anth.a er.

4g. Column LWC difference

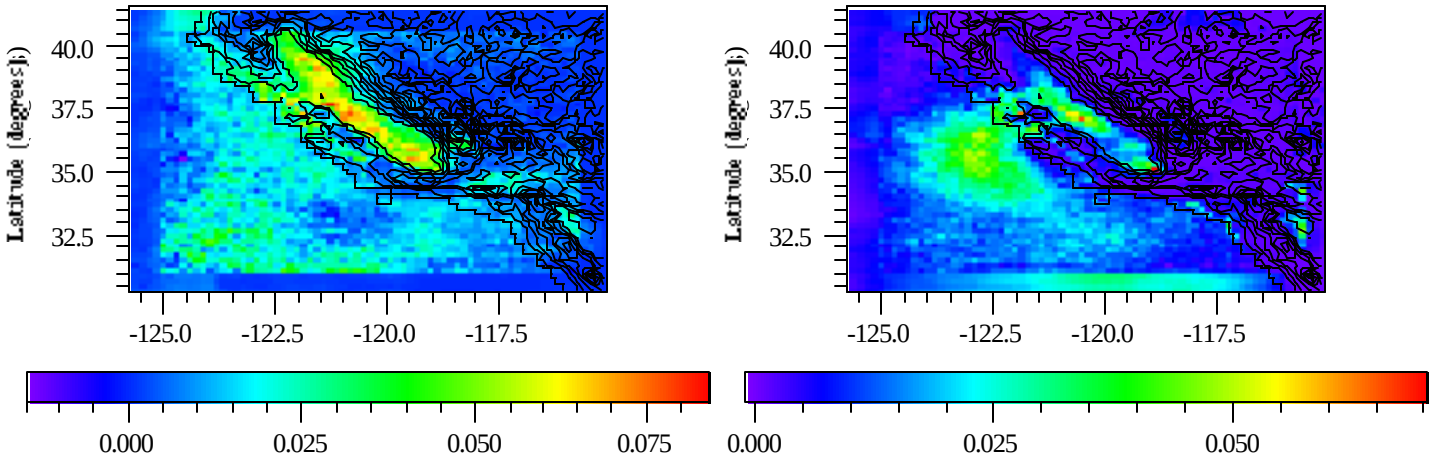


February column aerosol LWC dif. (g/m2) w-w/o anth. aer.

August column aerosol LWC dif. (g/m2) w-w/o anth. aer.

4h. Column total aerosol difference

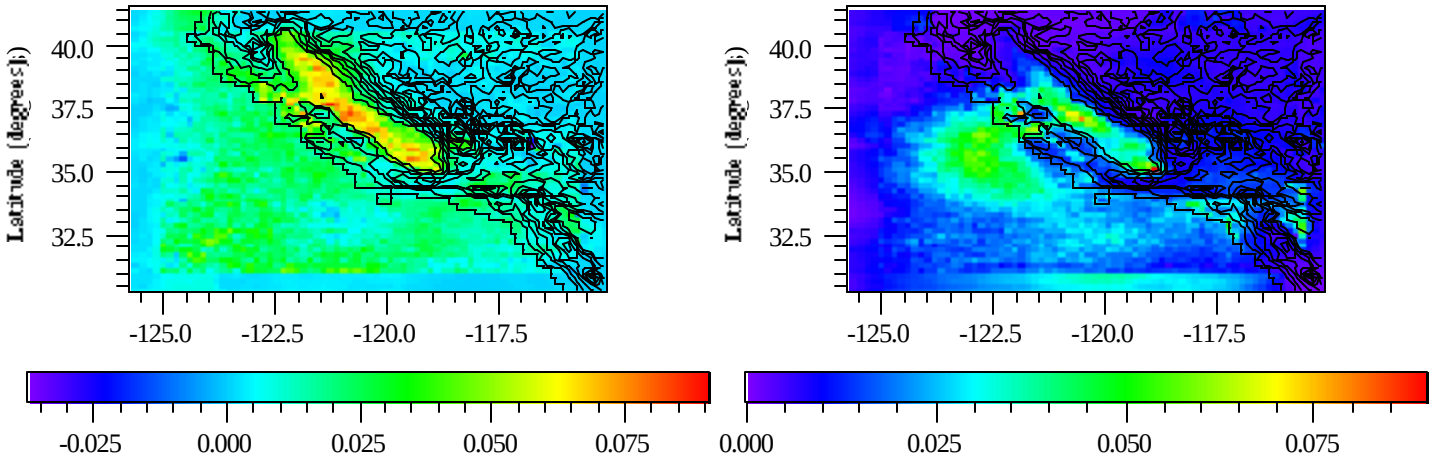


February column total aerosol dif. (g/m2) w-w/o anth. aer.

August column total aerosol dif. (g/m2) w-w/o anth. aer.

4i. Aerosol 550 nm optical depth difference

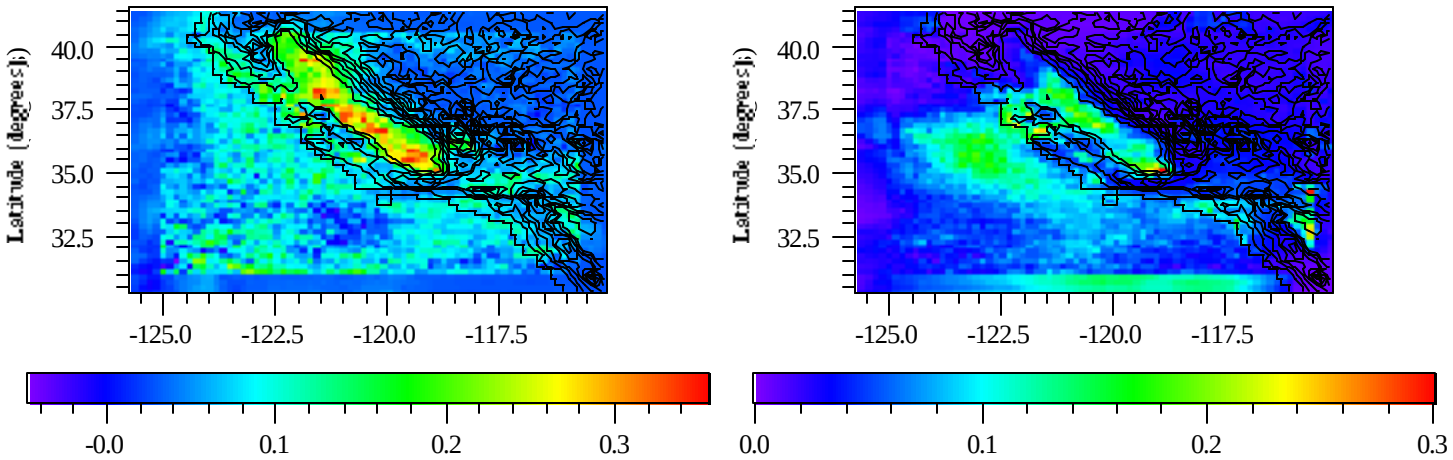


February aerosol 550 nm optical depth dif. w-w/o anth. aer.

August aerosol 550 nm optical depth dif. w-w/o anth. aer.

4j. Cloud total optical depth difference

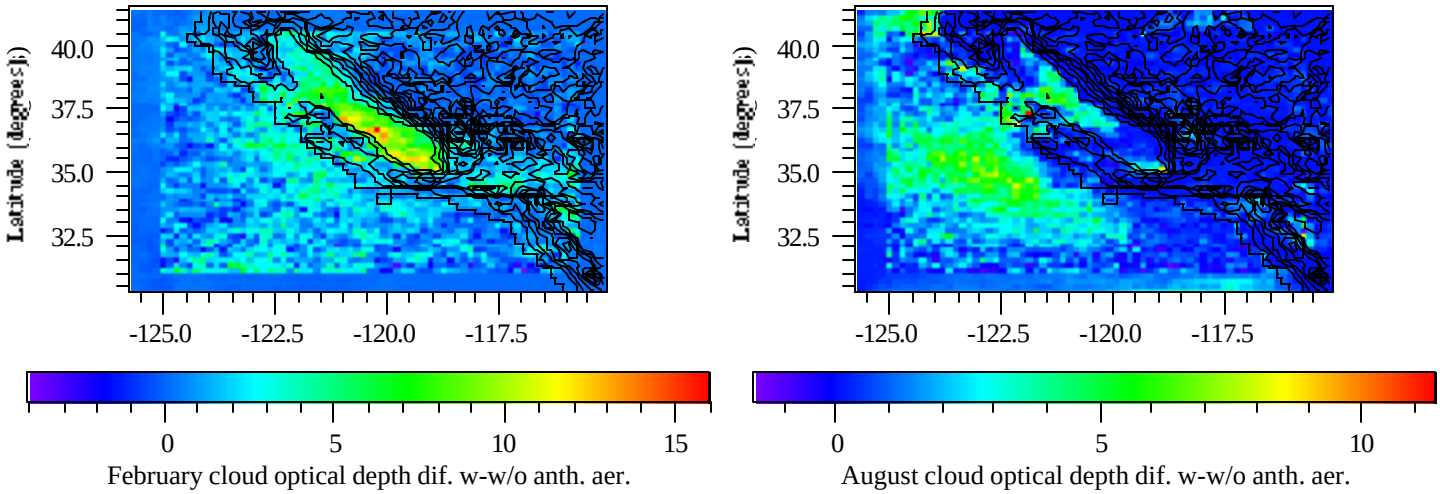


February cloud optical depth dif. w-w/o anth. aer.

August cloud optical depth dif. w-w/o anth. aer.

4k. Down-up surface solar irradiance difference

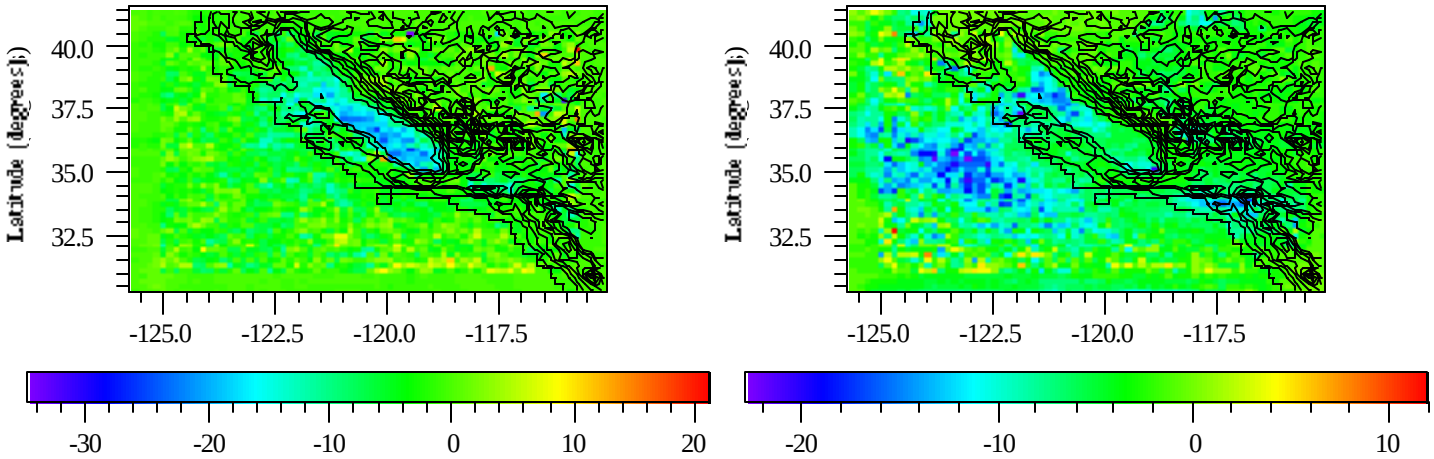


February down-up surface solar dif. (W/m2) w-w/o anth. aer.

August down-up surface solar dif. (W/m2) w-w/o anth. aer.

4l. Down-up surface thermal-IR irradiance difference

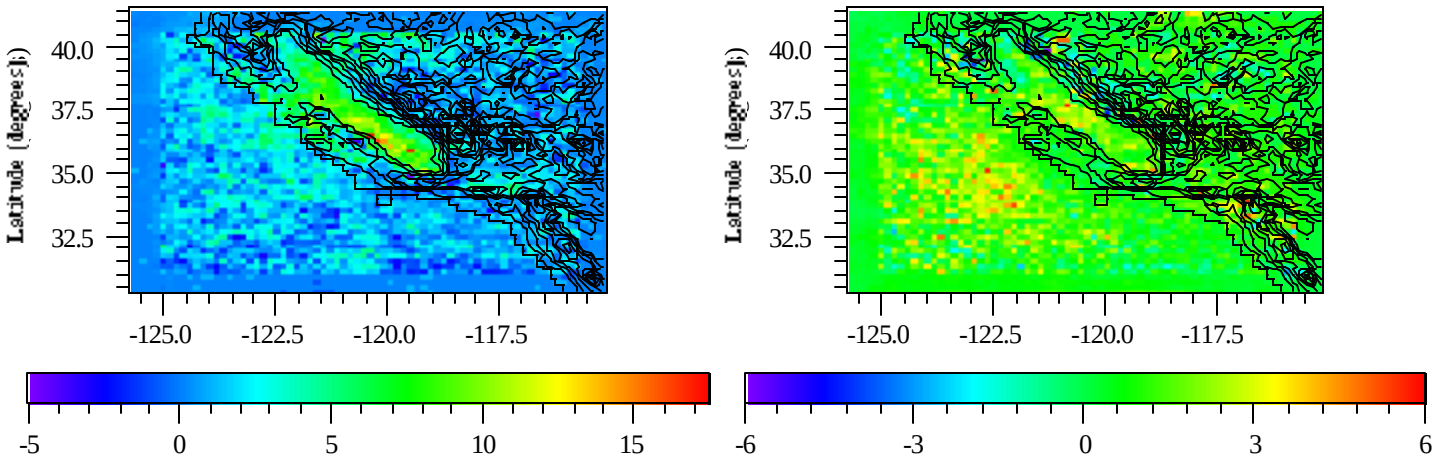


February down-up thermal-IR dif. (W/m2) w-w/o anth. aer.

August down-up surface thermal-IR dif. (W/m2) w-w/o anth. aer.

4m. Near-surface air temperature difference

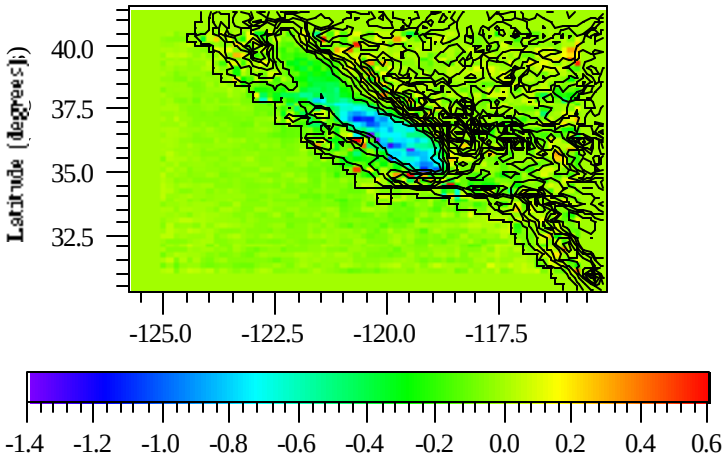


February near-surface temperature dif. (K) w-w/o anth. aer.

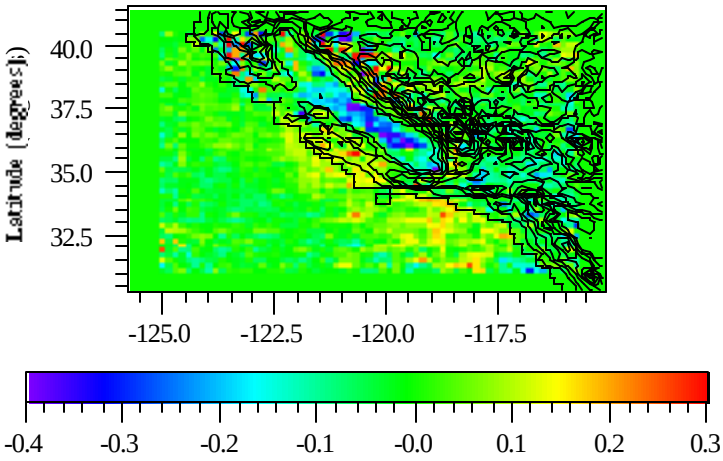


August near-surface temperature dif. (K) w-w/o anth. aer.

4n. Zonal temperature difference

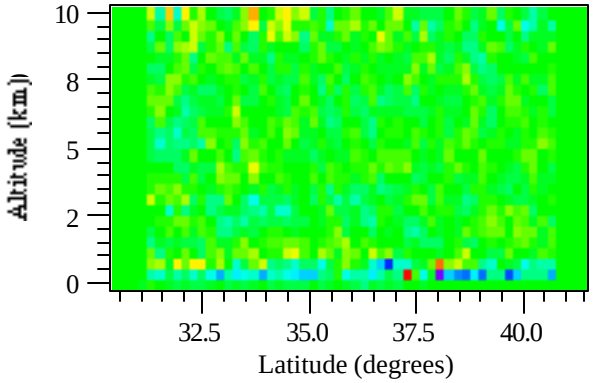


February zonal temperature dif. (K) w-w/o anth. aer.

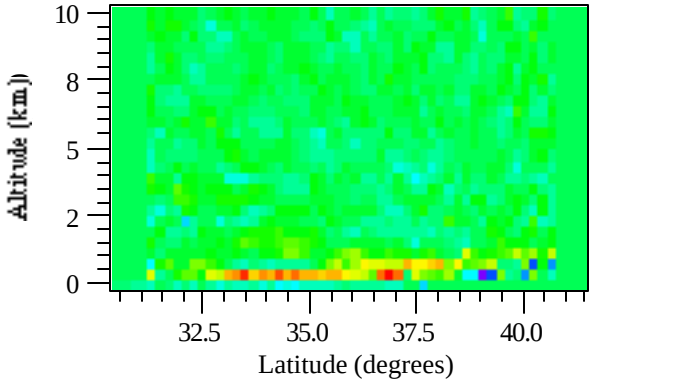


August zonal temperature dif. (K) w-w/o anth. aer.

4o. Pressure and near-surface wind difference

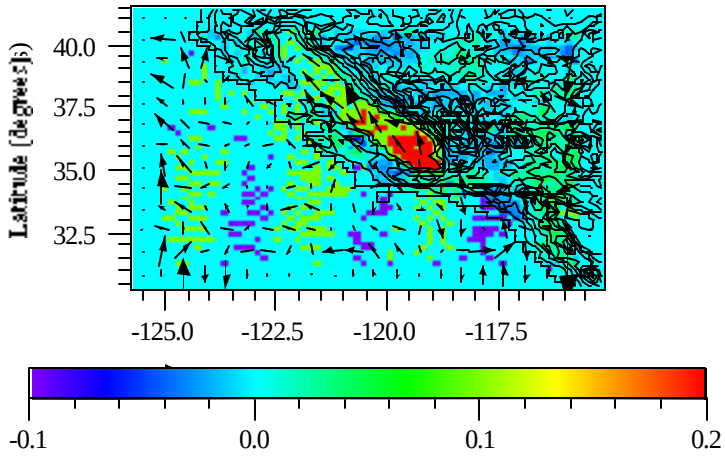


February pres. (hPa) and near-surface wind (m/s) dif. w-w/o anth. aer.

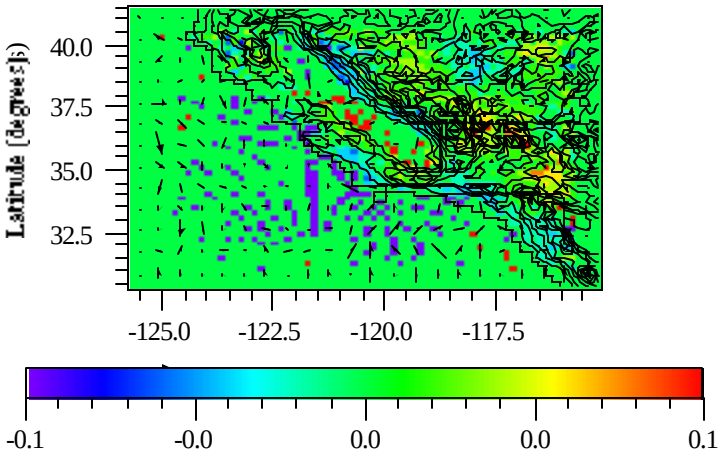


August pres. (hPa) and near-surface wind (m/s) dif. w-w/o anth. aer.

4p. Zonal pressure difference

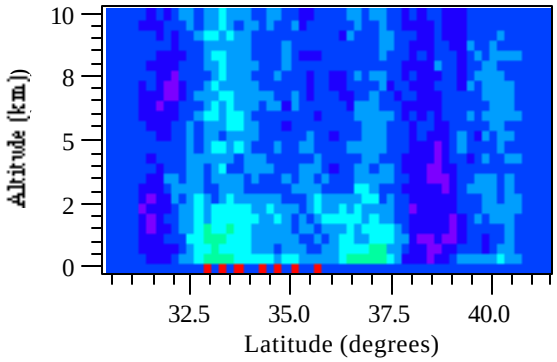


February zonal pressure dif. (hPa) w-w/o anth. aer.

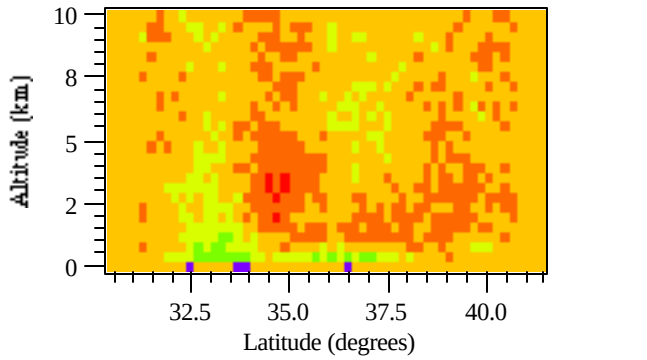


August zonal pressure dif. (hPa) w-w/o anth. aer.

4q. Zonal U-wind difference

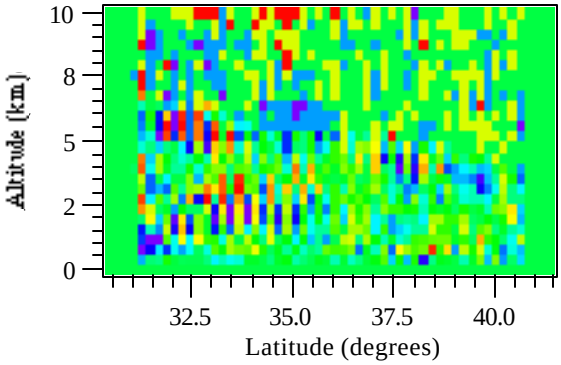


February zonal wind dif. (m/s) w-w/o anth. aer.

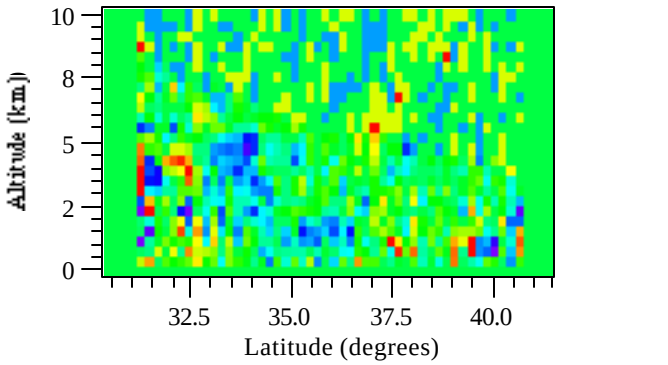


August zonal u-wind dif. (m/s) w-w/o anth. aer.

4r. Near-surface relative humidity difference

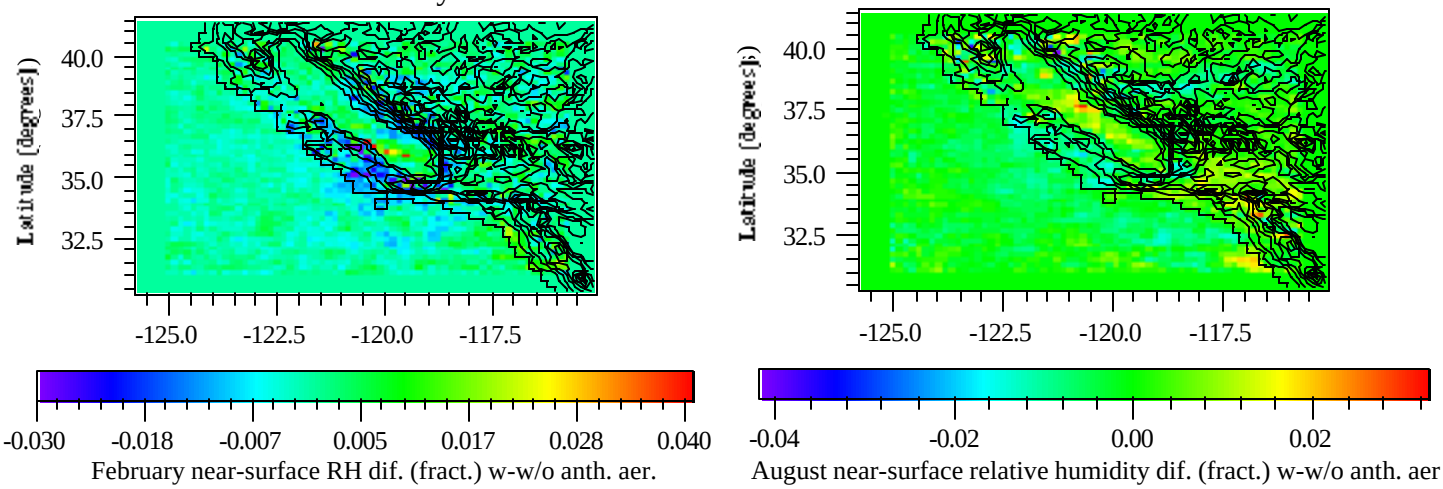


February near-surface RH dif. (fract.) w-w/o anth. aer.

August near-surface relative humidity dif. (fract.) w-w/o anth. aer

4s. Zonal relative humidity difference

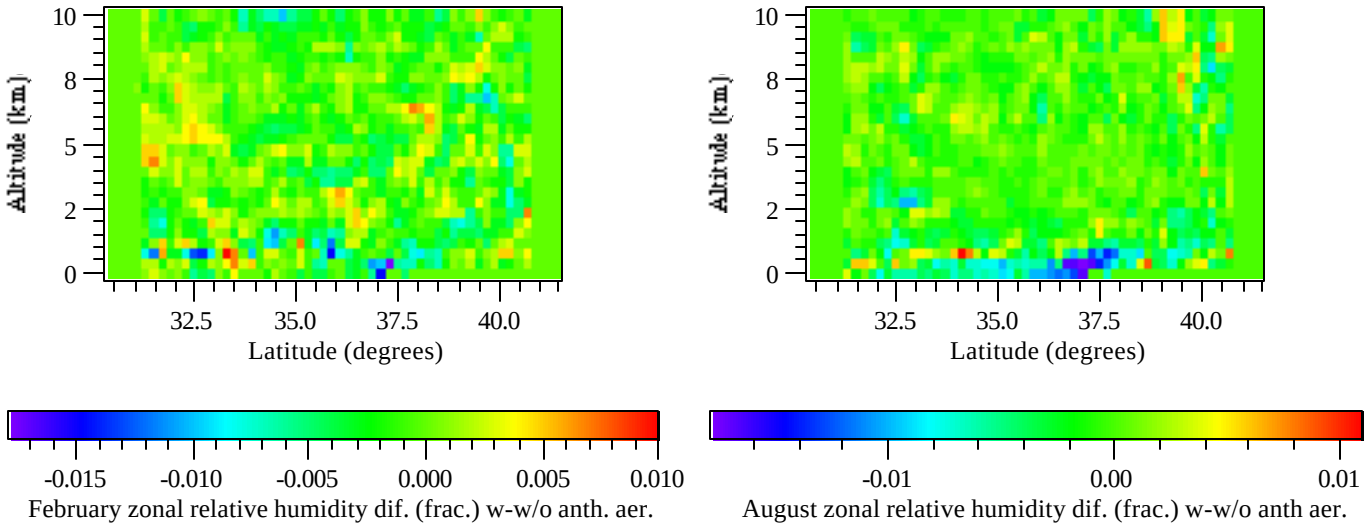


February zonal relative humidity dif. (frac.) w-w/o anth. aer.

August zonal relative humidity dif. (frac.) w-w/o anth aer.

4t. Zonal water vapor difference

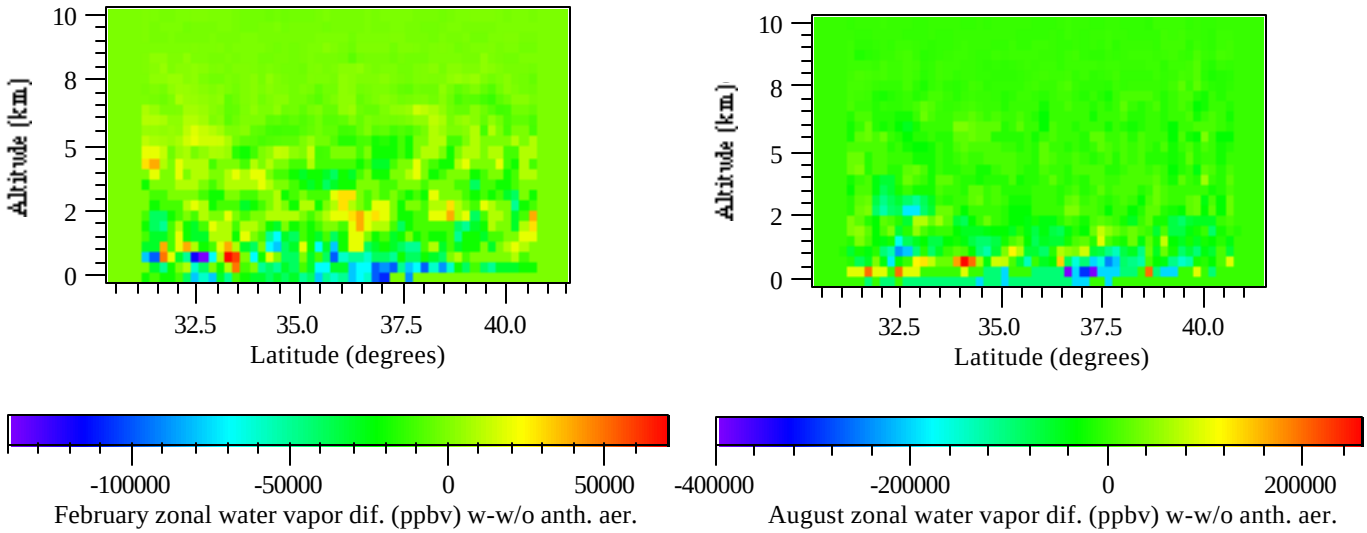


February zonal water vapor dif. (ppbv) w-w/o anth. aer.

August zonal water vapor dif. (ppbv) w-w/o anth. aer.

4u. Precipitation difference

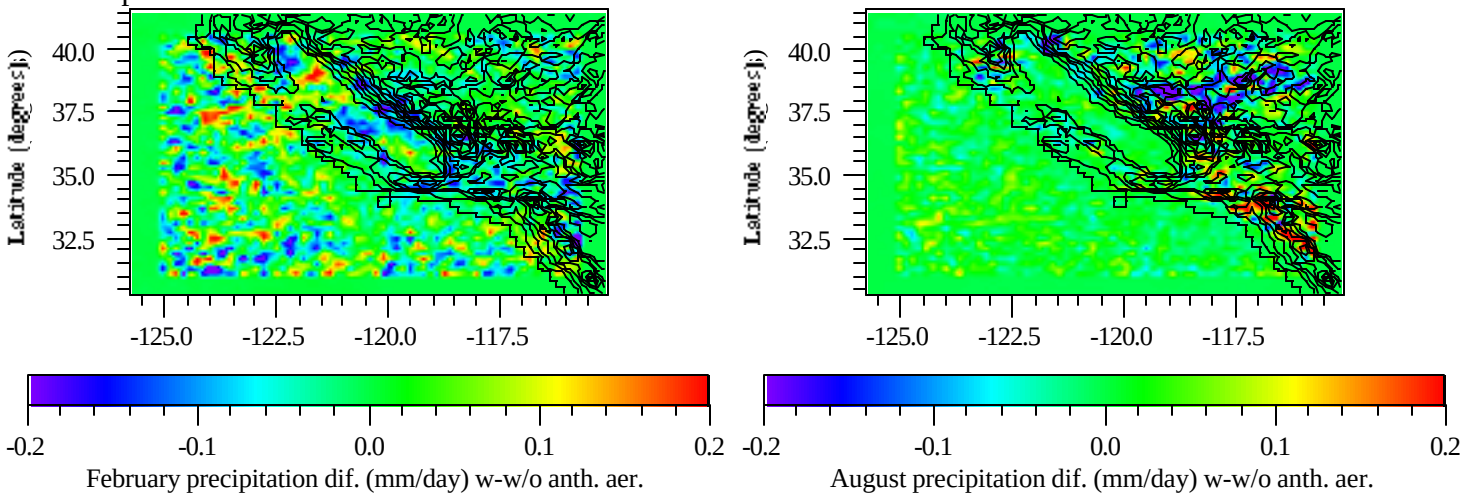


(Same as above, but without topography)

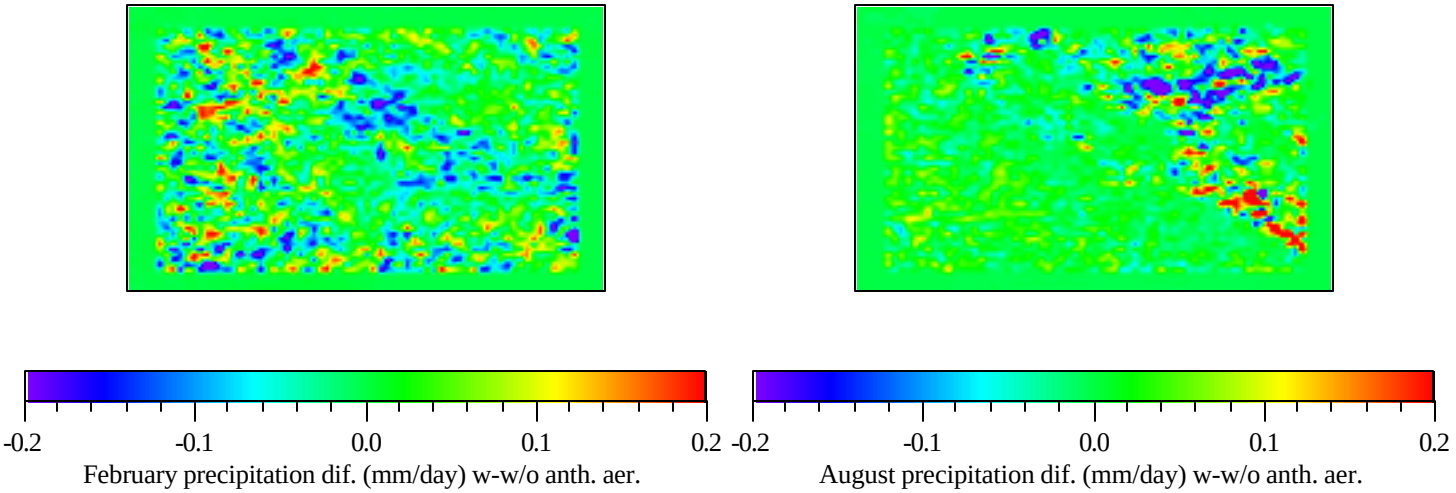


4v. Column cloud liquid water content difference

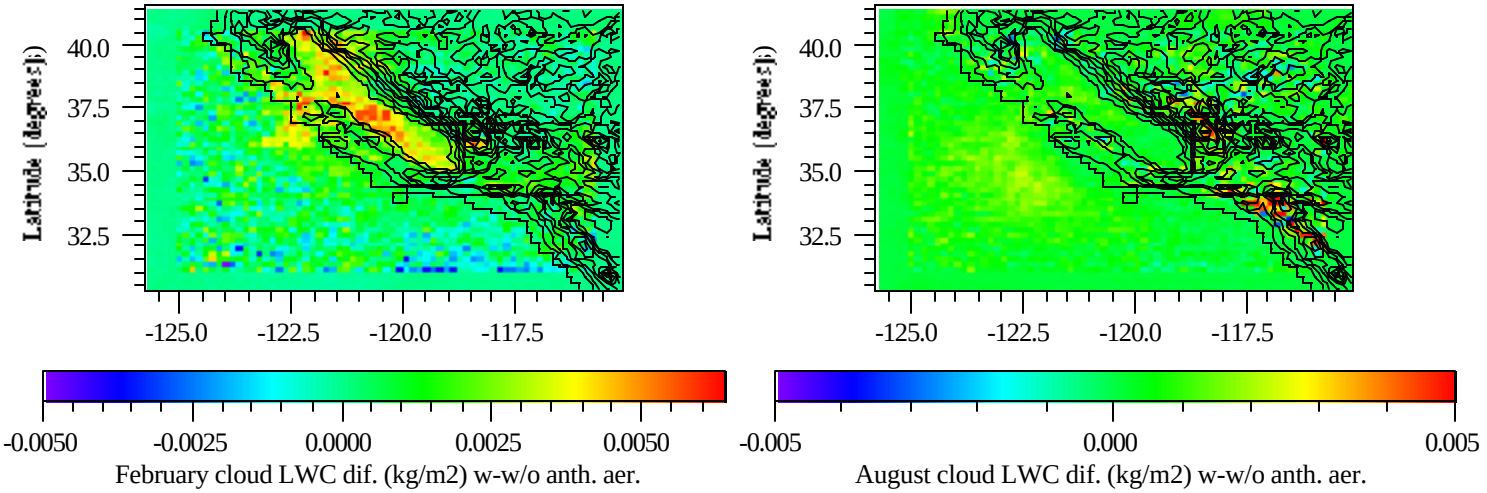

4w. Cloud fraction difference

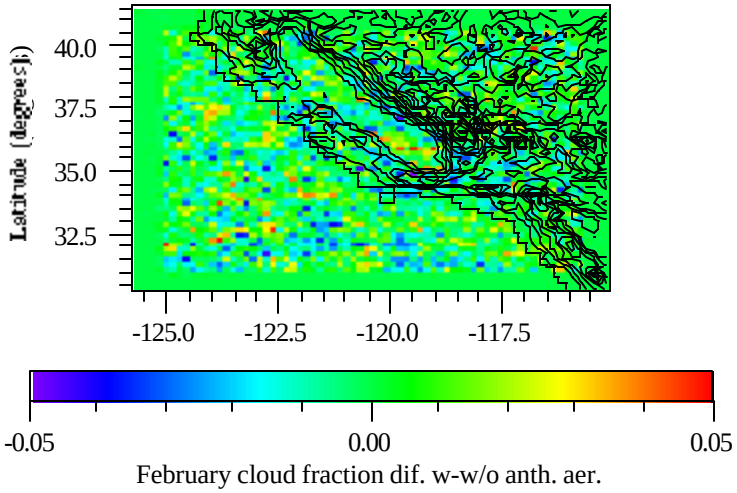


February cloud fraction dif. w-w/o anth. aer.

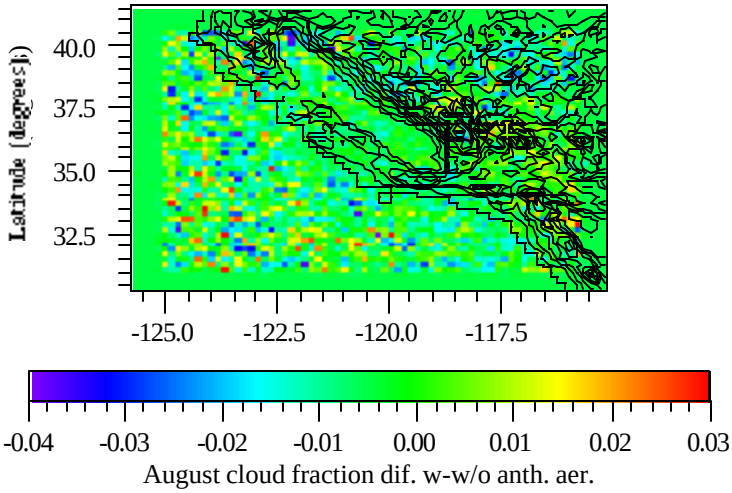


August cloud fraction dif. w-w/o anth. aer.

**Figure 5.** Model baseline predictions on the South Coast grid for February (left) column and August (right column), averaged over the respective months, of several variables.

5a. Baseline near-surface BC

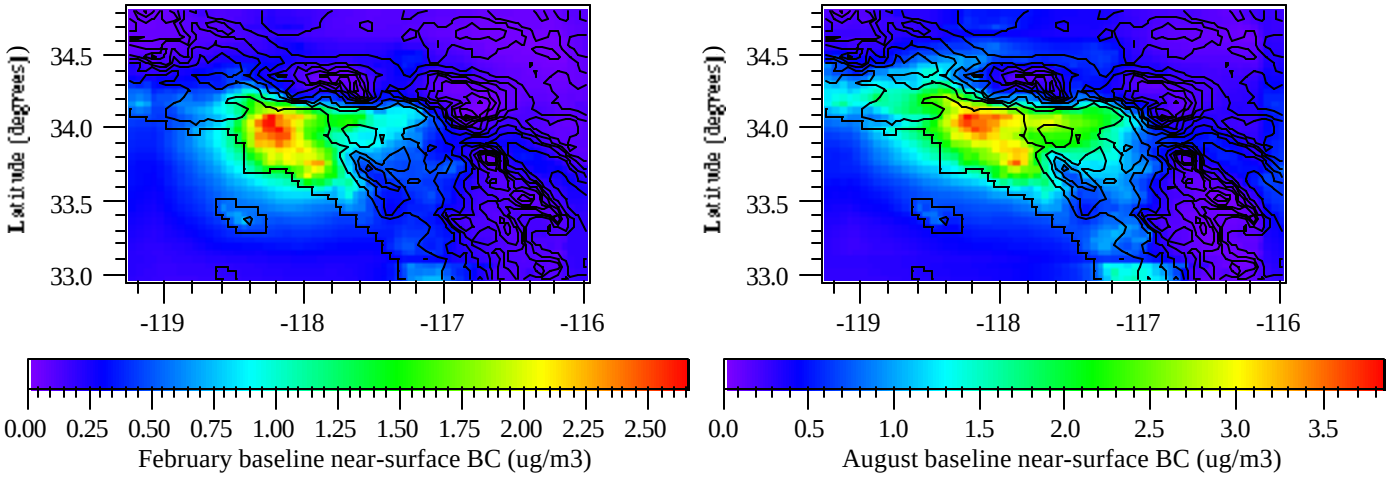


5b. Baseline near-surface nitrate

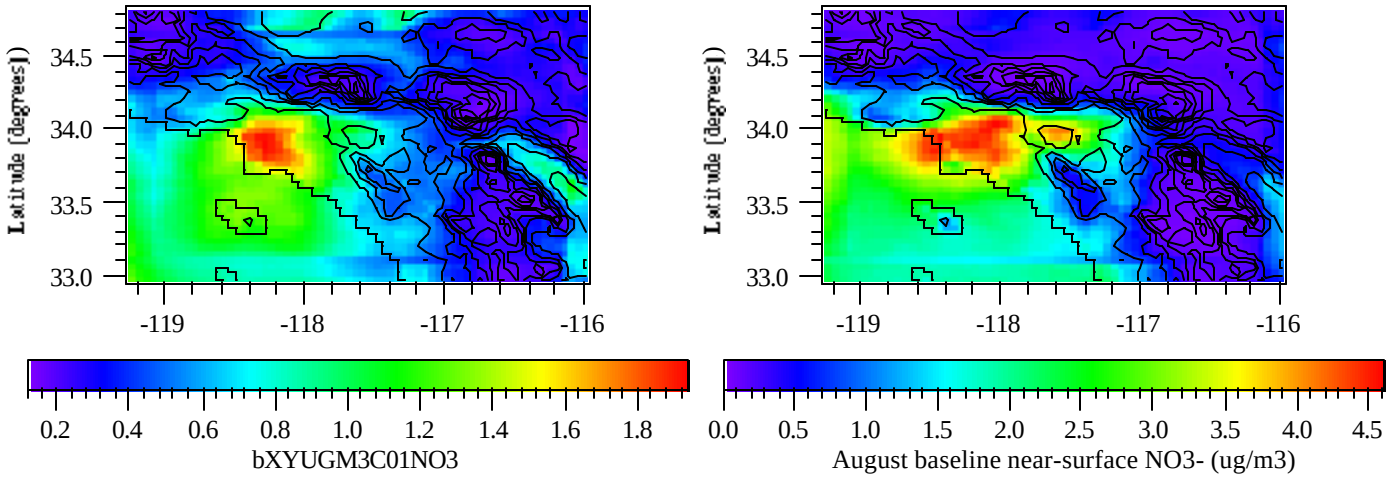


5c. Baseline aerosol optical depth

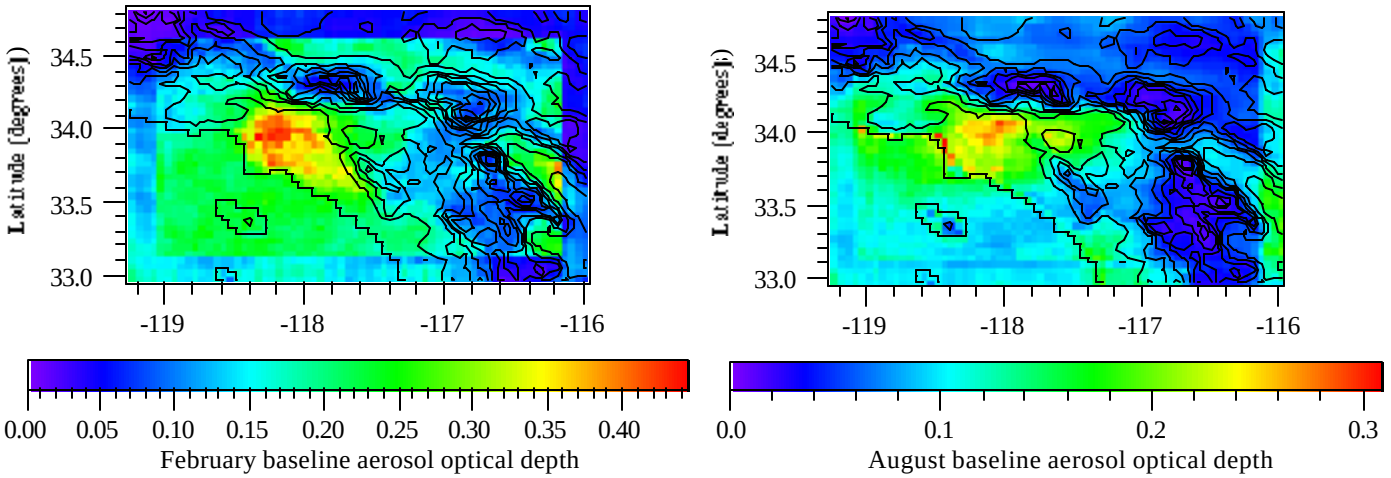

5d. Baseline cloud fraction

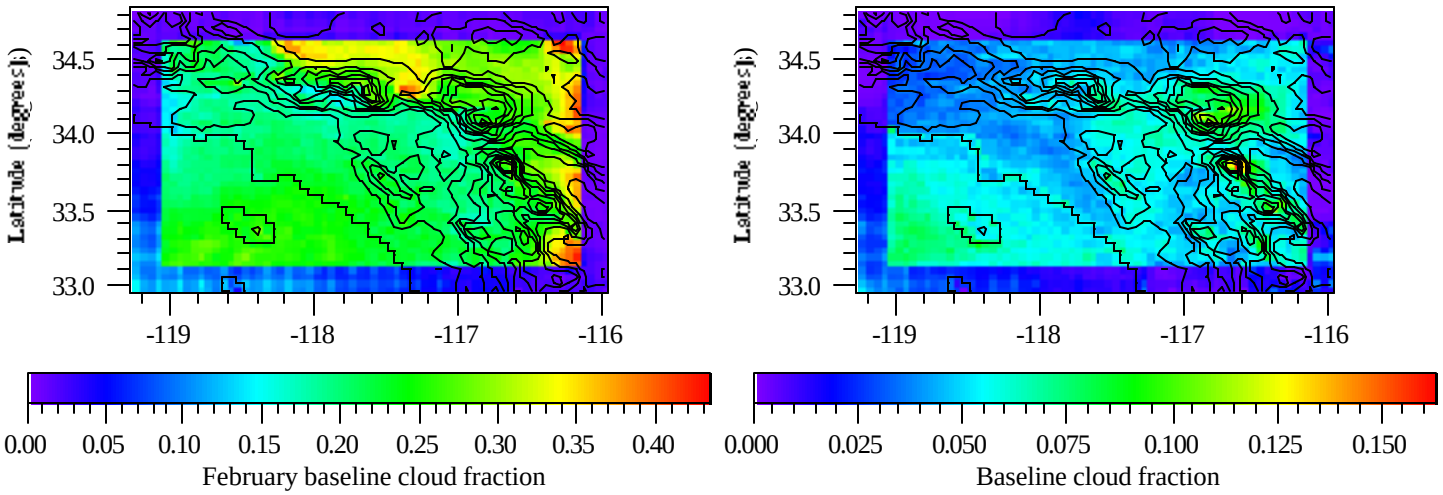


5e. Baseline cloud liquid water content

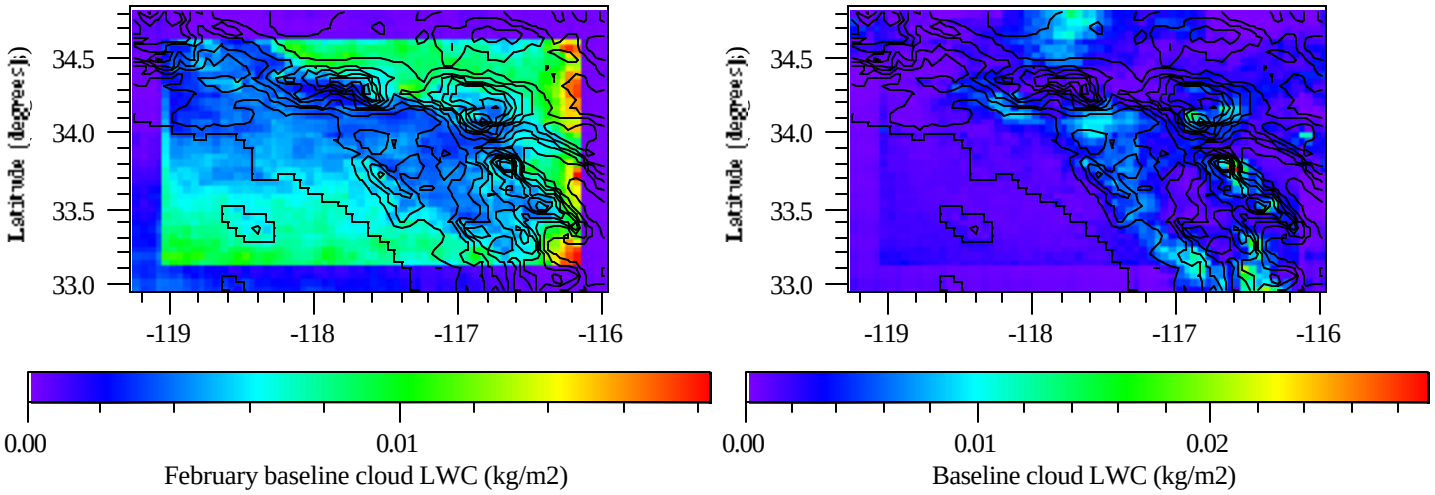


5f. Baseline cloud optical depth

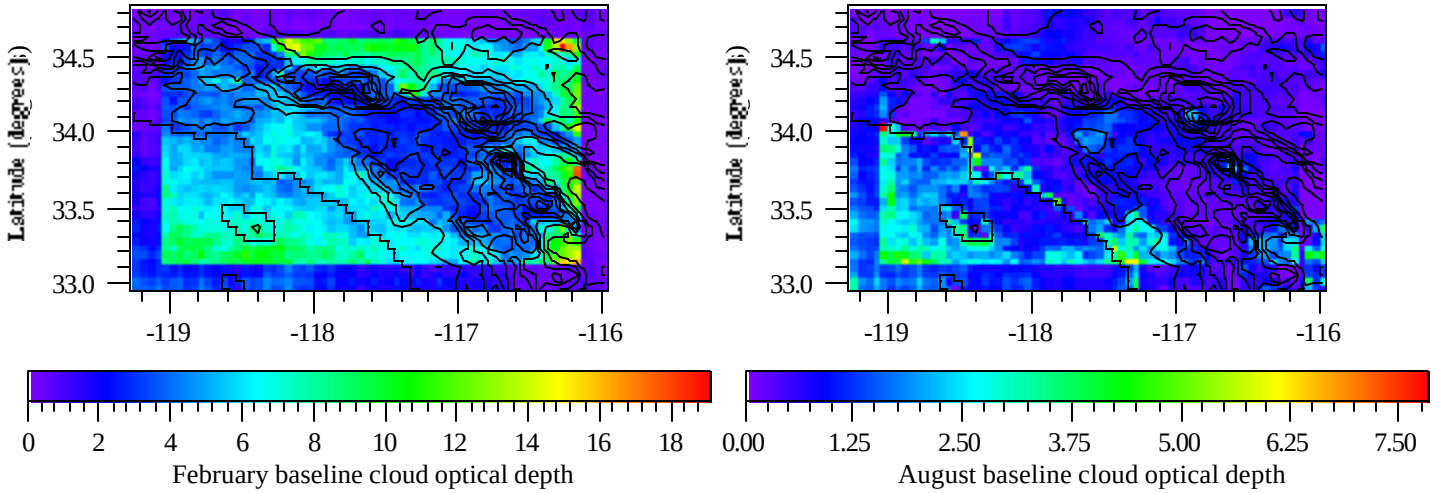

5g. Baseline precipitation

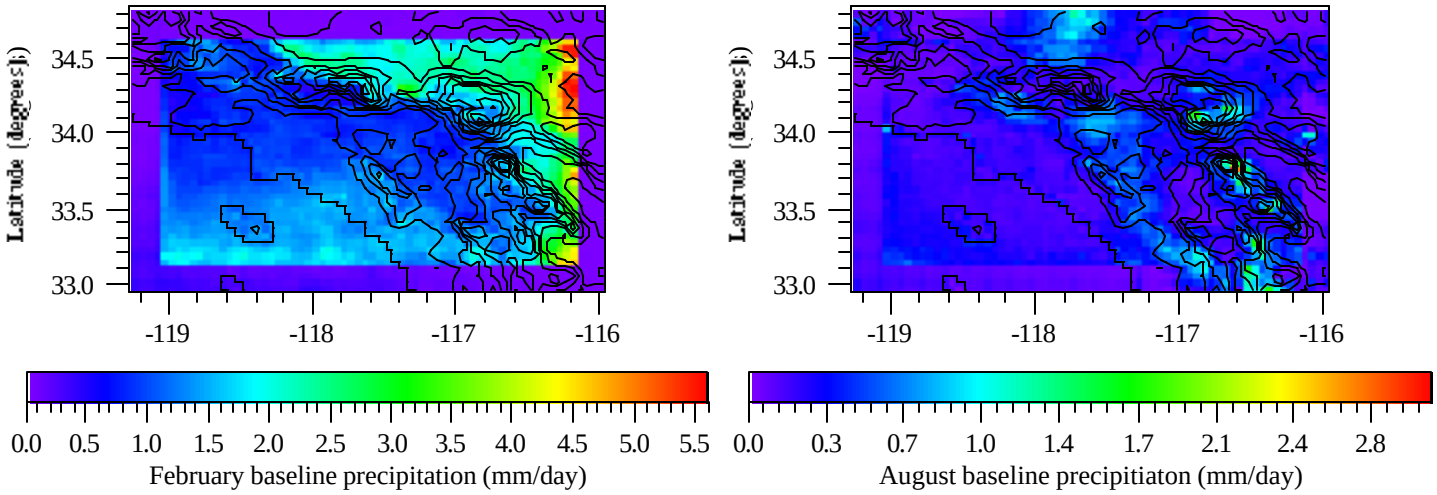

size of the grid cell. The cumulus parameterization is valid for the California grid, because clouds on that scale are smaller than the grid cell size. Second, the calculation of precipitation depends on the inflow of water vapor from the larger scale, and water vapor on the largest scale was initialized with NCEP reanalysis fields. Because such fields have very coarse resolution (e.g., 2.5 x 2.5 degrees in the horizontal) relative to the size of the SCAB grid (near 5 x 5 km), it is likely that the initial fields for moisture and other meteorological parameters were less accurate than they could be, giving rise to errors in precipitation in the SCAB grid. Finally, the calculation of precipitation in the model accounts for settling of fog drops as well as rain drops (e.g., fog drops that drop to the ground, even if they subsequently evaporate, are considered precipitation). Rain gauges account for net precipitation and cannot account for evaporated rainfall.

Figure 6 shows the monthly averaged and South-Coast-grid-averaged effect of AAPPGs in the vertical profile of several parameters. Figure 6a shows that AAPPGs increased cloud scattering optical depth in the SCAB, just as in the California grid. Cloud liquid water content increased in February but slightly decreased in August due to AAPPGs (Figure 6b). The increase in February may have been due to the decrease in precipitation. The slight decrease in February was most likely due to the increase in air temperatures (Figure 6f), decrease in water vapor (Figure 6d) and decrease in relative humidity in August due to AAPPGs. AAPGs generally decreased cloud ice contents in February and August. Decreases may have been due to increases in temperatures within clouds and decreased convection due to increased atmospheric stability caused by AAPPGs.

Figure 6d shows that AAPPGs decreased water vapor near the surface in February and August, most likely due to reduced vertical mixing due to a more stable boundary layer (Figure 6f). Above the surface, water vapor decreased in August and increased in February.

Figure 6e shows that AAPPGs decreased net down minus up surface solar irradiance and increased net down minus up surface thermal-IR irradiance in both February and August, just like over the California grid. Solar minus infrared irradiance losses were greater in August than in February, just like over the California grid.

Figure 6f shows that AAPPGs decreased ground temperatures in both February and August. They caused no net change in near-surface air temperatures in February but increased them in August. The increase in near-surface air temperature in August was due to aerosol particle absorption of solar radiation and reemission of thermal-IR radiation to the air around the particles. The net increase in near-surface air temperatures in August (averaged over day and night during the month) is consistent with the result of *Jacobson* (1997b) who found that aerosol particles in Los Angeles decreased daytime surface and air temperatures slightly but increased nighttime temperatures to a greater extent, causing a net two-day warming. The present study found a similar result over 30 days in August. Figure 5f also shows that AAPPGs increased the stability of the boundary layer.

Figure 7 shows spatial monthly-averaged differences in several parameters over the South Coast grid when aerosols were and were not included. The left column in the figure shows February differences and the right column shows August differences.

Figures 7a–g show differences in the near-surface concentrations of several aerosol parameters. Whereas BC and POM (Figures 7a,b) are emitted, sulfate, nitrate, and ammonium (Figures 7c–e) have emission and gas-to-particle conversion sources. Thus, the differences in these species were generally spread over a greater area than were the differences in BC or POM. An exception is sulfate, whose major sources (sulfur dioxide

**Figure 6.** Model monthly grid-averaged and South-Coast-Air-Basin-grid-averaged differences in the vertical profiles of some parameters for February and August. The bottom value for temperatures is ground temperature.

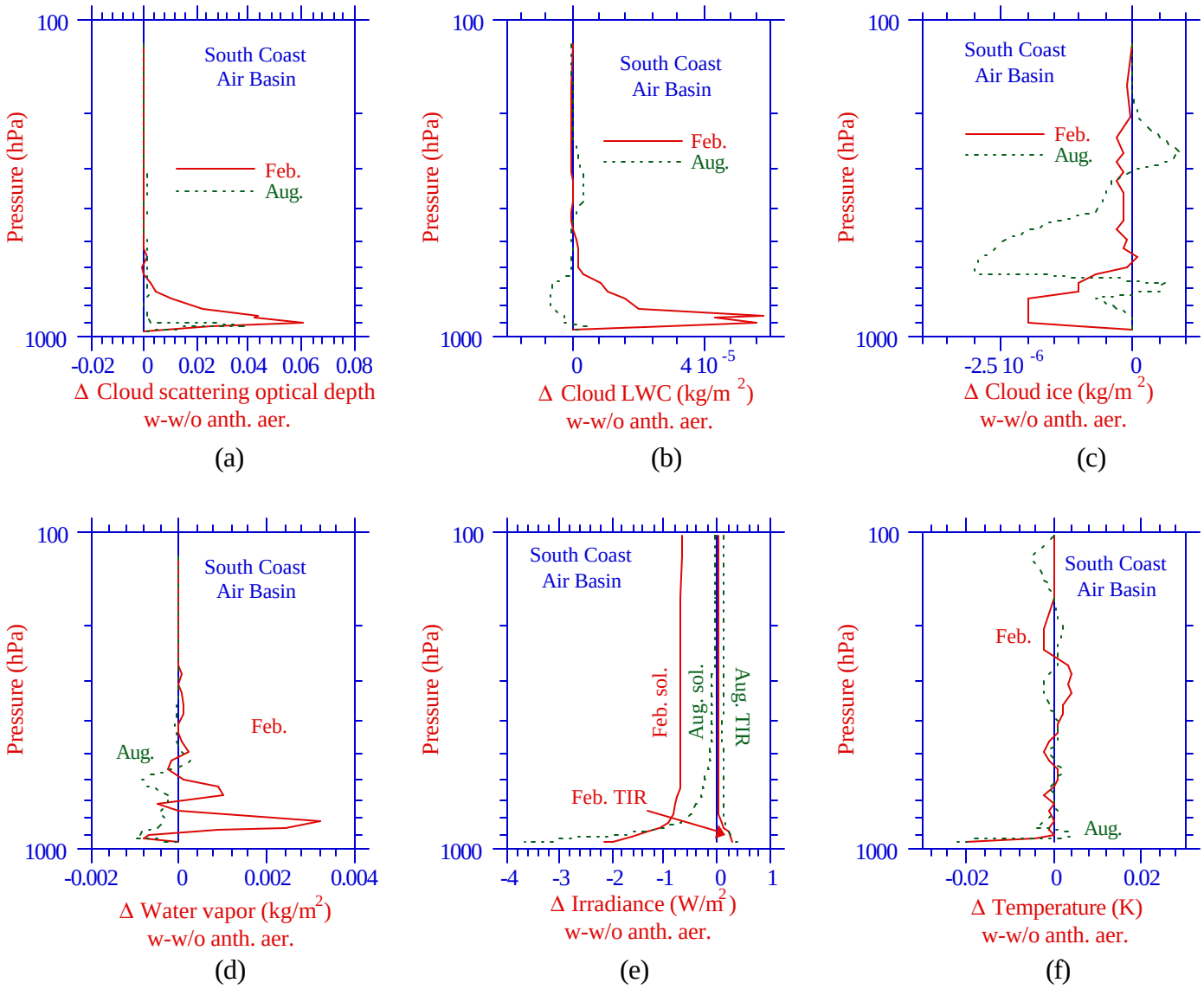

and sulfate emission) were concentrated over a narrow area near the coast, so were not spread out so much as BC and POM, whose sources covered a larger areal extent.

Although sodium (Figure 7f) was not a component of anthropogenic emission for the simulation, its near-surface concentration changed in the model due to the feedback of AAPPGs to near-surface winds. Changes in winds changed the emission rate of sea spray (daytime stability effect and smudgepot effect), which contains sodium.

Figure 7g shows that AAPPGs increased the aerosol liquid water, primarily near the coast, where the addition of sufficient hygroscopic aerosols and a high relative humidity enhanced water contents there. The total aerosol column difference due to AAPPGs (Figure 7h) mirrored the difference in near-surface aerosol liquid water content to some degree. The aerosol optical depth difference (Figure 7i) similarly mirrored the aerosol column difference for the most part.

Figures 7j and 7k shows that AAPPGs decreased the column-integrated aerosol single scattering albedo at 440 nm and 550 nm, respectively. The reduction in aerosol single-scattering albedo (ASSA) was greater at 440 nm than at 550 nm because of the stronger aerosol absorption at 440 nm. The stronger absorption is due to the linear inverse dependence of absorption on wavelength as well as the preferential UV absorption of organic aerosol particle components.

Figure 7l shows that AAPPGs increased cloud optical depth in February and August in the SCAB. Increases in August were primarily along the coast. Figure 7m shows that the greatest increases in cloud absorption optical depth occurred in locations were BC was present and clouds were also abundant.

Figures 7n and 7o show that AAPPGs reduced downward surface UV irradiance and net down minus up surface total solar irradiance. Reductions in both occurred primarily in locations where aerosol optical depths were decreased. Figure 7p shows that AAPPGs increased net down minus up thermal-IR irradiance in similar locations.

Figure 7q shows that AAPPGs decreased near-surface air temperatures within the basin itself in February and August (although to a lesser extent in August). Temperatures increased in the mountains and around the basin in both February and August. The net effect of AAPPGs was to increase near-surface air temperatures in the SCAB grid in August and to cause no net change in February (Figure 6f).

The increased stability of air in the basin reduced vertical mixing (thus groundwater evaporation), reducing near-surface water vapor contents (Figure 7r) and generally increasing soil moisture (Figure 7s) in the basin. The decrease in water vapor had a greater effect on the relative humidity in the basin than did the decrease in temperature, resulting in a decrease in the relative humidity over much of the basin (Figure 7t), except along the coast in February, where water vapor increased in some locations and temperature decreased.

Figure 7u shows that AAPPGs increased the cloud liquid water content in many parts of the basin and mountains.

Figure 7v shows that AAPPGs caused a clear reduction of precipitation in the basin and on the upslope side of mountain regions. Precipitation increased beyond the mountains in both February and August. Both results again appear consistent with those of *Givati and Rosenfeld* (2004).

Figure 7w shows that AAPPGs increased the BC content of precipitation, which was expected since rainout and washout together are the main removal mechanisms of aerosol particles globally.

Figure 7x shows that AAPPGs slightly decreased westerly wind speeds in the lower troposphere in February but slightly increased them in August. Westerly winds decreased in the mid troposphere in both February and August.

Finally, Figure 8 compares model predictions of: (a) downward surface solar irradiance, (b) sea-level air pressure, (c) temperature and relative humidity, and (d) wind speed and direction at some locations in the SCAB with paired-in-time-and-space data from August (thus the model values were compared with the data at the same time and location as the data). The comparisons were made hourly.

**Figure 7.** Modeled differences between the baseline case (1999) and the sensitivity case (no anthropogenic aerosol or aerosol-precursor-gas emissions), for the South Coast Air Basin grid, averaged over February (left column) and August (right column).

7a. Near-surface BC difference

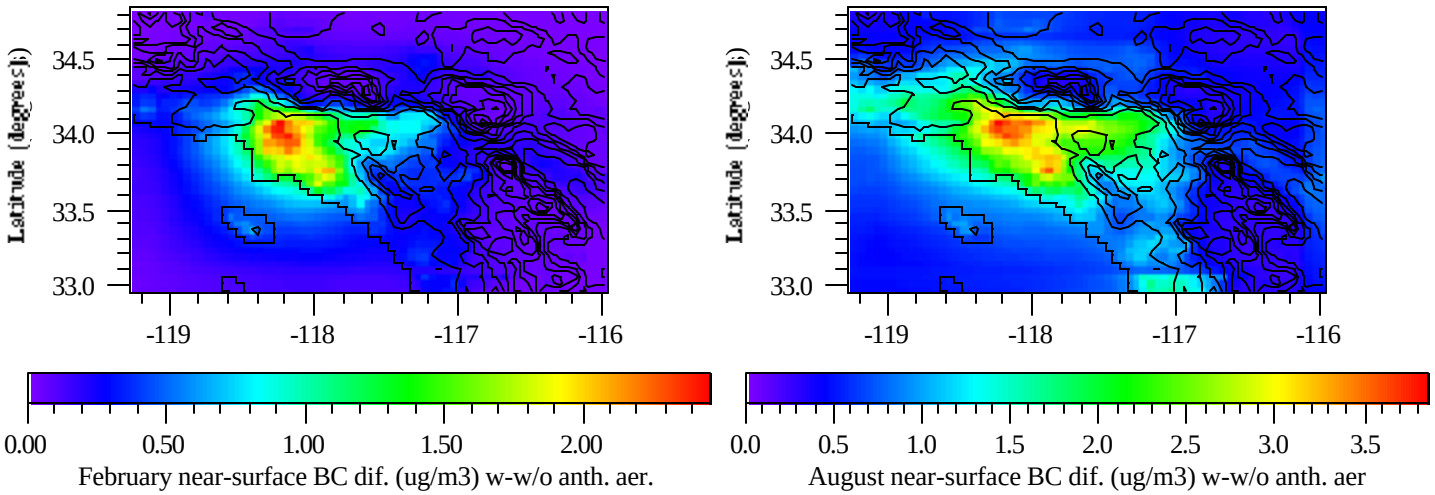


7b. Near-surface POM difference

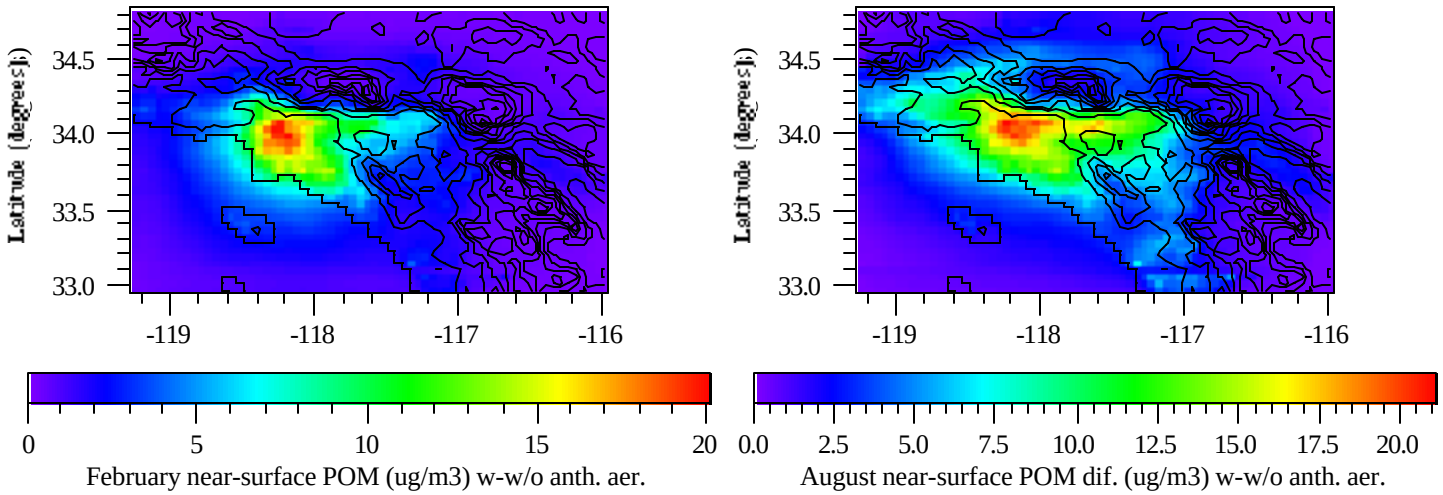

7c. Near-surface S(VI) difference

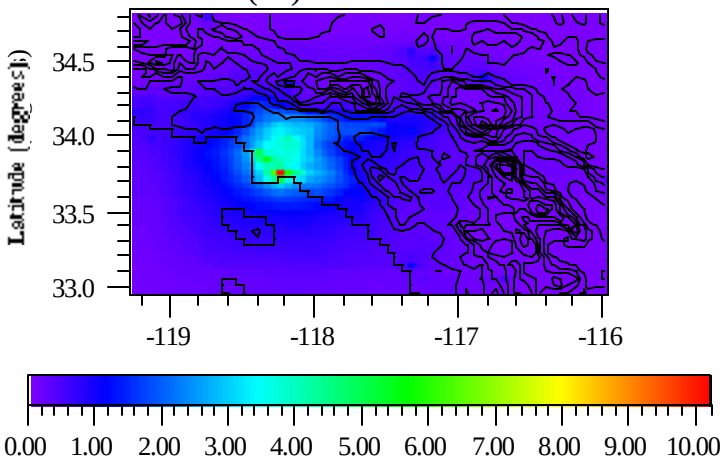


February near-surface S(VI) dif. (ug/m3) w-w/o anth. aer.

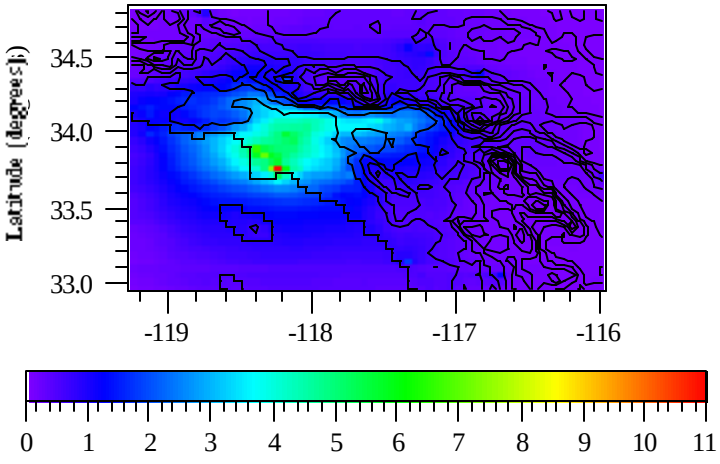


August near-surface S(VI) dif. (ug/m3) w-w/o anth. aer.

7d. Near-surface $NO_3^-$ difference

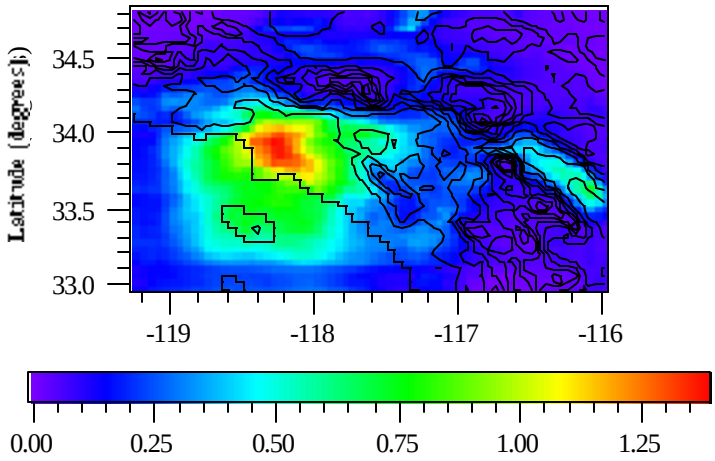


February near-surface NO3- dif. (ug/m3) w-w/o anth. aer.

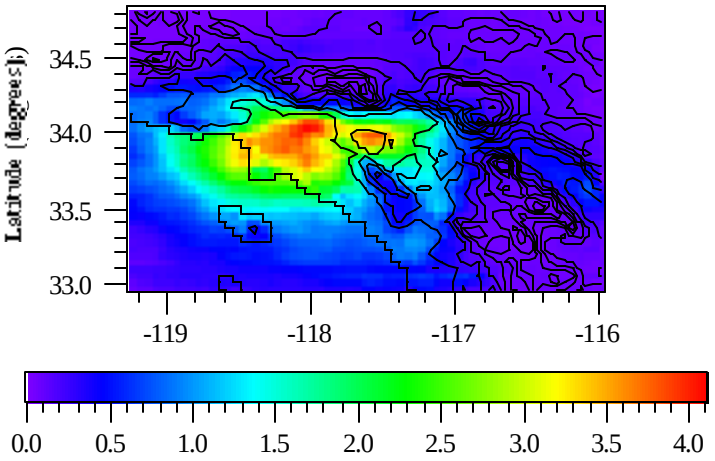


August near-surface NO3- dif. (ug/m3) w-w/w anth. aer.

7e. Near-surface $NH_4^+$ difference

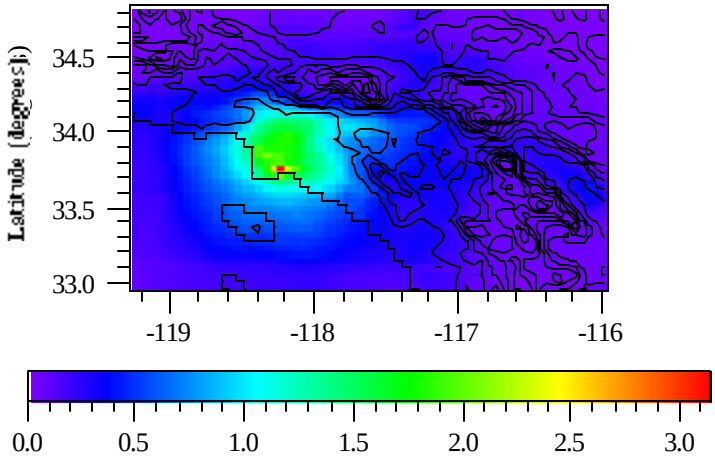


February near-surface NH4+ dif. (ug/m3) w-w/o anth. aer.

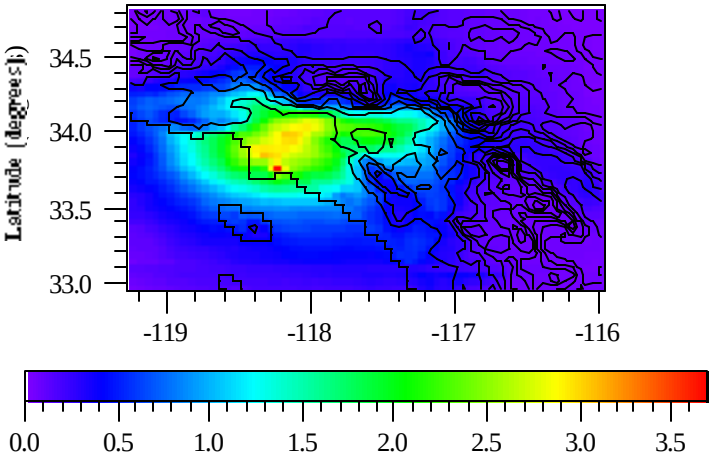


August near-surface NH4+ dif. (ug/m3) w-w/o anth. aer.

7f. Near-surface sodium difference

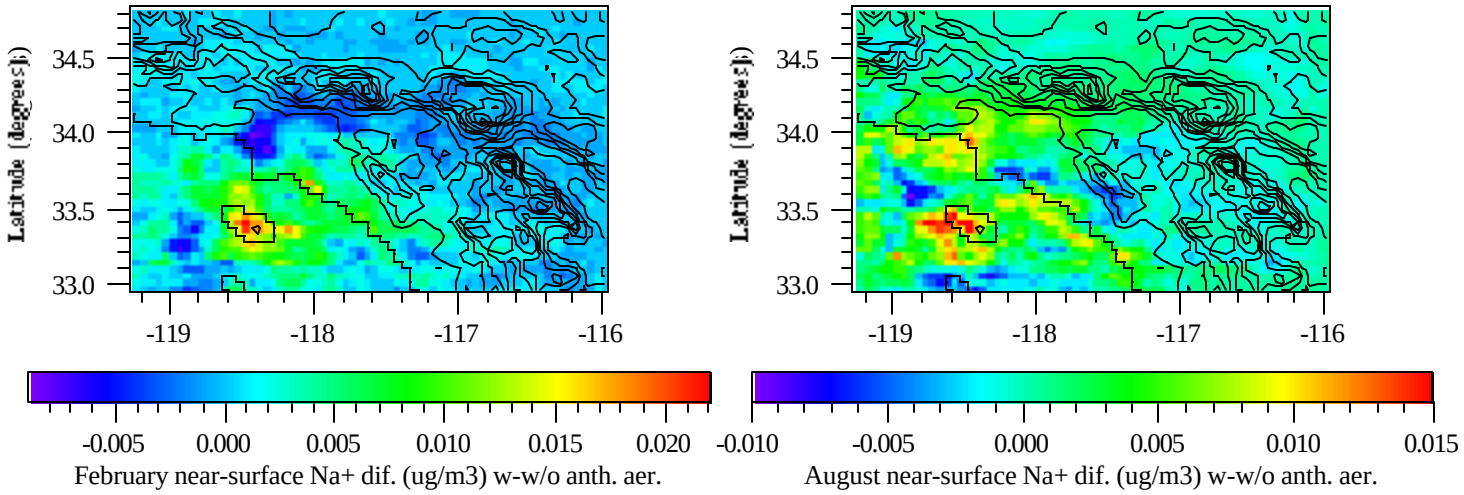


February near-surface Na+ dif. (ug/m3) w-w/o anth. aer.

August near-surface Na+ dif. (ug/m3) w-w/o anth. aer.

7g. Near-surface aerosol LWC difference

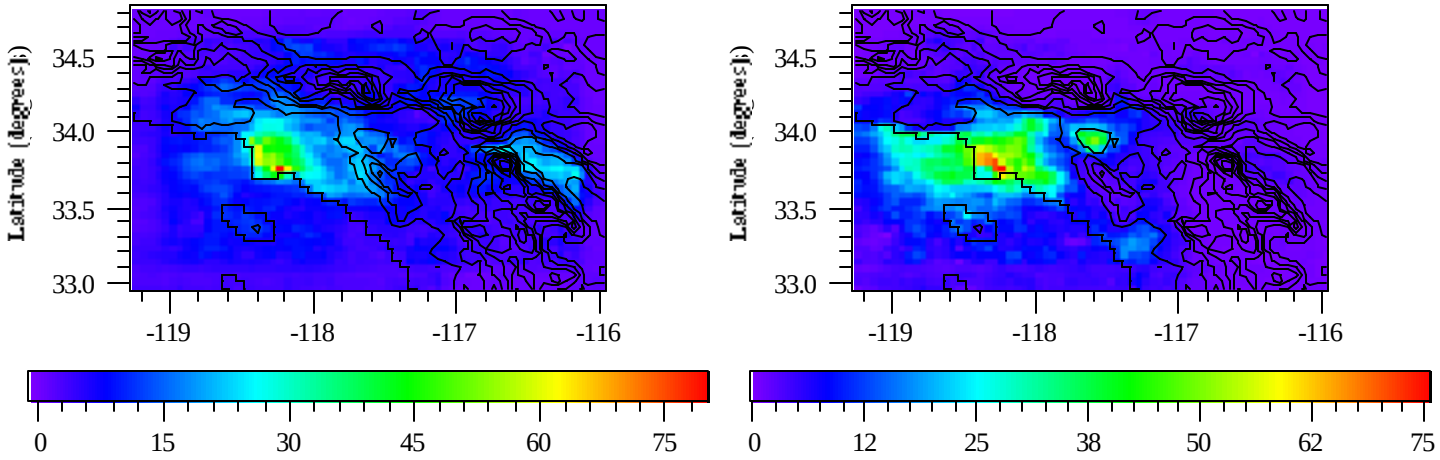


February near-surface aerosol LWC dif. (ug/m3) w-w/o anth. aer.

August near-surface aerosol LWC dif. (ug/m3) w-w/o anth. aer.

7h. Total aerosol column difference

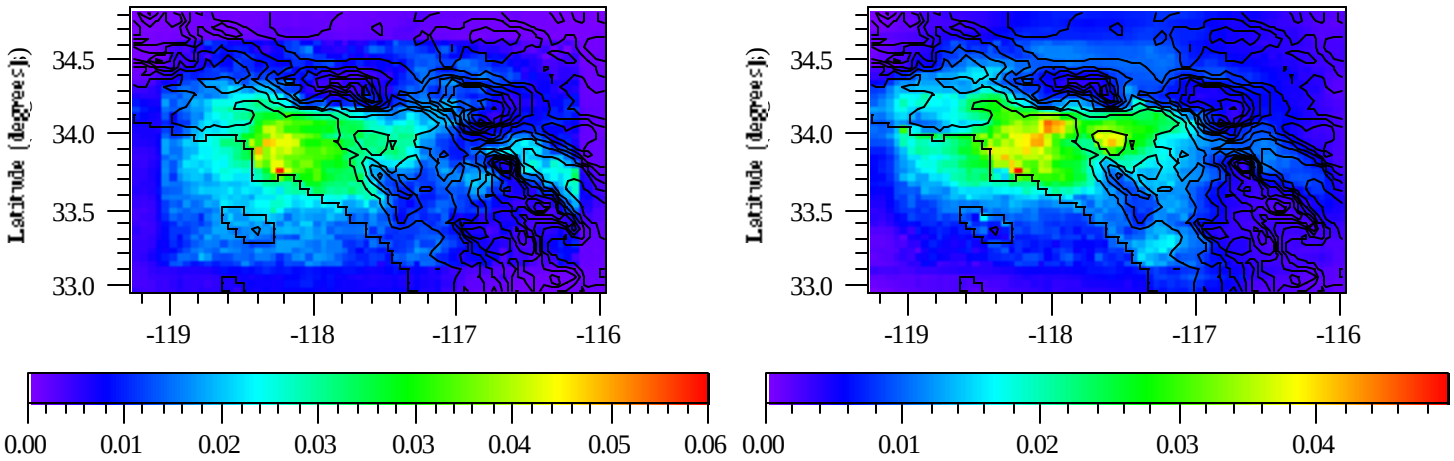


February column total aerosol dif. (g/m2) w-w/o anth. aer.

August column total aerosol dif. (g/m2) w-w/o anth. aer.

7i. Aerosol 550 nm optical depth difference

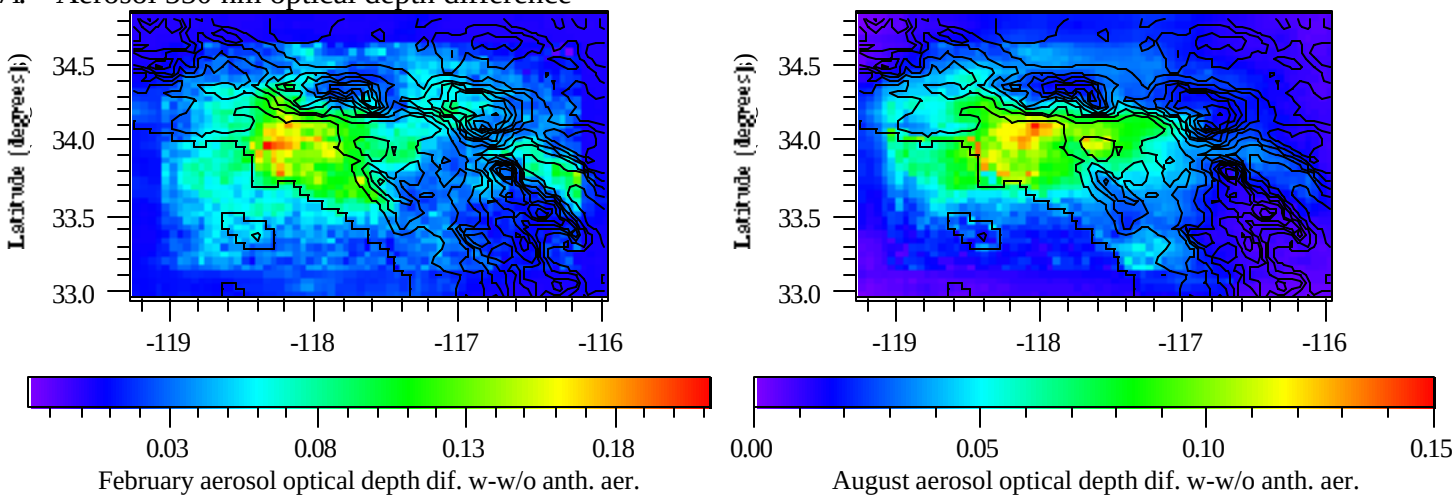


February aerosol optical depth dif. w-w/o anth. aer.

August aerosol optical depth dif. w-w/o anth. aer.

7j. Column aerosol SSA at 440 nm difference

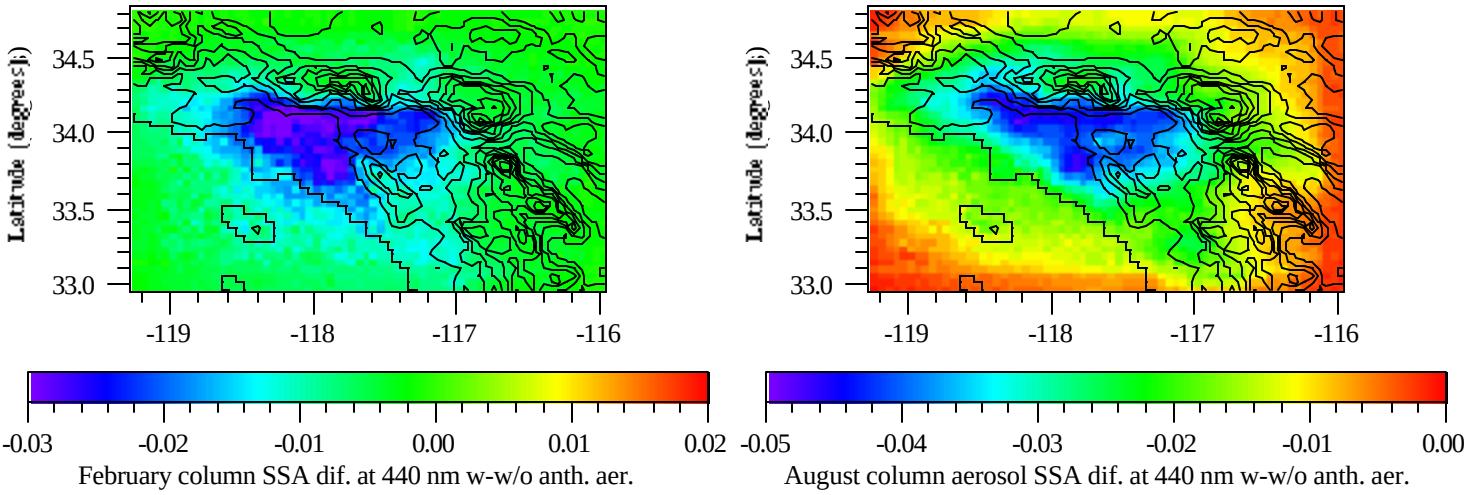


February column SSA dif. at 440 nm w-w/o anth. aer.

August column aerosol SSA dif. at 440 nm w-w/o anth. aer.

7k. Column aerosol SSA at 550 nm difference

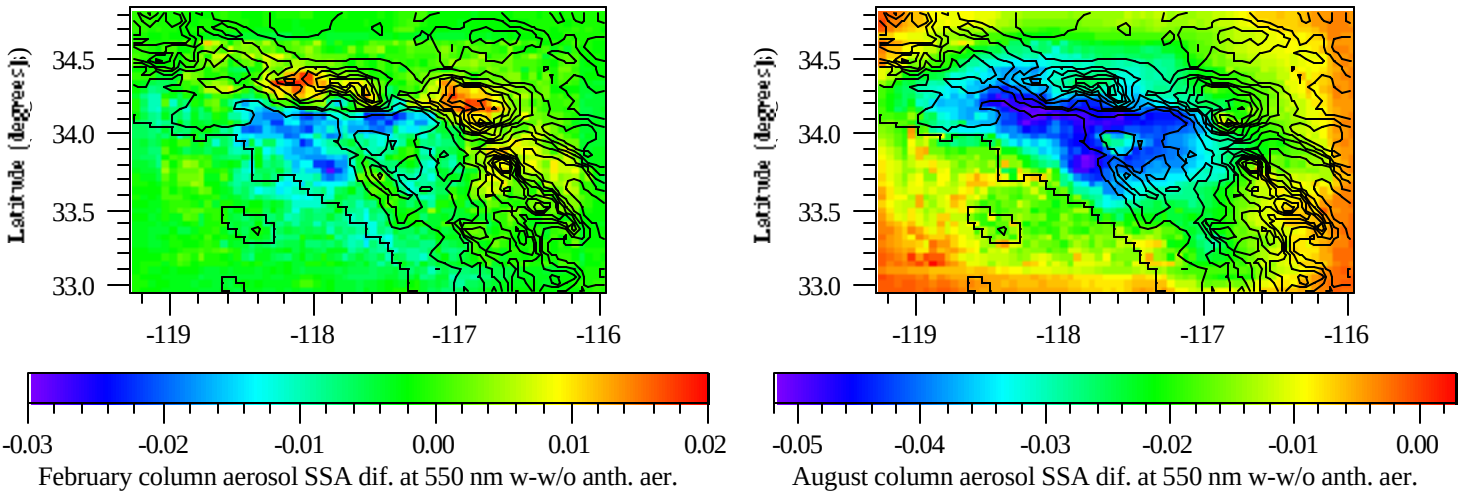


February column aerosol SSA dif. at 550 nm w-w/o anth. aer.

August column aerosol SSA dif. at 550 nm w-w/o anth. aer.

7l. Cloud optical depth difference

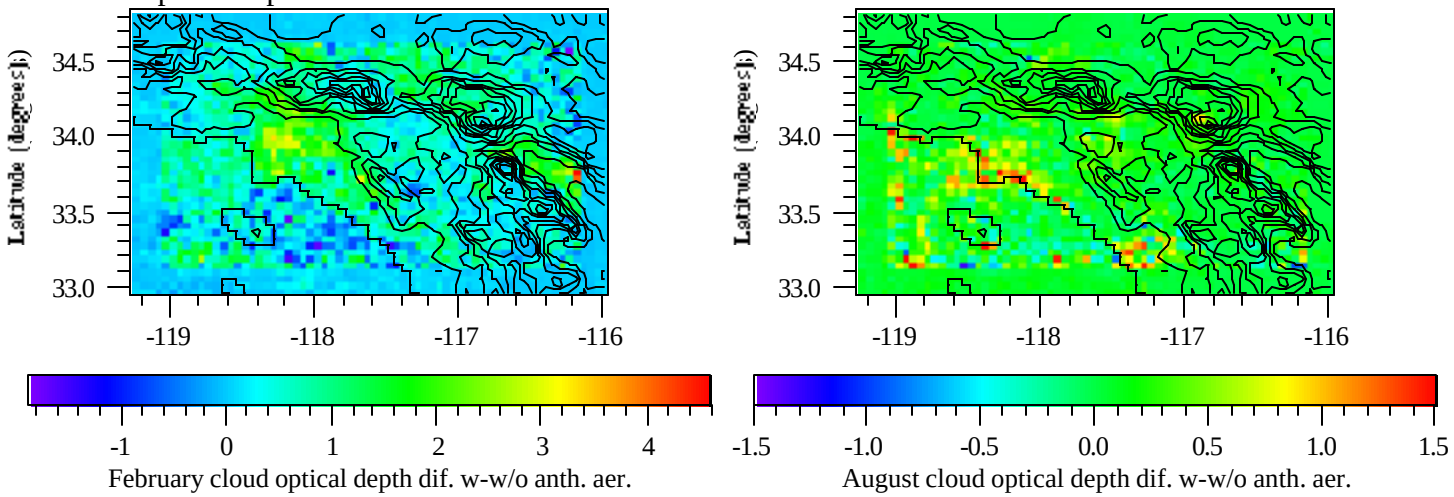


February cloud optical depth dif. w-w/o anth. aer.

August cloud optical depth dif. w-w/o anth. aer.

7m. Cloud absorption optical depth difference

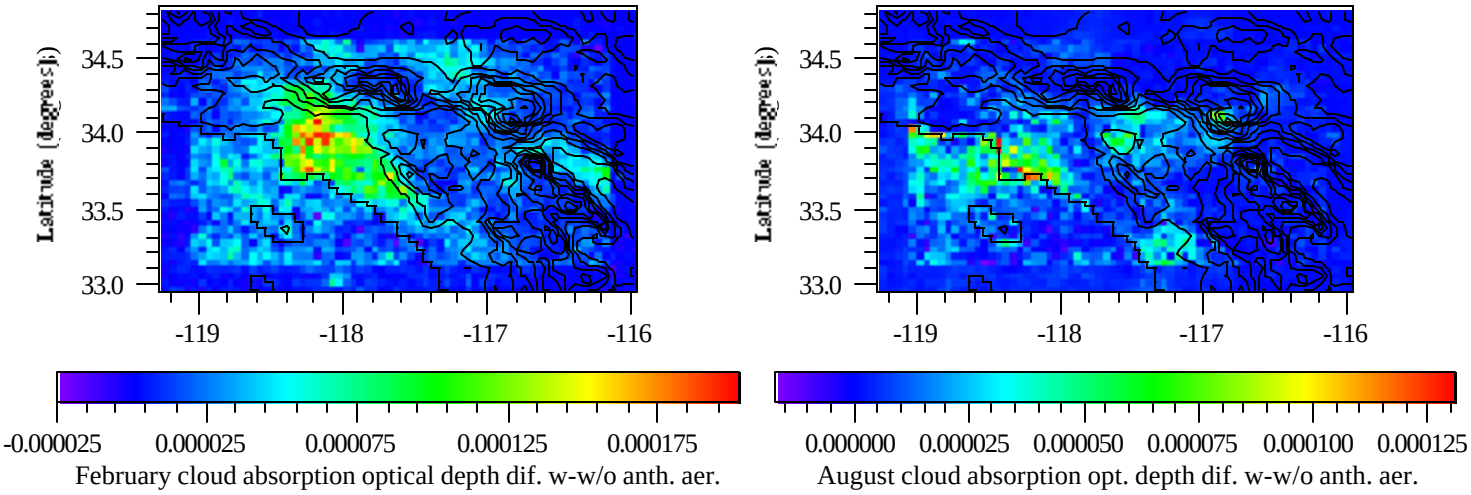


February cloud absorption optical depth dif. w-w/o anth. aer.

August cloud absorption opt. depth dif. w-w/o anth. aer.

7n. Downward UV difference at the surface

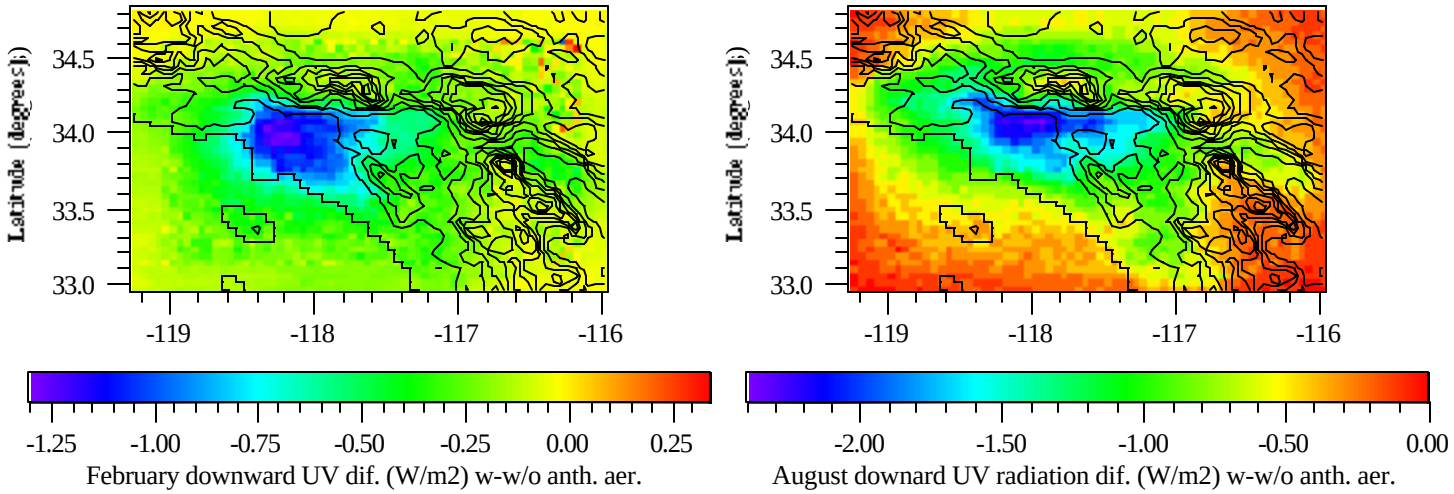


February downward UV dif. (W/m2) w-w/o anth. aer.

August downard UV radiation dif. (W/m2) w-w/o anth. aer.

7o. Down-up surface solar irradiance difference

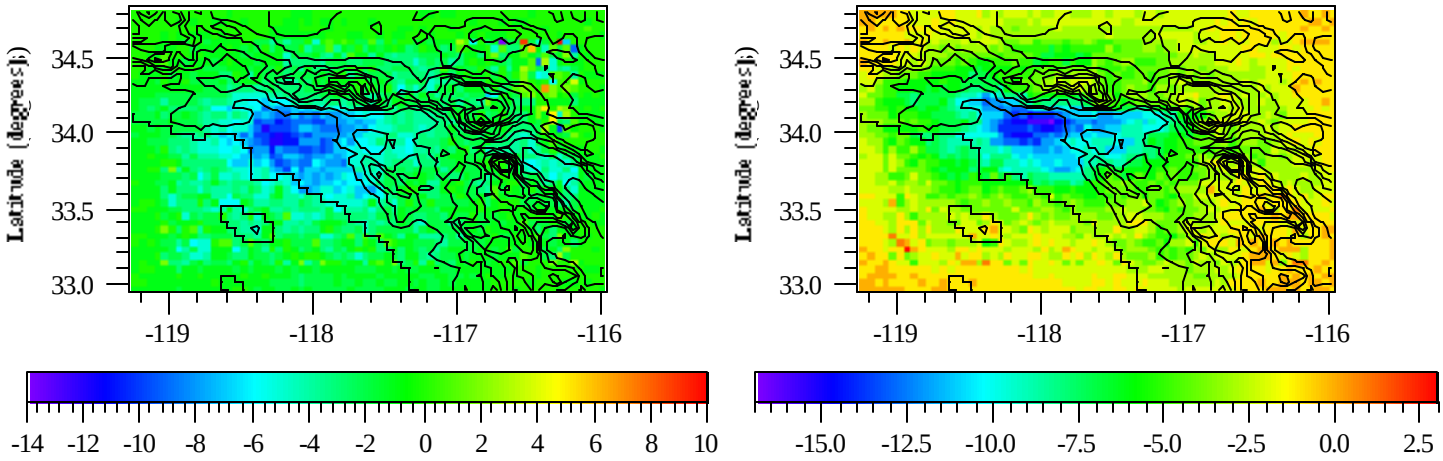


February down-up surface solar dif. (W/m2) w-w/o anth. aer.

August down-up surface solar dif. (W/m2) w-w/o anth. aer.

7p. Down-up thermal-IR irradiance difference

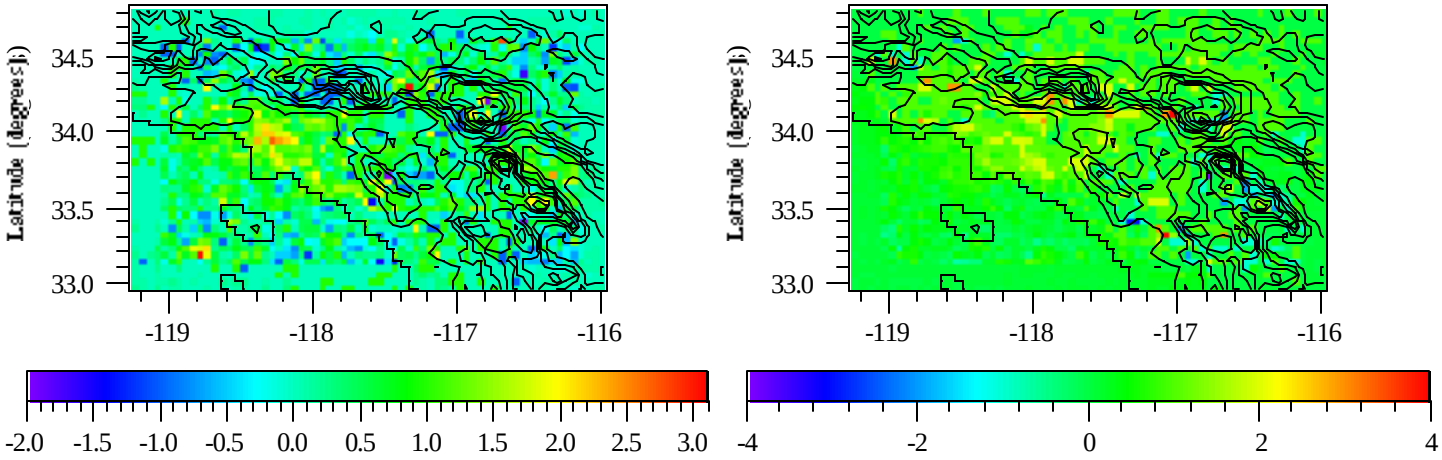


February down-up surface thermal-IR (W/m2) w-w/o anth. aer.

August down-up surface thermal-IR dif. (W/m2) w-w/o anth. aer.

7q. Near-surface air temperature difference

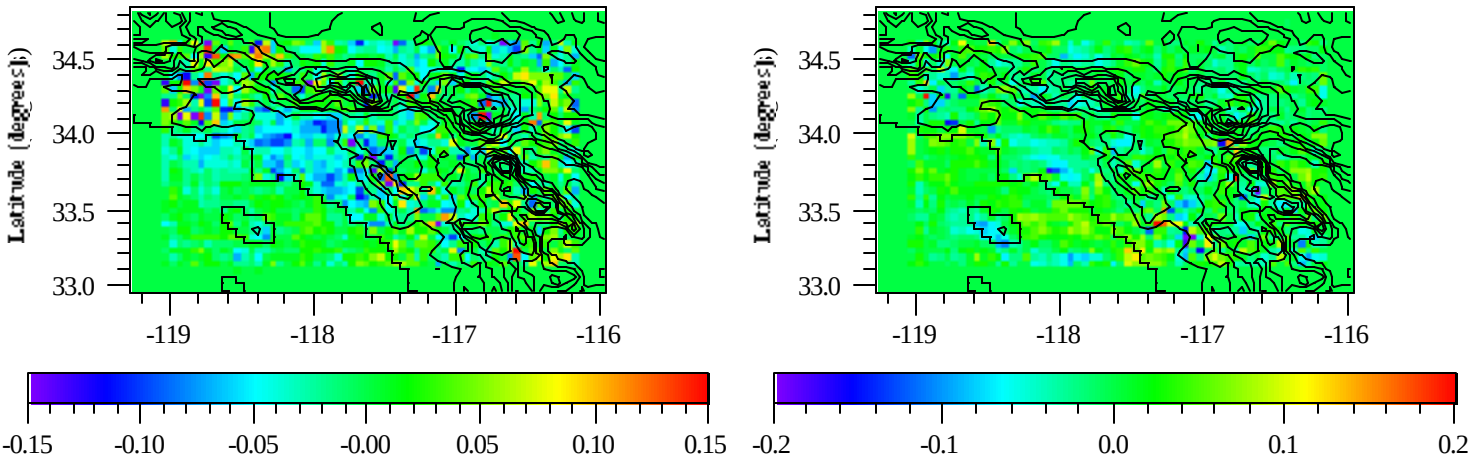


February near-surface air temperature dif. (K) w-w/o anth. aer.

August near-surface temperature dif. (K) w-w/o anth. aer.

7r. Near-surface water vapor difference

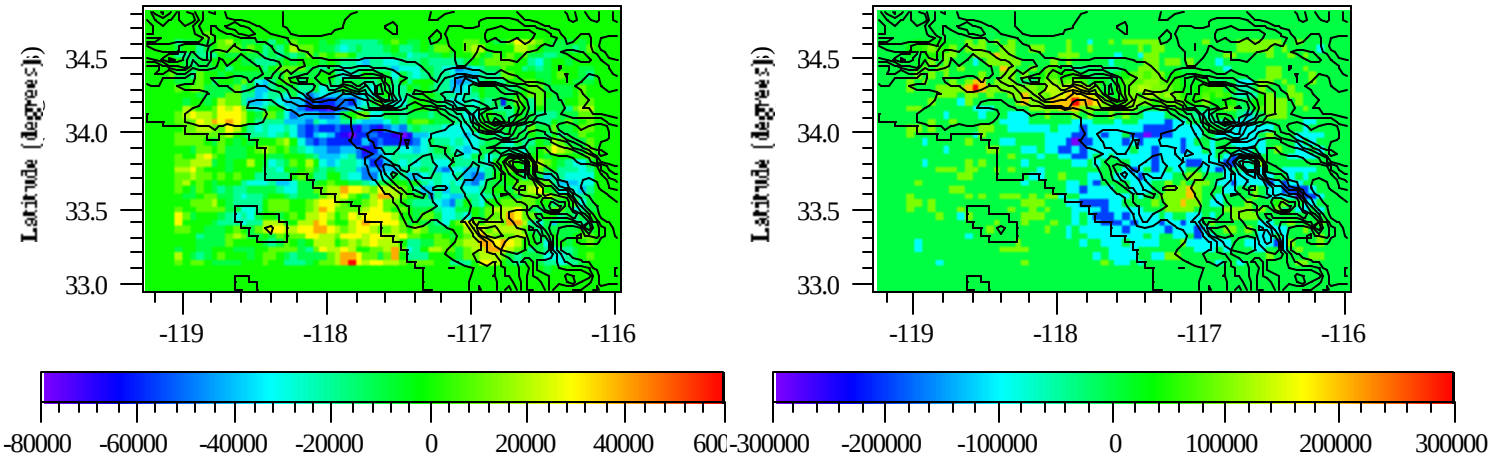


August near-surface water vapor dif. (ppbv) w-w/o anth. aer.

August near-surface water vapor dif. (ppbv) w-w/o anth. aer.

7s. Soil LWC difference

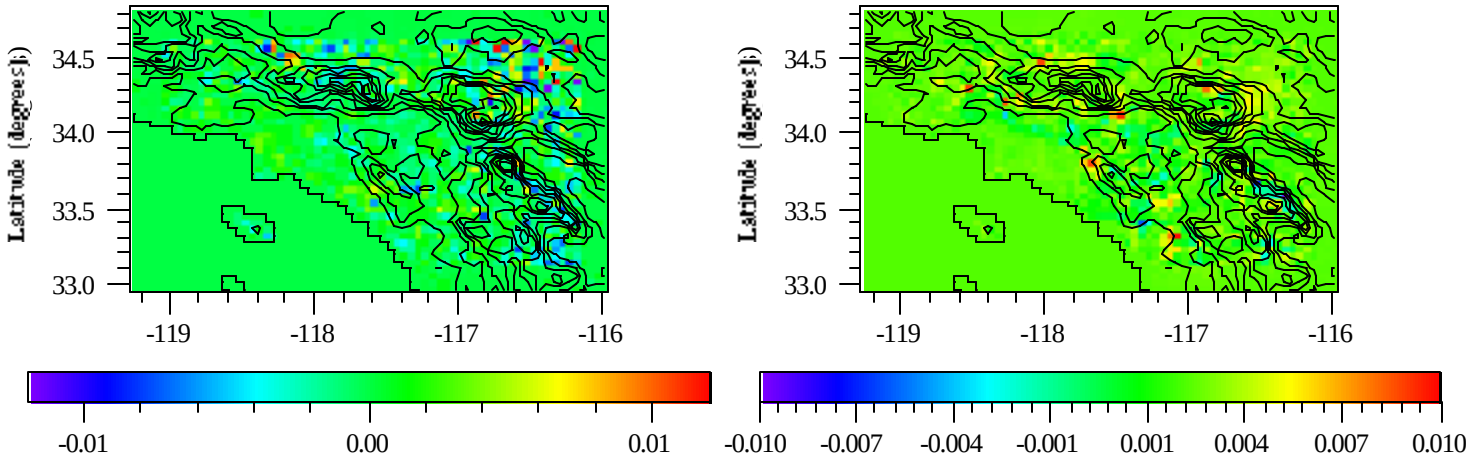


February soil LWC dif. (m3/m3) w-w/o anth. aer.

August soil LWC dif. (m3/m3) w-w/o anth. aer.

7t. Near-surface relative humidity difference

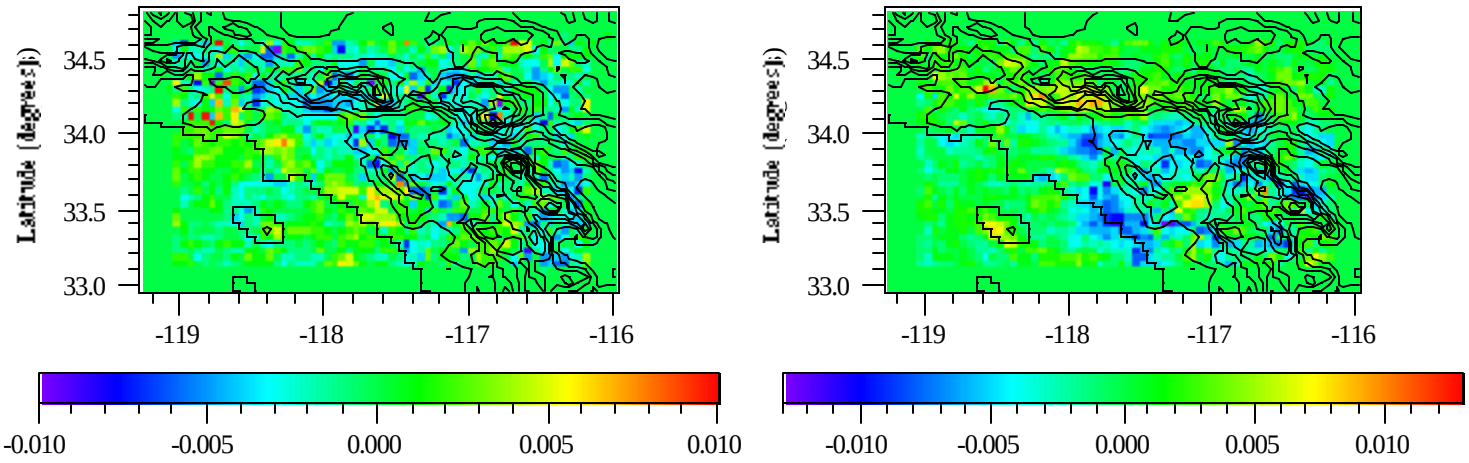


February near-surface relative humidity dif. (frac.) w-w/o anth. aer.

August near-surface relative humidity dif. (frac.) w-w/o anth. aer.

7u. Column cloud liquid water content difference

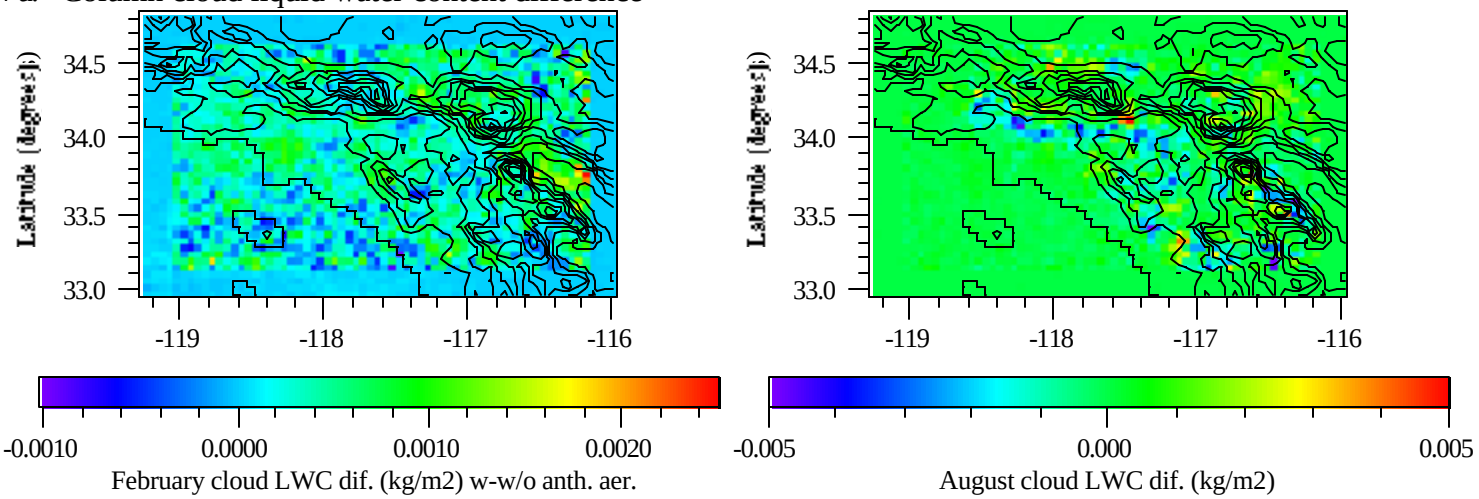


7v. Precipitation difference

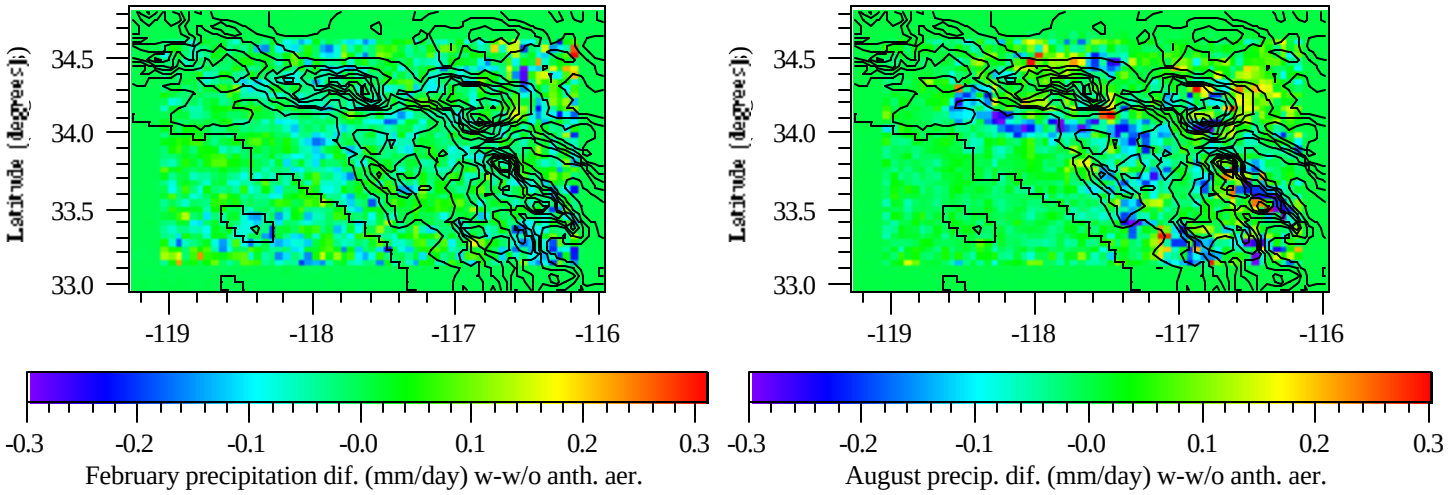


7w. BC in precipitation difference

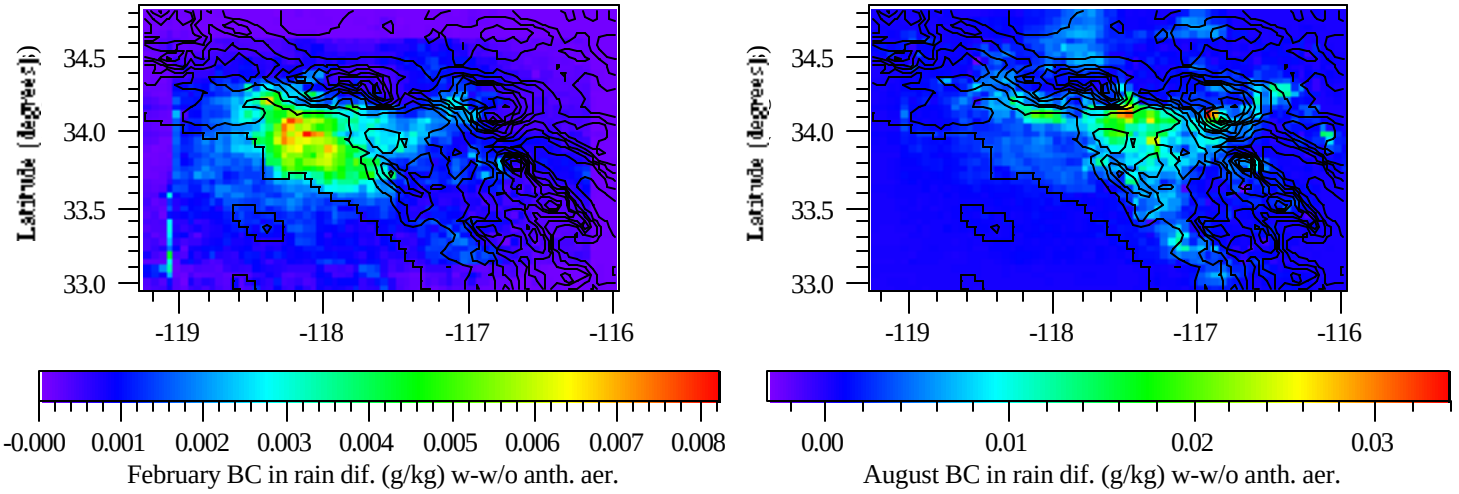

7x. Zonal west-east wind velocity difference

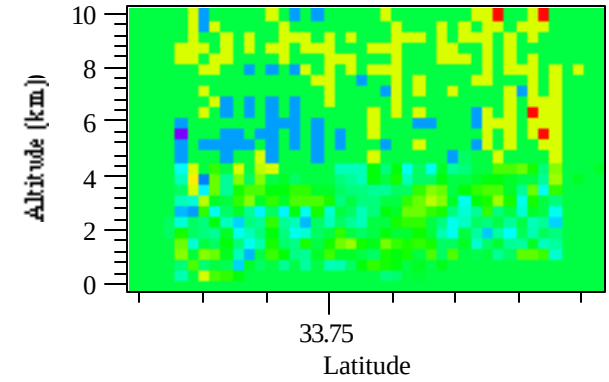


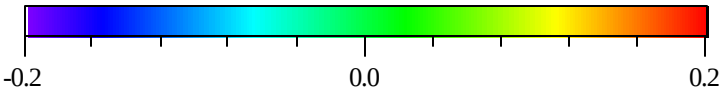


February zonal u-wind dif. (m/s) w-w/o anth. aer.

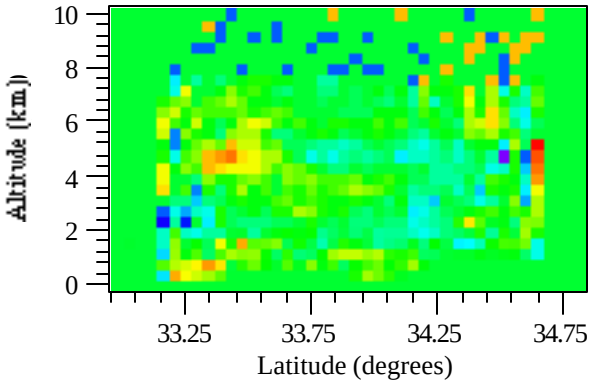


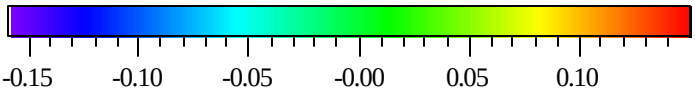


August zonal u-wind dif. (m/s) w-w/o anth. aer.

**Figure 8.** Paired-in-time-and-space comparisons of model predictions (solid lines) with data (dashed lines) from the Environmental Protection Agency AIRs database. Measured values were compared every hour for the month of August.

8a. Downward surface solar irradiance

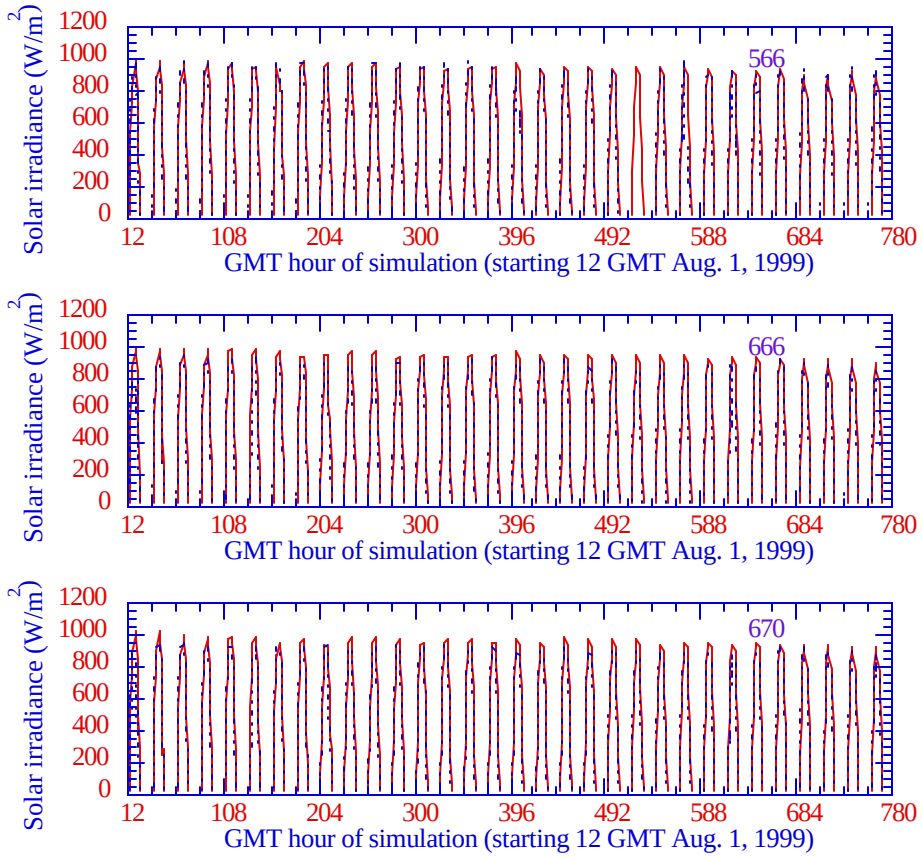


8b. Sea-level air pressure

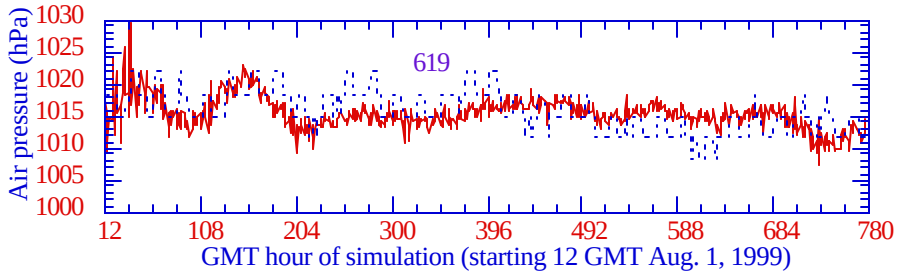

8c. Near-surface air temperature and relative humidity

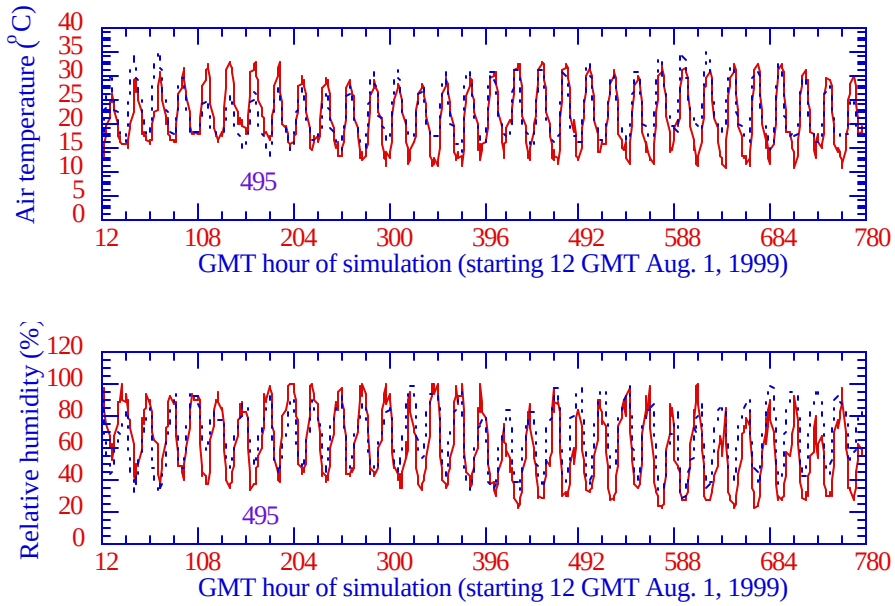


8d. Near-surface wind speed and direction

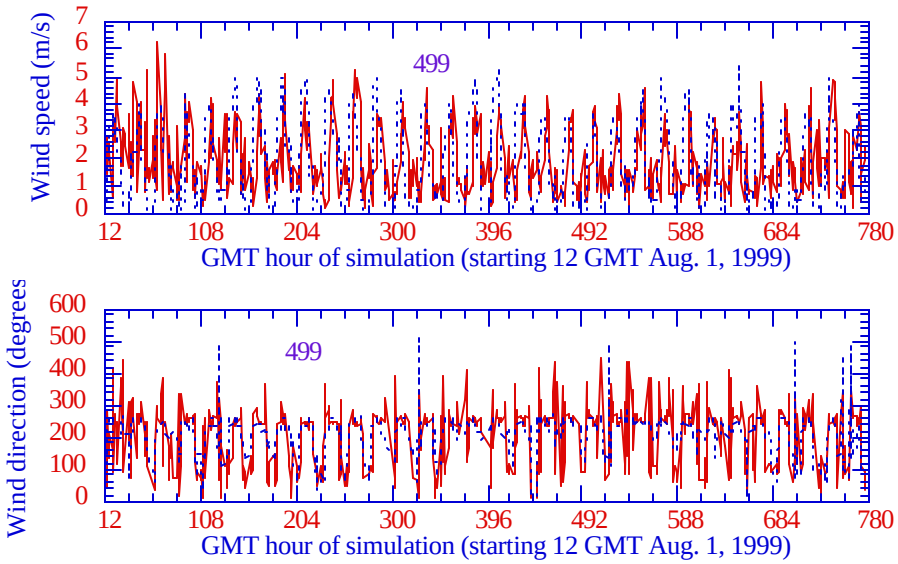

## 7. Summary

This report first presented a review of previous work on the climate response of anthropogenic aerosol particles. It then described results of model simulations of the effects of anthropogenic aerosol particles and their precursor gases on California and South Coast Air Basin climate during two months, February and August, 1999. Because the simulations were run for a relatively short period and under only two sets of initial conditions, further verification would be beneficial. With this caveat, some findings of the study are as follows:

1) Anthropogenic aerosol particles and their precursor gases (AAPPG) were modeled to reduce precipitation in the Sierra-Nevada Mountains and the Central Valley in February and August. Slight increases in precipitation in some locations beyond the mountains were also seen in both months, but the net effect was a precipitation reduction over land. Similarly, AAPPG were modeled to reduce precipitation in February and August over most of the SCAB grid, including mountainous regions. Increases in precipitation occurred beyond the mountains in both months. Again, the net effect of particles was to reduce precipitation.

2) AAPPG were modeled to decrease both California-grid-averaged and South-Coast-grid-averaged ground temperatures in both August and February.

3) AAPPG decreased near-surface air temperatures in February in both grids, but slightly increased near-surface air temperatures in the South-Coast grid and caused no net change in near-surface air temperatures in the California grid in August.

4) AAPPG increased California temperatures in the boundary layer and lower troposphere above the boundary layer in August and keep them relatively constant in February. A similar result was found over the SCAB grid. The effects of individual aerosol components were not isolated. The effect of historic changes in GHG changes, which would enhance warming, were not also not isolated. Present emission of GHGs was treated in all cases to isolate the effect of aerosols and their precursor gases.

5) In all cases, AAPPG stabilized the boundary layer. More stable boundary layers enhance pollutant concentrations.

6) AAPPG were modeled to reduce net downward minus upward surface solar radiation and increase net downward thermal-IR radiation in the Central Valley and South Coast Air Basin in February and August. Increases in thermal-IR offset decreases in solar to a greater extent in February than in August. The reduction in solar radiation has implications for photosynthesis rates and crop yields, although such effects were not quantified.

7) AAPPG were modeled to increase cloud optical depths by up to a factor of two in some areas (reducing visibility through clouds) in the California and SCAB grids in February and August, demonstrating the first indirect effect of aerosols in all cases.

8) AAPPG were modeled to increase cloud liquid water and decrease cloud ice in California in February and August. Increases in cloud liquid may have been due to the longer lifetimes of clouds and the reduction in precipitation caused by aerosol particles. In the SCAB, liquid water contents increased in February and slightly decreased in August.

9) AAPPG were modeled to decrease downward surface UV radiation in the Central Valley and SCAB in February and August. The reduction in UV come at the expense of high particle and gas pollutant loadings. Increases in particle loadings, in particularly, exacerbate adverse impacts to human health to a greater extent than reductions in UV radiation improve it.

10) AAPPG were modeled to increase the rainwater concentration of aerosol particles. Thus, rainwater contamination is a consequence of air pollution buildup.

## 8. References


Ackerman, A. S.,. B. Toon, D. E. Stevens, A. J. Heymsfield, V. Ramanathan, and E. J. Welton, Reduction of tropical cloudiness by soot, *Science*, *288*, 1042-1047, 2000.

Ackerman, T.P., K.N. Liou, and C.B. Leovy, Infrared radiative transfer in polluted atmospheres, *J. Appl. Meteorol., 15*, 28-35, 1976.

Ackerman, T. P., A model of the effect of aerosols on urban climates with particular applications to the Los Angeles basin, *J. Atmos. Sci., 34*, 531-546, 1977.

Albrecht, B. A., Aerosols, cloud microphysics, and fractional cloudiness, *Science*, *245*, 1227-1230, 1989.

Andreae, M.O., D. Rosenfeld, P. Artaxo, A.A. Costa, G.P. Frank, K.M. Longo, and M.Z.F. Silva-Dias, Smoking rain clouds over the Amazon, *Science, 303*, 133-342, 2004.

Aoki, T., T. Aoki, M. Fukabori, A. Hachikubo, Y. Tachibana, and F. Nishio, Effects of snow physical parameters on spectral albedo and bi-directional reflectance of snow surface, *J. Geophys. Res., 105*, 10,219-10,236, 2000.

Arakawa, A., and V. R. Lamb, A potential enstrophy and energy conserving scheme for the shallow water equations, *Mon. Wea. Rev., 109*, 18-36, 1981.

Atwater, M. A., The radiation budget for polluted layers of the urban environment, *J. Appl. Meteorol., 10*, 205-214, 1971a.

Atwater, M. A., Radiatve effects of pollutants in the atmospheric boundary layer, *J. Atmos. Sci., 28*, 1367-1373, 1971b.

Atwater, M. A., Thermal effects of urbanization and industrialization in the boundary layer: A numerical study. *Bound.-Layer Meteorol., 3*, 229-245, 1972.

Atwater, M. A., Thermal changes induced by urbanization and pollutants, *J. Appl. Meteorol.*, 14, 1061-1071, 1975.

Balling, R.C., and S.B. Idso, Historical temperature trends in the United States and the effect of urban population growth, *J. Geophys. Res., 94*, 3359-3363, 1989.

Bergstrom, R.W. Jr., Predictions of the spectral absorption and extinction coefficients of an urban air pollution aerosol model, *Atmos. Environ., 6*, 247-258, 1972.

Bergstrom, R. W., and R. Viskanta, Modeling of the effects of gaseous and particulate pollutants in the urban atmosphere, Part I: Thermal structure, *J. Appl. Meteorol., 12*, 901-912, 1973a.

Bergstrom, R.W., and R. Viskanta, Modeling of the effects of gaseous and particulate pollutants in the urban atmosphere. Part II: Pollutant dispersion, *J. Appl. Meteorol., 12*, 913-918, 1973.

Berner, A., S. Sidla, Z. Galambos, C. Kruisz, R. Hitzenberger, H. M. ten Brink, and G. P. A. Kos, Modal character of atmospheric black carbon size distributions, *J. Geophys. Res., 101*, 19,559-19,565, 1996.

Binenko, V.I., and H. Harshvardhan, Aerosol effects in radiation transfer. In *Aerosol Effects on Climate*, S.G. Jennings, et., pp. 190-232, 1993.

Bohren, C. F., Applicability of effective-medium theories to problems of scattering and absorption by nonhomogeneous atmospheric particles, *J. Atmos. Sci., 43*, 468-475.

Borys, R.D., D.H. Lowenthal, S.A. Cohn, and W.O.J. Brown, Mountaintop and radar measurements of anthropogenic aerosol effects on snow growth and snowfall rate, *Geophys. Res. Lett., 30*, 1538, doi:10.1029/2002GL016855, 2003.

Bretherton, C. S., E. Klinker, A. K. Betts, and J. Coakley, Comparison of ceilometer, satellite, and synoptic measurements of boundary layer cloudiness and the ECMWF diagnostic cloud parameterization scheme during ASTEX, *J. Atmos. Sci., 52*, 2736-2751, 1995.

Cess, R.D., G.L. Potter, S.J. Ghan, and W.L. Gates, The climatic effects of large injections of atmospheric smoke and dust: A study of climate feedback mechanisms with one- and three-dimensional models, *J. Geophys. Res., 90*, 12,937-12,950, 1985.

Charlock, T.P., and W.D. Sellers, Aerosol effects on climate: Calculations with time-dependent and steady-state radiative-convective models, *J. Atmos. Sci., 37*, 1327-1341, 1980.

Chung, C.E., V. Ramanathan, and J.T. Kiehl, Effects of the South Asian absorbing haze on the northeast monsoon and surface-air heat exchange, *J. Climate, 15*, 2462-2476, 2002.

Chung, S.H., and J.H. Seinfeld, Global distribution and climate forcing of carbonaceous aerosols, *J. Geophys. Res., 107 (D19*), 4407, doi:10.1029/2001JD001397, 2002.

Chylek, P., V. Ramaswamy, and V. Srivastava, Albedo of soot-contaminated snow, *J. Geophys. Res., 88*, 10,837-10,843, 1983.

Chylek, P., V. Srivastava, R. G. Pinnick, and R. T. Wang, Scattering of electromagnetic waves by composite spherical particles: experiment and effective medium approximations, *Appl. Optics, 27*, 2396-2404, 1988.

Chylek, P., G. Videen, D. Ngo, R. G. Pinnick, and J. D. Klett, Effect of black carbon on the optical properties and climate forcing of sulfate aerosols, *J. Geophys. Res., 100*, 16,325-16,332, 1995.

Clark, R.N., and P.G. Lucey, Spectral properties of ice-particulate mixtures and implications for remote sensing, 1, Intimate mixtures, *J. Geophys. Res., 89*, 6341-6348, 1984.

Coakley Jr., J.A., and R.D. Cess, Response of the NCAR Community Climate Model to the radiative forcing by naturally occurring tropospheric aerosols, *J. Atmos. Sci., 42*, 1677-1692, 1985.

Cook, J., and E.J. Highwood, Climate response to tropospheric absorbing aerosols in an intermediate general circulation model, *Q.J.R. Meteorol. Soc., 130*, 175-191, 2004.

Covey, C., S.H. Schneider, and S.L. Thompson, Global atmospheric effects of massive smoke injections from a nuclear war: Results from general circulation model simulations, *Nature, 308*, 21-25, 1984.

Dickerson, R. R., S. Kondragunta, G. Stenchikov, K. L. Civerolo, B. G. Doddridge, and B. N. Holben, The impact of aerosols on solar ultraviolet radiation and photochemical smog, *Science, 278*, 1997.

Dickinson, R.E., R.M. Errico, F. Giorgi, and G.T. Bates, A regional climate model for the western United States, *Climatic Change, 15*, 383-422, 1989.

Ding, P., and D. A. Randall, A cumulus parameterization with multiple cloud-base levels, *J. Geophys. Res., 103*, 11,341-11,353, 1998.

Estournal, C., R. Vehil, D. Guedalia, J. Fontan, and A. Druilhet, Observations and modeling of downward radiative fluxes (solar and infrared) in urban/rural areas, J. Clim. And Appl. Meteorol., 22, 134-142, 1983.

Fuller, K. A., W. C. Malm, and S. M. Kreidenweis, Effects of mixing on extinction by carbonaceous particles, *J. Geophys. Res., 104*, 15,941-15,954, 1999.

Gillette, D. A., E. M. Patterson Jr., J. M. Prospero, and M. L. Jackson, Soil aerosols. In *Aerosol Effects on Climate.* S. G. Jennings, ed., University of Arizona Press, Tucson, 73-109, 1993.

Ghan, S.J., M.C. MacCracken, and J.J. Walton, Climatic response to large atmospheric smoke injections: Sensitivity studies with a tropospheric general circulation model, *J. Geophys. Res., 93*, 8315-8337, 1988.

Giorgi, F., and G.T. Bates, On the climatological skill of a regional model over complex terrain, *Monthly Weather Rev., 117*, 2325-2347, 1989.

Givati, A., and D. Rosenfeld, Quantifying precipitation suppression due to air pollution, J. Appl. Meteorol. 43, 1038-1056, 2004.

Goodridge, J.D., Urban bias influences on long-term California air temperature trends, Atmos. Environ., 26B, 1-7, 1992.

Gribbon, P.W.F., Cryoconite holes on Sermikavsak, West Greenland, *J. Glaciol, 22*, 177-181, 1979.

Groisman, P.Y., R.W. Knight, and T.R. Karl, Heavy precipitation and high streamflow in the contiguous United States: Trends in the twentieth century. *Bulletin of the American Meteorological Society, 82*, 219-246, 2001.

Groisman, P.Y., R.W. Knight, T.R. Karl, D.R. Easterling, B. Sun, J.H. Lawrimore, Contemporary changes of the hydrological cycle over the contiguous United States: Trends derived from in situ observations, *J. Hydrometeorology, 5*, 64-85, 2004.

Hansen, J., M. Sato, and R. Ruedy, Radiative forcing and climate response, *J. Geophys. Res*., *102*, 6831-6864, 1997.

Hansen, J. and L. Nazarenko, Soot climate forcing via snow and ice albedos, *Proc. Natl. Acad. Sci*., doi/10.1073/pnas.2237157100, 2003.

Haywood, J. M., D. L. Roberts, A. Slingo, J. M. Edwards, and K. P. Shine, General circulation model calculations of the direct radiative forcing by anthropogenic sulfate and fossil-fuel soot aerosol, *J. Climate*, *10*, 1562-1577, 1997.

Hegg, D. A., J. Livingston, P. V. Hobbs, T. Novakov, and P. B. Russell, Chemical apportionment of aerosol column optical depth off the mid-Atlantic coast of the United States, *J. Geophys. Res*., *102*, 25,293-25,303, 1997.

Hignett, P., J. P. Taylor, P. N. Francis, and M. D. Glew, Comparison of observed and modeled direct aerosol forcing during TARFOX, *J. Geophys. Res*., *104*, 2279-2287, 1999.

Higuchi, K., and A. Nagoshi, Effect of particulate matter in surface snow layers on the albedo of perennial snow patches, *IAHS AISH Publ., 1*18, 95-97, 1977.

Hitzenberger, R. and H. Puxbaum, Comparisons of the measured and calculated specific absorption coefficients for urban aerosol samples in Vienna, *Aerosol Sci. Technol*., *18*, 323-345, 1993.

Ishizaka, Y., and M. Adhikari, Composition of cloud condensation nuclei, *J. Geophys. Res.*, *108* (D4), 4138, doi:10.1029/2002JD002085, 2003.

Jacobson M. Z. (1994) *Developing, coupling, and applying a gas, aerosol, transport, and radiation model to study urban and regional air pollution*. Ph. D. Dissertation, Dept. of Atmospheric Sciences, University of California, Los Angeles, 436 pp.

Jacobson, M. Z., Development and application of a new air pollution modeling system. Part II: Aerosol module structure and design, *Atmos. Environ*., *31A*, 131-144, 1997a.

Jacobson, M. Z., Development and application of a new air pollution modeling system. Part III: Aerosol-phase simulations, *Atmos. Environ*., *31A*, 587-608, 1997b.

Jacobson, M. Z., Studying the effects of aerosols on vertical photolysis rate coefficient and temperature profiles over an urban airshed, *J. Geophys. Res*., *103*, 10,593-10,604, 1998a.

Jacobson, M. Z., Improvement of SMVGEAR II on vector and scalar machines through absolute error tolerance control. Atmos. Environ., 32, 791–796, 1998b.

Jacobson, M.Z., *Fundamentals of Atmospheric Modeling*, Cambridge University Press, New York, 1999a.

Jacobson, M. Z., Isolating nitrated and aromatic aerosols and nitrated aromatic gases as sources of ultraviolet light absorption, *J. Geophys. Res.*, *104*, 3527-3542, 1999b.

Jacobson, M. Z., Studying The effects of calcium and magnesium on size-distributed nitrate and ammonium with EQUISOLV II, *Atmos. Environ.*, *33*, 3635-3649, 1999c.

Jacobson, M. Z., A physically-based treatment of elemental carbon optics: Implications for global direct forcing of aerosols, *Geophys. Res. Lett*., *27*, 217-220, 2000.

Jacobson, M. Z., Strong radiative heating due to the mixing state of black carbon in atmospheric aerosols, *Nature*, *409*, 695-697, 2001a.

Jacobson, M. Z., GATOR-GCMM: A global through urban scale air pollution and weather forecast model. 1. Model design and treatment of subgrid soil, vegetation, roads, rooftops, water, sea ice, and snow., *J. Geophys. Res*., *106*, 5385-5402, http://www.stanford.edu/group/efmh/jacobson/GATORglob.html, 2001b.

Jacobson, M. Z., GATOR-GCMM: 2. A study of day- and nighttime ozone layers aloft, ozone in national parks, and weather during the SARMAP Field Campaign, *J. Geophys. Res*., *106*, 5403-5420, 2001c.

Jacobson, M. Z., Control of fossil-fuel particulate black carbon plus organic matter, possibly the most effective method of slowing global warming, *J. Geophys. Res.*, *107*, (D19), 4410, doi:10.1029/ 2001JD001376, 2002a.

Jacobson, M. Z., Analysis of aerosol interactions with numerical techniques for solving coagulation, nucleation, condensation, dissolution, and reversible chemistry among multiple size distributions, *J. Geophys. Res*., *107* (D19), 4366, doi:10.1029/ 2001JD002044, 2002b.

Jacobson, M. Z., Development of mixed-phase clouds from multiple aerosol size distributions and the effect of the clouds on aerosol removal, *J. Geophys. Res*., *108* (D8), 4245, doi:10.1029/2002JD002691, 2003.

Jacobson, M. Z., The short-term cooling but long-term global warming due to biomass burning, *J. Clim.*, 17 (15), 2909-2926, 2004a.

Jacobson, M.Z., The climate response of fossil-fuel and biofuel soot, accounting for soot's feedback to snow and sea ice albedo and emissivity, *J. Geophys. Res.*, *109*, doi:10.1029/2004JD004945, 2004b.

Jacobson, M.Z., Updates to "Control of fossil-fuel black carbon plus organic matter, possibly the most effective method of slowing global warming," http://www.stanford.edu/group/efmh/fossil/fossil.html, 2004c.

Jacobson, M. Z., J. H. Seinfeld, G. R. Carmichael, and D.G. Streets, The effect on photochemical smog of converting the U.S. fleet of gasoline vehicles to modern diesel vehicles, *Geophys. Res. Lett.*, *31*, L02116, doi:10.1029/2003GL018448, 2004.

Jacobson, M.Z., and J.H. Seinfeld, Evolution of nanoparticle size and mixing state near the point of emission, *Atmos. Environ*., 38, 1839-1850, 2004.

Jayaraman, A., D. Lubin, S. Ramachandran, V. Ramanathan, E. Woodbridge, W. D. Collins, and K. S. Zalpuri, Direct observations of aerosol radiative forcing over the tropical Indian Ocean during the January-February 1996 pre-INDOEX cruise, *J. Geophys. Res*. *103*, 13,827-13,836, 1998.

Joseph, J.H., The effect of a desert aerosol on a model of the general circulation, Proc. Symp. On Radiation in the Atmosphere. H.J. Bolle, Ed., Science Press, 487-492, 1976.

Kahle, A.B., and D. Deirmendjian, The black cloud experiment, Rep. R-1263-ARPA, Rand, Santa Monica, 1973.

Karl, T.R., H.F. Diaz, and G. Kukla, Urbanization: Its detection and effect in the United States climate record, *J. Clim.*, *1*, 1099-1123, 1988.

Karl, T.R., R.W. Knight, D.R. Easterling, and R.G. Quayle, Indices of climate change for the United States, Bull. Am. Met. Soc., 77, 279-292, 1996.

Ketefian, G., and M. Z. Jacobson, Development and application of a 2-D potential-enstrophy-, energy-, and mass-conserving mixed-layer ocean model with arbitrary boundaries, in preparation, 2004.

Kilsby, C.G., A study of aerosol properties and solar radiation during a straw-burning episode using aircraft and satellite measurements, *Q.J.R. Meteorol. Soc.*, *116*, 1173-1192, 1990.

Klein, S. A., Synoptic variability of low-cloud properties and meteorological parameters in the subtropical trade wind boundary layer, *J. Clim.*, *10*, 2018-2039, 1997.

Koren, I., Y.J. Kaufman, L.A. Remer, and J.V. Martins, Measurements of the effect of Amazon smoke on inhibition of cloud formation, *Science*, *303*, 342-345, 2004.

Krishnan, R., and V. Ramanathan, Evidence of surface cooling from absorbing aerosols, *Geophys. Res. Lett.*, *29* (9), doi:10.1029/2002GL014687, 2002.

Kristjansson, J. E., Studies of the aerosol indirect effect from sulfate and black carbon aerosols, J. Geophys. Res., *107*, (*D15*), 10.1029/2001JD000887, 2002.

Lammel, G., and T. Novakov, Water nucleation properties of carbon black and diesel soot particles, *Atmos. Environ.*, *29*, 813-823, 1995.

Lesins, G., P. Chylek, and U. Lohmann, A study of internal and external mixing scenarios and its effect on aerosol optical properties and direct radiative forcing, *J. Geophys. Res*., *107*(D10), 10.1029/2001JD000973, 2002.

Lu, R., and R. P. Turco, Air pollutant transport in a coastal environment, II, Three-dimensional simulations over Los Angeles basin, *Atmos. Environ*., *29*, 1499-1518, 1995.

Lubin, D., and A. S. Simpson, The longwave emission signature of urban pollution: Radiometric FTIR measurement, Geophys. Res. Lett., 21, 37-40, 1994.

Malone, R.C., L.H. Auer, G.A. Glatzmaier, M.C. Wood, and O.B. Toon, Nuclear winter: Three-dimensional simulations including interactive transport, scavenging, and solar heating of smoke, J. Geophys. Res., 91, 1039-1054, 1986.

Mellor, G. L., and T. Yamada, Development of a turbulence closure model for geophysical fluid problems, *Revs. of Geophys. and Space Phys*., *20*, 851-875, 1982.

Menon, S., J. Hansen, L. Nazarenko, and Y. Luo, Climate effects of black carbon aerosols in China and India, *Science*, *297*, 2250-2253, 2002.

National Centers for Environmental Prediction (NCEP), 2.5 degree global final analyses, distributed by the Data Support Section, National Center for Atmospheric Research, 2003.

Nemani, R.R., M.A. White, D.R. Cayan, G.V. Jones, S.W. Running and J.C. Coughlan, Asymmetric climatic warming over coastal California and its impact on the premium wine industry. *Climate Research, 19*, 25-34, 2001.

Nicholls, S., The dynamics of stratocumulus: Aircraft observations and comparisons with a mixed layer model, *Quart. J. Roy. Meteor. Soc., 110*, 783-820, 1984.

Park, R.J., G.L. Stenchikov, K.E. Pickering, R.R. Dickerson, D.J. Allen, and S. Kondragunta, Regional air pollution and its radiative forcing: Studies with a single column chemical and radiation transport model, *J. Geophys. Res., 106*, 28751-28770, 2001.

Peterson, J.T., E.C. Flowers, and J.H. Rudisill, Urban-rural solar radiation and atmospheric turbidity measurements in the Los Angeles basin, J. Appl. Meteorol., 17, 1595-1609, 1978.

Podgorny, I.A., and T.C. Grenfell, Absorption of solar energy in a cryoconite hole, *Geophys. Res. Lett., 23*, 2465-2468, 1996.

Raga, G.B., T. Castro, and D. Baumgardner, The impact of megacity pollution on local climate and implications for the regional environment: Mexico City, *Atmos. Environ.*, 35, 1805-1811, 2001.

Ramanathan, V., et al., Indian Ocean Experiment: An integrated analysis of the climate forcing and effects of the great Indo-Asian haze, *J. Geophys. Res., 106*, 28,371-28,398, 2001a.

Ramanathan, V., P.J. Crutzen, J.T. Kiehl, and D. Rosenfeld, Aerosols, climate, and the hydrological cycle, *Science, 294*, 2119-2124, 2001b.

Rasool, S., and S. Schneider, Atmospheric carbon dioxide and aerosols: Effects of large increases on global climate, *Science, 173*, 138-141, 1971.

Riemer, N., H. Vogel, B. Vogel, and F. Fiedler, Modeling aerosols on the mesoscale-g: Treatment of soot aerosol and its radiative effects, *J. Geophys. Res., 108 (D19)*, 4601, doi:10.1029/2003JD003448, 2003.

Rosenfeld, D., Suppression of rain and snow by urban and industrial air pollution, *Science, 287*, 1793-1796, 2000.

Russell, P. B., P. V. Hobbs, and L. L. Stowe, Aerosol properties and radiative effects in the United States East Coast haze plume: An overview of the tropospheric aerosol radiative forcing observational experiment (TARFOX). *J. Geophys. Res., 104*, 2213-2222, 1999a.

Russell, P. B., J. M. Livingston, P. Hignett, S. Kinne, J. Wong, A. Chien, R. Bergstrom, P. Durkee, and P. V. Hobbs, Aerosol-induced radiative flux changes off the United States mid-Atlantic coast: Comparison of values calculated from sunphotometer and in situ data with those measured by airborne pyranometer, *J. Geophys. Res., 104*, 2289-2307, 1999b.

Satheesh, S.K., and V. Ramanathan, Large differences in tropical aerosol forcing at the top of the atmosphere and Earth's surface, *Nature, 405*, 60-63, 2000.

Schnaiter, M., H. Horvath, O. Mohler, K.-H. Naumann, H. Saathoff, and O.W. Schock, UV-VIS-NIR spectral optical properties of soot and soot-containing aerosols, *J. Aerosol Sci., 34*, 1421-1444, 2003.

Sokolik, I., A. Andronova, and C. and Johnson C., Complex refractive index of atmospheric dust aerosols. *Atmos. Environ., 27A*, 2495-502, 1993..

Tett, S., et al., Estimation of natural and anthropogenic contributions to twentieth century temperature change, *J. Geophys. Res., 107 (D16)*, doi:10.1029/2000JD000028, 2002.

Toon, O. B., and T.P. Ackerman, Algorithms for the calculation of scattering by stratified spheres, *Appl. Opt. 20*, 3657-60, 1981.

Twohy, C. H., A. D. Clarke, S. G Warren, L. F. Radke, and R. J. Charlson, Light-absorbing material extracted from cloud droplets and its effect on cloud albedo, *J. Geophys. Res. 94*, 8623-8631, 1989.

Twomey, S. A., The effect of cloud scattering on the absorption of solar radiation by atmospheric dust, *J. Atmos. Sci., 29*, 1156-1159, 1977.

USEPA, United States National Emission Inventory for 1999, /www.epa.gov/ttn/chief, 2002.

Vehkamaki, H., M. Kulmala, I. Napari, K.E.J. Lehtinen, C. Timmreck, M. Noppel, and A. Laaksonen, An improved parameterization for sulfuric acid-water nucleation rates for tropospheric and stratospheric conditions, *J. Geophys. Res., 107* (D22), 4622, doi:10.1029/2002JD002184, 2002.

Venkataraman, C, J. M. Lyons, and S. K. Friedlander, Size distributions of polycyclic aromatic hydrocarbons and elemental carbon. 1. Sampling, measurement methods, and source characterization, *Environ. Sci. Technol, 28*, 555-562, 1994.

Venkataraman, C. and S. K. Friedlander, Size distributions of polycyclic aromatic hydrocarbons and elemental carbon. 2. Ambient measurements and effects of atmospheric processes. *Environ. Sci. Technol*., *28*, 563-572, 1994.

Venkatram, A., and R. Viskanta, Effects of aerosol-induced heating on the convective boundary layer, *J. Atmos. Sci., 34*, 1918-1933, 1977a.

Venkatram, A., and R. Viskanta, Radiative effects of elevated pollutant layers, *J. Appl. Meteorol*., *16*, 1256-1272, 1977b.

Vogelmann, A. M., A. Robock, and R. G. Ellingson, Effects of dirty snow in nuclear winter simulations, *J. Geophys. Res*., *93*, 5319-5332, 1988.

Wang, C., A modeling study on the climate impacts of black carbon aerosols, J. Geophys. Res., *109*, D03106, doi:10.1029/2003JD004084, 2004.

Wang, W., and G.M. Domoto, The radiative effect of aerosols in the earth's atmosphere, J. Appl. Meteorol., 13, 521-534, 1974.

Warren, S. G., and W. J. Wiscombe, A model for the spectral albedo of snow. II: Snow containing atmospheric aerosols. *J. Atmos. Sci*., *37*, 2734-2745, 1980.

Warren, S.G., Optical properties of snow, *Rev. Geophys., 20*, 67-89, 1982.

Warren, S. G., Impurities in snow: Effects on albedo and snowmelt, *Ann. Glaciol*., *5*, 177-179, 1984.

Warren, S.G., and W.J. Wiscombe, Dirty snow after nuclear war, *Nature, 313*, 467-470, 1985.

Warren, S. G., and A. D. Clarke, Soot in the atmosphere and snow surface of Antarctica, *J. Geophys. Res*., *95*, 1811-1816, 1990.

Welch, R., and W. Zdunkowski, A radiation model of the polluted atmospheric boundary layer, *J. Atmos. Sci., 33*, 2170-2184, 1976.

Wigley, T.M.L., Input needs for downscaling of climate data, Discussion paper prepared for the California Energy Commission Public Interest Energy Research Program, 2004.

Woo, M.-K., and M.-A. Dubreuil, Empirical relationship between dust content and arctic snow albedo, *Cold Reg. Sci. Technol*., *10*, 125-132, 1985.

Yu, H., S.C. Liu, and R.E. Dickinson, Radiative effects of aerosols on the evolution of the atmospheric boundary layer, *J. Geophys. Res., 107*, doi:10.1029/2001JD000754, 2002.

Yu, S., V. K. Saxena, and Z. Zhao, A comparison off signals of regional aerosol-induced forcing in eastern China and the southeastern United States, Geophys. Res. Letters, 28, 713-716, 2001a.

Yu, S., C.S. Zender, and V.K. Saxena, Direct radiative forcing and atmospheric absorption by boundary layer aerosols in the southeastern U.S.: model estimates on the basis of new observations, *Atmos. Environ*., 35, 3967-3977, 2001b.

Zdunkowski, W.G., and N.D. McQuage, Short-term effects of aerosol on the layer near the ground in a cloudless atmosphere, *Tellus, 24*, 237-254, 1972.

Zdunkowski, W. G., R. M. Welch, and J. Paegle, One dimensional numerical simulation of the effects of air pollution on the planetary boundary layer, *J. Atmos. Sci*., *33*, 2399-2414, 1976.